B cell intrinsic gain of function mutations in B cell development and function: a story of activated CARD11 and PI3K

Michelle Dutra

A dissertation

submitted in partial fulfillment of the

requirements for the degree of

Doctor of Philosophy

University of Washington

2018

Reading Committee:

David Rawlings, chair

Richard James

Ram Savan

Program Authorized to Offer Degree

Immunology

©Copyright 2018

Michelle Dutra

University of Washington

Abstract

The impact of B cell intrinsic gain of function mutations on B cell development and function: a story of activated CARD11 and PI3K

Michelle Dutra

Chair of Supervisory Committee:
Adjunct Professor David J. Rawlings
Department of Immunology

Abstract: Gain of function mutations in key signaling molecules downstream of the B cell receptor have been linked to both malignancy and monogenic primary immunodeficiencies. This study is focused on characterizing the impact of such mutations in *Card11* and *Pik3cd* when restricted to the B cell lineage. Dominant, activating mutations in the adapter protein CARD11 induce inappropriate activation of NF-κB signaling. Somatic mutations in CARD11 are predicted to arise during GC responses in lymphomas, whereas germline CARD11 mutations drive a mild immunodeficiency, B cell expansion with NF-κB and T cell anergy (BENTA). Activated PIK3-delta syndrome (APDS) is an immunodeficiency caused by gain-of-function mutations in PIK3CD. Both diseases exhibit complex immune phenotypes including recurrent infection and impaired vaccine responses. Here, we modeled the B cell-intrinsic impact of: 1) the L251P activating mutation in CARD11 (aCARD11) and 2) the common APDS mutation (h*PIK3CD*-E1021K; referred to as 'aPIK3CD'). Global B cell aCARD11 expression led to a modest increase in splenic B cells and severe reduction in B1 B cell numbers, respectively. Following T cell-dependent immunization, aCARD11 cells exhibited increased rates of GC formation, resolution and differentiation. In this model, aCARD11 promoted dark zone skewing along with increased cycling, AID levels and class switch recombination. Furthermore, aCard11 GC B cells displayed increased biomass and mTORC1 signaling,

suggesting a novel strategy for targeting aCARD11-driven DLBCL. Global B cell expression of aPIK3CD drove expansion of the peripheral innate, B1a and MZ, B cell compartments. aPIK3CD blunted T-independent immune responses and reduced class-switched antibodies following T-dependent immunization. Thus, aPIK3CD and aCARD11 differentially alter B cell development and function post immunization, providing insight into B cell intrinsic contributions of these mutations to APDS and BENTA, as well as post GC malignancy.

Table of Contents

Abstract iii

List of Figures viii

Acknowledgements x

Chapter 1: Introduction 1

T-independent response 1

T-dependent response 2

B cell receptor signaling to NF-κB 3

CARD11 loss of function and dominant negative isoforms 4

CARD11 gain of function risk variants 5

B cell receptor signaling to PI3K 7

PI3K loss of function 8

Hyperactive PI3K signaling and Activated PI3K delta syndrome (APDS) 9

Questions to address 10

How does activated CARD11 impact B cell development and T dependent immune responses? 11

How does activated PI3K impact B cell development and humoral responses? 12

Chapter 2: Activated CARD11 accelerates germinal center kinetics, promoting mTORC1 and terminal differentiation 14

Introduction 14

Materials and methods 15

Results 20

aCARD11 promotes follicular over marginal zone B cell development and alters the B1 compartment 20

aCARD11 promotes more rapid formation and contraction of the GC response 21

GC B cell intrinsic aCARD11 expression is sufficient to alter the kinetics of the GC response 22

aCARD11 enhances cycling in vivo and skews GC polarization 23

GC B cells expressing aCARD11 demonstrate elevated mTORC1 signaling 25

Cells overexpressing aCARD11 manifest an NF-κB-independent elevation in mTORC1 signaling . 26

aCARD11 signaling likely enhances class switch recombination 27

Discussion 28

Figures 35

Chapter 3: Activated PIK3CD drives innate B cell expansion yet limits B cell intrinsic immune responses 47

Introduction 47

Materials and methods 48

Results 51

A cell intrinsic model for tissue-specific knock-in of activated PIK3CD 51

Expression of aPIK3CD in developing B cells leads to BM B lymphopenia 52

aPIK3CD expression promotes expansion of peripheral innate B cell compartments 53

aPIK3CD B cells exhibit differential selection within the immature vs. MZ and B1a compartments . 53

aPIK3CD does not alter cycling but differentially impacts immature vs. innate B cell survival 54

aPIK3CD expression drives plasma cell formation that correlates with elevated natural IgM 55

B-intrinsic aPIK3CD expression blunts TI immune responses 56

B-intrinsic aPIK3CD expression skews GCs toward a light zone fate and limits Ig class-*switching* . 57

Discussion 58

Figures 61

Chapter 4: Concluding Remarks 72

References 77

List of Figures

Table 1. Comparison of murine model phenotypes and human clinical features in the setting of LOF and GOF mutations in CARD11 and PI3KCD 13

Figure 2-1. B lineage aCARD11 expression leads to modest alterations in mature B2 B cells but near absence of B1 B cells 35

Figure 2-2. B cell intrinsic aCARD11 expression alters the kinetics of the GC response 36

Figure 2-3. GC B cell intrinsic aCARD11 expression induces rapid GC peak and contraction with increased terminal differentiation 37

Figure 2-4. aCARD11 promotes GC B cell cycling and DZ skewing 38

Figure 2-5. GC B cells expressing aCARD11 exhibit increased mTORC1 signaling 39

Figure 2-6. DLBCL B cells expressing aCARD11 exhibit increased pS6 independent of NF-kB signaling 40

Figure 2-7. aCARD11 promotes Ig class-switching in GC B cells and generation of IgG1 secreting PCs 41

Figure 2-S1. Mb1-aCard11 mice have mild splenomegaly with unaltered bone marrow B cell Development 42

Figure 2-S2. Cγ1-aCard11 mice have normal peritoneal B cells and serum Ig titers 43

Figure 2-S3. aCARD11 enhances cycling of GC B cells and PCs, with no impact on cycling in the bone Marrow 44

Figure 2-S4. aCARD11 enhances cell biomass and mTORC1 signaling 45

Figure 2-S5. aCard11 enhances CSR 46

Figure 3-1. Mb1-aPIK3CD mice exhibit BM B lymphopenia and expanded peripheral, innate B cell compartments 61

Figure 3-2. aPIK3CD B cells exhibit a competitive disadvantage in the BM but outcompete WT B cells in innate B cell compartments 62

Figure 3-3. aPIK3CD does not alter B cell cycling but differentially impacts survival in immature vs. innate B cell subsets 63

Figure 3-4. aPIK3CD enhances plasma cell differentiation and IgM and IgG3 production in the absence of Immunization 64

Figure 3-5. B cell intrinsic aPIK3CD expression limits both TI and TD humoral responses 65

Figure 3-S1. Inducible PIK3CD-E1020K (aPIK3CD) murine model and representative gating strategies to identify B cell subsets in B-cell specific aPIK3CD models 67

Figure 3-S2. Analysis of B cell cycling and survival in B-cell specific aPIK3CD models 69

Figure 3-S3. Selection for GC, plasma B cells and B1 progenitors, natural IgM specificities, and TI-II IgG3 responses in B-cell specific aPIK3CD models 70

Acknowledgements

Regarding my studies of activated CARD11, I would like to thank Raghav Chawla, Kerri Thomas, Brenda J. Seymour, and Tanvi Arkatkar for assistance with designing, performing, and interpreting experiments. Karen Sommer and David J. Rawlings designed the murine model. Cole Trapnell and Raghav Chawla were my collaborators for the single-cell RNAsequencing studies, and helped design and perform experiments, as well as analyze and interpret the findings. Thanks to Richard G. James, Iana Meitlis, Emma Suchland, and Nate Camp for assistance in designing, performing, and interpreting all biochemical studies. Thanks to Genita Metzler, Eric Allenspach, Richard G. James, and Shaun Jackson for critical review of the manuscript resulting from these studies.

Regarding my studies of activated PI3K, I would like to thank Fahd Al Qureshah and Genita Metzler for assistance with designing, performing, and interpreting experiments. Mohammed Oukka and David J. Rawlings designed the murine model. I, Fahd Al Qureshah, Genita Metzler, Richard G. James, and David J. Rawlings all contributed to the manuscript resulting from these studies.

Chapter 1

Introduction

Dysregulation of signaling pathways downstream of the B cell receptor (BCR), which is critical for the development, survival, and function of B cells, have been implicated in autoimmunity, primary immunodeficiency (PID), and lymphomagenesis. Gain of function (GOF) mutations in two distinct pathways downstream of the antigen receptor (Agr) identified in patients with immunodeficiency syndromes place these individuals at greater risk for development of B cell malignancies: 1) canonical NF-κB pathway and 2) PI3K pathway. Genome-wide association studies (GWAS), along with whole-exome sequencing, have identified target genes with recurrent mutations in key molecules, such as CARD11 and PI3K, involved in B cell intrinsic signaling in both PIDs and non-Hodgkins lymphomas (NHLs). However, the contribution of single mutations in lymphoma are difficult to discern as they are often identified after significant progression of disease. Similarly, while monogenetic PIDs have been identified, the extent to which individual cell lineages act as drivers of disease and/or pathogenesis remain unknown. The clinical phenotype of patients with loss of function (LOF) and GOF mutations bear similarities in a shared inability to respond to certain types of vaccines and recurrence of sinopulmonary and viral infections. B cells are the primary effectors that drive humoral immunity, which can be broken down into T cell-independent and -dependent responses and is decided by the type of antigen the B cells are responding to. This study focuses on characterizing individual GOF mutations in CARD11 and Pi3kcd/p110δ restricted to the B cell lineage, specifically interrogating the impact of these GOF during an immune response.

T-independent response

Resting B cells become activated by acquisition of soluble or membrane bound antigen[(1)]. Innate B cells, comprised of the marginal zone (MZ) and B1 B cell compartments, can respond to antigens independent of T cell help. Thymus-independent (TI) antigens can be subdivided into: 1) TI type 1 (TI-1) antigens are mitogenic, polyclonal B cell activators such as LPS, CpG and polyIC, and activate B cells

through toll-like receptors (TLRs); and 2) TI-2 antigens that feature repeating structures on a polysaccharide backbone - found in capsules of pathogens that impact the mortality of young adults such as *Haemophilus influenzae* b and *Streptococcus pneumoniae* – and engage the BCR driving an antigen specific response[2-4]. T independent responses are characterized by early B cell proliferation and differentiation into antibody producing cells beginning at three days post immunization, with a subsequent drop in the number of plasma cells during the second week following immunization. TI-2 antigens drive formation of extrafollicular foci where plasma cells are produced. TI-2 antigens induce a strong, long-lasting primary antibody response in mice, while polysaccharide vaccines confer long-term humoral protection in humans. These antigens do not induce recall responses upon secondary challenge, however, adoptive transfer of splenocytes from immunized mice into naïve irradiated recipients results in response to secondary challenge. Injection of immune serum from immunized mice into naïve recipients precludes this response prior to adoptive transfer.

T-dependent response

T-dependent antigens are proteins that are processed and loaded into MHC II complexes for presentation to cognate helper T cells[4]. Activated B cells that have successfully interacted with their cognate T cell are recruited/migrate into the germinal center (GC). GCs are specialized structures in which mature B cells undergo repeated rounds of clonal expansion and diversification of their immunoglobulin (Ig) genes. The GC gives rise to high-affinity B cells that differentiate into memory or plasma cells. GCs are polarized into two distinct compartments: the dark zone (DZ) and the light zone (LZ). The DZ is the site of clonal expansion and Ig somatic hypermutation (SHM), while the LZ is the site of selection of B cell clones expressing high-affinity BCRs through recognition of antigen on the surface of follicular dendritic cells (FDCs) and/or costimulatory signals from T follicular helper cells (Tfhs)[5]. The LZ is also thought to be the site of class-switch recombination (CSR), however, there is no conclusive study indicating that the LZ is where TD CSR occurs. Positive selection within the LZ allows the B cell clone to differentiate and exit the GC or re-enter the DZ for subsequent rounds of expansion and SHM. The

mutagenic nature of the GC is thought to contribute to the occurrence of GC- and post-GC derived malignancies.

B cell receptor signaling to NF-κB

In naïve, resting mature B cells NF-κB proteins are retained in the cytoplasm by the inhibitor IκBα. Antigen recognition through the B cell receptor (BCR) recruits Src family kinases, which phosphorylate conserved immunoreceptor tyrosine activation motifs (ITAMs) on the Igα/β (CD79a/b) subunits of the BCR complex. Subsequent recruitment of Syk tyrosine kinases to phosphorylated ITAMs results in phosphorylation of adapter molecules (Blnk). These adapters act as scaffolds for the assembly of signaling molecules (such as Btk) resulting in the activation of PLCγ2 to process phosphatidylinositol-4,5-bisphosphate (PIP_2) into second messengers, diacylglycerol (DAG) and inositol-1,4,5-trisphosphate (IP_3). DAG activates PKCβ, which mediates the phosphorylation of CARD11 (or CARD-containing MAGUK protein 1, CARMA1). Upon phosphorylation, CARD11 undergoes a conformational change allowing for its interaction with downstream binding partners, Bcl10 and MALT1, yielding the CARD11-Bcl10-MALT1 (CBM) signalosome. This signalosome is required for NF-κB and JNK signaling leading to B cell proliferation, survival, and differentiation[6]. Formation of the CBM complex ultimately activates the IκB kinase (IKK comprising IKKα, IKKβ, and IKKγ/NEMO) complex to phosphorylate IκBα. Phosphorylation of IκBα releases NF-κB for translocation into the nucleus to regulate transcription of its target genes, while pIκBα is degraded by the proteasome [7].

CARD11 expression is predominantly restricted to lymphocytes[8-10]. CARD11 proteins are made up of five domains involved in protein-protein interactions: an N-terminal caspase recruitment domain (CARD); a coiled coil (CC); a PDZ; and C-terminal SH3 (Src homology 3) and a GUK (guanylate-kinase)-like domain. CARD11 is phosphorylated at PKC consensus site serine residues within the linker region between the CC and PDZ domains in response to BCR engagement. Mutation of consensus serines abrogates PMA/ionomycin induced NF-κB activation[11]. The linker region interacts with the N-terminus of CARD11, resulting in intermolecular inhibition, holding CARD11 in a closed conformation. This

intermolecular inhibition is released upon phosphorylation of consensus serine residues within the linker region by PKCβ. In its open/activated conformation the CARD domain mediates oligomerization and interaction with the CARD11 of Bcl10.

CARD11 loss of function and dominant negative isoforms

Loss of function mutations (LOF) in CARD11 results in severe combined immunodeficiency (SCID) in patients[12, 13]. Patients with germline, LOF *Card11* mutations display progressive hypogammaglobulinemia and a block in peripheral B cell differentiation, with an increase in transitional B cells and loss of T regulatory cells (Tregs)[14]. Patients also exhibit defects in antigen receptor signaling and increased susceptibility to *Pneumocystis jirovecii* pneumonia (PjP)[12]. CARD11 deficiency is fatal within the first year of life and is treated with hematopoietic stem cell transplant. Heterozygous parents of CARD11 deficient patients are asymptomatic, thus haploinsufficiency does not result in disease.

CARD11 deficient mice, in which the CARD domain has been deleted (ΔCard)[9] or exons 3 and 4 were deleted[8], exhibit a complete defect in antigen-induced proliferation of T and B cells. However, ectopic expression of CARD11 has been shown to rescue NF-κB signaling in these animals and overexpression of CARD11 has been shown to enhance PMA- and Bcl-10 dependent NF-κB activation[8, 9]. Loss of CARD11 has no effect on conventional T cell development, whereas reduced marginal zone (MZ) and B1 B cells are observed in CARD11 deficient animals. These animals display decreased serum antibody titers, specifically IgM, IgG3, and IgA. Deletion of CARD11 shows no impact on bone marrow B cell development however B cell precursors were only characterized using limited markers[8], and requires additional study. B cells from CARD11 deficient mice fail to respond to BCR and CD40 signals, however there is inconsistency in the data regarding their responsiveness to lipopolysaccharide (LPS). Similar to CARD11$^{-/-}$ mice, Bcl10$^{-/-}$ mice are defective in propagating signals from the antigen receptor to NF-κB. Bcl10 deficient B cells are unresponsive to BCR and CD40 but can respond to LPS stimulation. It has also been previously shown that deficiency in components of the NF-κB signaling pathway downstream of

CARD11, Rel$^{-/-}$ and NFkB1$^{-/-}$ mice, have decreased serum Ig levels, and decreased CD5^{+} peritoneal B cells and diminished mitogen responsiveness.

Rare hypomorphic, dominant negative mutations in CARD11, which lead to dominantly inherited severe atopy with variable infection beyond the skin[14] have been recently described. A subset of patients displayed B cell lymphopenia and low IgM levels. Transfection of the identified CARD11 mutants into CARD11 deficient Jurkat T cells (JPM50.6) resulted in diminished NF-κB and mTORC1 activation after CD3/CD28 and PMA/iono stimulation. When co-transfected with WT CARD11, mutant CARD11 was found to interfere with the ability of WT CARD11 to activate downstream signaling pathways. These dominant, interfering mutants are thought to disrupt assembly of the CBM complex, as MALT1 protease activity was diminished in mutant transfected Jurkats as well as co-transfected cells. An ENU-mutagenesis derived CARD11^{UNM} mutant murine model, bearing pLeu298Gln in the CC domain, also displays elevated IgE and severe eczema, but no atopic phenotype[15]. Additional work in CARD11-deficient Jurkat T cells and primary mouse CARD11 deficient CD4^{+} T cells demonstrated decreased mTORC1 activity in the absence of CARD11[16].

CARD11 gain of function risk variants

CARD11 gain of function (GOF) mutations, were first identified in diffuse large B cell lymphomas (DLBCLs). Lymphomas are predominantly B cell derived (~95%)[17], while a subset are T cell derived. DLBCL is the most common type of non-Hodgkin's lymphoma (NHL)[18], accounting for ~30-40% of cases[17, 19]. DLBCL is a heterogeneous disease that is divided into three subtypes based on gene expression profiling studies. While ~50% of DLBCL cases are curable with current treatment, the activated B cell like (ABC) subtype, accounting for ~1/3 of cases, has an inferior prognosis[10, 19, 20]. A hallmark of ABC-DLBCL is constitutive NF-κB signaling, and inhibition of this pathway is toxic to these lymphomas[21]. RNA interference screens showed that the survival of most ABC-DLBCL lines depends on the CBM complex[19, 21]. GOF mutations in CARD11 are predominantly found in the N-terminal portion of CARD11 (CARD, LATCH, and CC domains), which mediates oligomerization of CARD11 and binding to

Bcl10 and MALT1, independent of upstream signaling. Somatic mutations within the coiled-coil domain of CARD11 are present in ~10% of ABC-DLBCL tumors[19], and expression of these mutants in cell lines induces strong NF-κB activity without stimulation[19]. DLBCLs accumulate ~30 mutations on average, and the contribution of individual of mutations is unknown.

In 2012, a novel congenital disorder featured the first known germline, GOF mutation of CARD11[(22)]. Individuals with BENTA (B cell expansion with NF-κB and T cell anergy) present with recurrent childhood sinopulmonary and viral infections, B cell expansion, splenomegaly and lymphadenopathy. Patients' T cells are within normal pediatric ranges but remain hyporesponsive upon stimulation *ex vivo*. Serum antibodies are skewed, with decreased IgM and normal-low levels of IgG and IgA. Patient B cells display elevated NF-κB signatures in the absence of stimulation, but fail to terminally differentiate into long lived plasma cells in vitro[(23)]. There is an increase in transitional and naïve, mature B cells with a concomitant decrease in switched and memory B cells. A subset of patients have gone on the develop B cell lymphomas in adulthood[(24)]. Enhanced expansion and survival of B cell clones may predispose BENTA patients to acquire additional mutations overtime, promoting lymphomagenesis.

The first study of GOF CARD11 mutants in isolation, with expression restricted to activated B cells, demonstrated that oncogenic mutations in CARD11 switched the response of recognizing self-antigen from death to proliferation and autoantibody production[(25)]. DLBCL CARD11 mutants were introduced into antigen-primed/activated B cells *ex vivo* and transplanted into $Rag1^{-/-}$ recipients with or without self-antigen in circulation. Mutant CARD11 expression in mature B cells broke tolerance, induced aberrant proliferation, plasmacyctic differentiation and antibody secretion. Notably the plasmacytic differentiation observed occurs in the absence of T cells. ABC-DLBCL has a plasmablast-like phenotype and is thought to derive from germinal center (GC) B cells that acquired oncogenic hits[(10, 20, 26)]. However, because introduction of mutant CARD11 was achieved by retroviral transduction into artificially activated cells, which were transplanted into lymphocyte deficient recipients, the findings in this study may not reflect the consequences of induction of mutant CARD11 in a germinal center reaction.

The DLBCL CARD11-L225LI mutation, resulting in an isoleucine insertion, has been previously shown to be the most potent NF-κB activating mutation in human DLBCL lines[(19)]. In a B intrinsic

CARD11-L225LI mouse model, pups succumbed to early postnatal lethality resulting from aggressive B-cell lymphoproliferation. At 5 days post birth, transgenic mice displayed histopathological features of a high-grade lymphoma, with blastoid cells infiltrating solid organs and bone marrow. B cells isolated from transgenic mice showed elevated NF-κB and JNK activity compared to wildtype. This phenotype was completely rescued when transgenics were crossed to either $Bcl10^{-/-}$ or $MALT1^{-/-}$ mice, demonstrating that disruption of the CBM complex resolves aberrant NF-κB activation[27]. While this study demonstrated that a single mutation in CARD11 can yield a disease phenotype mirroring ABC-DLBCL, whether other CARD11 mutants - that result in a spectrum of NF-κB activity - will behave similarly is unknown. Also, since these animals did not survive past 6 days post birth we have no insight into how CARD11 mutants impact a germinal center response.

BCR signaling to PI3K

The PI3K-Akt signaling axis is responsible for the inactivation of FOXO1 as well as the activation of mTORC1 downstream of the BCR, as well as providing pro-survival signals. Phosphatidylinositol 3-kinase (PI3K) signaling plays a critical role at several stages of B cell development. Class 1A PI3K proteins function as heterodimers between activating (p110α, β, and δ) and regulatory (p85) subunits. These heterodimeric complexes are critical for the activation of downstream kinases that regulate B cell survival, differentiation and metabolism including, but not limited to, Btk, Akt and mTOR. The activating subunits of class 1A PI3Ks have overlapping expression patterns. PIK3CA and PIK3CB are expressed ubiquitously, whereas PIK3CD (p110δ) is restricted to immune cells. Despite the structural and expression similarities, loss of function studies have revealed that PIK3CD and its regulatory subunit PIK3R1 (p85) are the primary class 1A PI3K downstream of the BCR. Class I PI3Ks phosphorylate membrane phosphatidylinositol lipids on the D3 position of the inositol ring to generate the lipids PIP, PIP_2 and PIP_3[28]. Phosphatidylinositol 4,5-bisposphate (PIP_2) and phosphatidylinositol 3,4,5-trisposphate (PIP_3) function as a membrane tether for plextrin homology domain (PH) containing proteins such as PDK1, Akt, and Btk, among others. Two SH2 domains within the p85 subunit of PI3K interact with phosphotyrosine residues in the cytoplasmic tails of surface receptors (BCR and CD19). Binding of PI3K

to the cytoplasmic tail of surface receptors brings it in proximity of its substrates. Recruitment to the plasma membrane also brings PI3K in proximity of Src-family kinases (Lyn), which can further potentiate PI3K activity via interaction between the SH3 domain, within the Src, and the proline-rich region of PI3K. Negative regulators of PI3K signaling hydrolyze PIP_3 back to PIP_2; 1) phosphatase and tensin homolog (PTEN) hydrolyzes the 3-phosphate of PIP_3 to phosphatidylinositol 4,5-bisposphate (PIP_2), and 2) phosphatidylinositol 3,4,5-trisphosphate 5-phosphatase 1(SHIP-1/INPP5D) hydrolyzes the 5-phosphate of PIP_3 to phosphatidylinositol 3,4-bisposphate (PIP_2).

PI3K loss of function

While deletion of either gene, *Pi3kcd/p110δ* or *Pi3kr1/p85α*, in mice has minimal impact on central B cell development, mature B cell development is significantly altered, resulting in development of fewer B1 and marginal zone (MZ) B cells[29]. PI3K signaling is required for B cell homeostasis, as demonstrated by deletion of Pdk1 ($CD21^{Cre/+}Pdk1^{Flox/Flox}$) resulting in reduced numbers of both splenic and peritoneal B cell subsets[30]. Similarly, $p110\delta^{-/-}$ mice have reduced B1 and MZ compartments[31], while mice homozygous for catalytically inactive p110δ ($p110\delta^{D910A/D910A}$) also lack splenic MZ and peritoneal B1 cells[32]. These cellular defects contribute to decreased immunoglobulin production, weak responses to TI antigens and lack of response to TD antigens in mice[29, 32] or humans deficient in either *PIK3CD*[33] or *PIK3R1*[34].

The contribution of p110δ in early B cell development in the bone marrow is murkier. One report showed $p110\delta^{-/-}$ mice, in which exons 1-9 of the *Pi3kcd* gene are deleted, have no apparent defect in BM B cell development[31]. Whereas another study using mice homozygous for catalytically inactive p110δ ($p110\delta^{D910A/D910A}$) have decreased numbers of $B220^{+}IgM^{+}$ B cells in the BM and a 1:1 ratio of pre:pro B cells, whereas WT mice exhibit a 4:1 pre:pro ratio[32]. Complete loss of p110α or p110β results in embryonic lethality. Use of $p110\alpha^{fl/fl}$ mice, in which exons 18 and 19 of *Pi3kca* are flanked by loxp sites, crossed to the CD2-Cre strain deletes p110α in all lymphocytes. In vitro stimulation of B cells from $p110\alpha^{fl/fl}CD2^{Cre/+}$ mice showed no change in responses to BCR, IL4, CD40 or LPS stimulation.

p110α$^{fl/fl}$CD2$^{Cre/+}$ mice[35] also demonstrated normal primary and secondary responses to hapten immunization as well. This shows that p110α is dispensable for B cell maturation and function. However, compound loss of p110α and p110δ (p110α$^{fl/fl}$CD2$^{Cre/+}$ p110δ$^{D910A/D910A}$), results in a substantial block at the pre-B cells stage (fraction C, B220^{+}CD19^{+}cKit^{+}CD25^{-}Bp1^{+}) with significant loss in immature and mature B cells in the bone marrow. Also, p110α-p110δ double deficient B cells failed to suppress Rag gene expression and exhibit attenuated proliferation in response to IL-7. Treatment of B cells with p110δ-specific inhibitor IC87114 ablated responses to BCR, IL4, CD40 or LPS. Compound loss of p110β, exons 21 and 22 of *Pi3kcb* flanked by loxp sites, and p110δ (p110β$^{fl/fl}$CD2$^{Cre/+}$ p110δ$^{D910A/D910A}$) showed no impairment in B cell development[35]. Thus p110α, but not p110β, can compensate for a lack of p110δ during B cell development in the bone marrow.

Hyperactive PI3K signaling & Activated PI3K delta syndrome (APDS)

B cell-specific activation of class 1A PI3Ks, as assessed using genetic models of PI3K hyper-activity, also leads to defects in both TI and TD responses. For example, deficiency of either the PI3K phosphatases, INPP5D[36, 37] or PTEN[38], or forced expression of membrane-tethered Pi3kca[39], results in loss of B cell class-switch recombination and maturation in response to TD antigens. BCR stimulation in immature splenic B cells fails to activate Akt, correlating with a loss of mitochondrial membrane potential and diminished viability. These events are reversed in the setting of increased PI3K activity as demonstrated by B cell intrinsic deletion of PTEN (CD19$^{Cre/+}$Pten$^{Flox/Flox}$), which allows splenic immature B cells to survive and proliferate after BCR-ligation[40]. PTEN deletion in CD19$^{-/-}$ mice also rescues the B1 and MZ compartments, which are absent in CD19$^{-/-}$ mice[41].

As suggested from the data in mice, primary immunodeficiency in humans can be caused by germline mutations in PIK3CD or PIK3R1 that increase class 1A PI3K signaling. Patients with activating mutations in either gene present with complex immune phenotypes that include susceptibility to bacterial and viral respiratory infections, B cell lymphopenia, effector-memory T cell hyperplasia and senescence, antibody dysregulation (increased IgM and decreased IgG2), impaired vaccine responses and acquisition

of B cell lymphoma[42-45]. The cell intrinsic roles for B and T cells in this newly identified immune dysregulation disease, called Activated Phosphoinositide 3-kinase-d Syndrome (APDS), have not been carefully elucidated. The most common APDS associated mutation E1021K occurs within the catalytic subunit p110δ, encoded by the PIK3CD gene[42].

In contrast to its impact on the peripheral B cell compartment, hyperactive PI3K signaling in BM B cells appears to be deleterious. The mechanistic explanation for the negative impact is less clear but likely reflects a requirement for a precise window of PI3K signaling during pro- and pre-B cell development. Consistent with this idea, both loss of function and hyperactivation of PI3K have similar deleterious effects in early B cell development, supporting the idea that early B cells are selected for an intermediate level of PI3K signaling[46]. Pten deletion in pre-B cells expressing oncogenic BCR-ABL1 drives rapid cell death of leukemia cells. Pten deletion was shown to result in downregulation of IL-7R, CD19, and components of the pre-BCR and lead to hyperactive Akt signaling. Pharmacological inhibition of Akt greatly reduced Pten deletion mediated toxicity. Bone marrow (BM) B cell phenotyping in a small number of APDS subjects has suggested that aPIK3CD may impact the pre-B-I stage leading to an increased proportion of apoptotic $CD19^{dim}$ B cell progenitors[47]. A proportional increase in the late pro-B cells (referred to as the pre-B-I population) in the BM correlated with absolute decrease in circulating B cell numbers. Another study, utilizing alternative markers and while not entirely consistent with data from Wentink et al., also showed a proportional increase in early $CD10^{hi}CD20^{-}$ “pro-B” cells and markedly reduced mature B cells[48]. While the full extent of hyperactivation of p110δ on early B cell development is unknown, data from human APDS patients supports a model where hyperactive PI3K signaling limits pre-B cell development, thereby restricting overall BM B lymphopoiesis.

Questions to address

While dysregulation of B cell intrinsic signaling results in altered development, homeostasis/survival, and response to antigen the contribution of individual mutations that perturb signaling requires additional study. Determining what roles, the B cells themselves play in propagating disease in PIDs such as BENTA and APDS has been up to this point based on findings using patient samples in which dysregulated signaling is not restricted to a single lineage, and the impact of altered

development cannot be separated from impaired immune responses. Regarding malignancies, determining the input of a single mutation in patient samples, or patient derived cell lines is difficult as many tumors have accumulated numerous mutations that impact multiple signaling pathways, all of which perturbed B cell biology. Interestingly, many clinical features of PIDs and developmental outcomes appear similar when comparing LOF and GOF mutations in the same signaling pathways (see Table 1). For example, SCID patients, with CARD11 deficiency, and BENTA patients display decreased mature B cells in circulation, with diminished Ig titers, and increased susceptibility to infection. Similarly, APDS patients, while having increased serum Ig titers, fail to respond to polysaccharide derived vaccines, as do BENTA patients. These similarities in clinical features demonstrate that signaling pathways central to B cell development, homeostasis and immune function must be finely tuned, and both too little and too much signal are detrimental.

How does activated CARD11 impact B cell development and T-dependent immune responses?

As the activating, somatic mutations in CARD11 that lead to DLBCL are predicted to occur during the B cell GC response, GC-specific analyses are likely to improve understanding of DLBCL biology. To evaluate the impact of aCARD11 on the GC response, we developed a transgenic model allowing inducible expression of aCARD11 (mouse CARD11-L251P) that mimics an analogous mutation identified in human DLBCL (L244P)[19]. This construct was introduced in association with a downstream T2A-linked GFP marker into the endogenous *Rosa26* locus. Crossing this strain to various B cell-intrinsic Cre-bearing strains gives rise to GFP^+ cells co-expressing aCARD11. Importantly, this model was designed to facilitate aCARD11 expression levels similar to that observed in heterozygotes that develop DLBCL. Further, this specific mutant activates NF-κB to a lesser extent than the previously modeled L225LI mutation[19, 27], demonstrated by differential induction of an NF-κB reporter and ability to spontaneously aggregate and form the CBM complex, and was anticipated to permit a relatively normal B cell developmental program wherein animals would establish a mature peripheral B cell compartment. Using several B cell intrinsic models, we assessed both how this mutation modulates B cell development and, most importantly, its impact within a GC response. Our findings indicate that cells expressing aCARD11

display enhanced NF-κB and mTORC1 signaling, significantly altered GC kinetics, cell fate determination and class switch recombination (CSR) during the primary response to T-dependent (TD) antigens.

How does activated PI3K impact B cell development and humoral responses?

APDS patients display an array of symptoms which multiple immune cell lineages contribute to[42-44, 49]. How dysregulated signaling of PI3K within a single cell lineage contributes to the APDS disease phenotype is unknown. To understand how activating mutations in the catalytic subunit of p110δ (Pik3cd) impact the differentiation, homeostasis, and function of B cells, we generated an inducible mouse model of PIK3CD-E1020K (equivalent to hE1021K, hereafter referred to as 'aPIK3CD'). With this model we can study the impact of this GOF mutation during different stages of B cell development and its impact on humoral immunity.

		CARD11		PIK3CD	
		LOF	GOF	LOF	GOF
Mouse models	BM	No effect	L225LI – premature lethality due to plasmacytic infilitrates in BM & organs **ROSA-CARD11-L251P** • B lymphopenia by % • ↑pro%, ↓immature% • Loss of B1 progenitors	**p110$^{-/-}$**: no impact **p110$^{D910A/910A}$**: increased pro B cells **p110$^{fl/fl}$p110$^{D910A/910A}$**: block at frac B→C transition due to inability to suppress Rag1/2 expression & fail to proliferate in response to IL7	**PIK3CD-E1020K** • B lymphopenia % & # • ↑pro%, ↓mature%, ↓small pre & mature #s • ↑B1 progenitors
	Periphery	• Normal T cell development • Loss of B1 & MZ B cells • Decreased Ig titers • Loss of AgR→NFκB signaling	• Switch from self-Ag induced death to proliferation & Plasmablast differentiation **ROSA-CARD11-L251P** • Trend ↑ Spln weight & counts • ↑ total B cells due to ↑FM • No spontaneous GCs • ↓ total B cells in PF due to loss of B1a & B1b • ↓IgM	• Loss of B1 & MZ B cells • Diminished TI & TD responses • Decreased serum IgM, IgG3, & IgA • Decreased BCR responsiveness • Decreased Ca-flux, decreased activation of PLCγ2 & Btk	**Pten$^{fl/fl}$**: B cell hyperplasia, lymphoma, hypergammagobulinemia **SHIP-1$^{-/-}$**: accelerated B cell development & hyperresponsiveness to BCR **PIK3CD-E1020K** • ↑B1a & MZ, ↓B2 • ↑IgM & IgG3 • Defect in CSR • Defect in TI response
Human clinical phenotype	BM				PTEN deletion in BCR-ABL1 pre-B leukemia drives rapid cell death **APDS** • Increase in late-pro-B (pre-B1) & decrease in in circulating B cells • Increase in early CD10^{hi}CD20^{-} (pro B) cells & decrease in mature cells
	Periphery	• Block at late transitional B cell stage, lack of mature B cells. • Decreased Treg/Th17 • Decreased Ig titers – fail to mount specific Ab response • Increased susceptibility to PjP	**BENTA (germline)** • B cell lymphocytosis, splenomegaly & lymphadenopathy • Recurrent sinopulmonary & viral infections • ↑transitional B cells, ↓SW/memory B cells • Decreased Ig titers, impaired PB formation in vitro • Diminished responses to polyssacharide vaccines • T cell anergy • Increased predisposition to B cell malignancy **Somatic mutations** • ~10% of ABC-DLBCL • Spontaneous CBM formation • Constitutive NFkB signaling • Plasmablast like gene expression & morphology • Chemo- & Ibrutinib resistant		**APDS (germline)** • Recurrent sinopulmonary infections & viral infections, progressive airway damage • Lymphoproliferation, lymphadenopathy & splenomegaly • Lymphomas in some patients • ↑ transitional B cells, ↓ SW/memory B cells • ↑ IgM, ↓ $IgG_{2/4}$ & IgA • Poor vaccine responses • Progressive CD4 T cell lymphopenia • Acceleration of terminally differentiated/senescent CD8 T cells • Decreased naïve T cells

Table 1. Comparison of murine model phenotypes and human clinical features in the setting of LOF and GOF mutations in CARD11 and PI3KCD. (Black) Phenotype and clinical features described in literature. (Red) Data generated from our murine studies.

Chapter 2

Activated CARD11 accelerates germinal center kinetics, promoting mTORC1 and terminal differentiation

Introduction

Diffuse large B-cell lymphoma (DLBCL) is the most common type of non-Hodgkin's lymphoma[18]. While nearly half of DLBCL are curable with current treatment, the activated B cell-like (ABC) subtype has an inferior prognosis[10, 19, 20]. ABC-DLBCL is derived from GC B cells that have acquired progressive oncogenic hits[10, 20, 26]. In normal B cells, B cell receptor (BCR) engagement induces phosphorylation of the molecular scaffold CARD11, leading to conformational changes that promote assembly of a CARD11, Bcl10, MALT1 (CBM) signalosome[11], required for NF-κB and JNK signaling and B cell proliferation, survival, and differentiation[6]. Activating mutations in CARD11 (referred to hereafter as aCARD11) occur in 10% of ABC-DLBCL[19]. Importantly, while aCARD11 expressing DLBCLs rely on constitutive NF-κB signals for survival[21], additional aberrant signals are also likely required for tumor growth. Thus, a better understanding of how aCARD11 alters GC biology may inform the design of future therapies.

An initial *in vivo* analysis of aCARD11 variants demonstrated that oncogenic mutations altered the response of self-reactive B cells, promoting proliferation and autoantibody production upon exposure to self-antigen[25]. In that study, DLBCL-derived aCARD11 mutants were introduced *ex vivo* (using retroviral gene delivery) into murine B cells following *in vivo* antigen-priming. Adoptive transfer of these cells into $Rag1^{-/-}$ recipients expressing the self-antigen, led to broken tolerance and aberrant proliferation, plasmacytic differentiation and autoantibody secretion. The impact of aCARD11 on T-dependent responses and the GC reaction were not addressed in this study.

A DLBCL-associated mutation resulting in an isoleucine insertion, CARD11-L225LI, is the most potent known NF-κB activating mutation[19]. In a B intrinsic CARD11-L225LI mouse model, pups succumbed to early postnatal lethality resulting from aggressive B-cell lymphoproliferation. Within 5 days post-birth, transgenic mice displayed histopathological features of high-grade lymphoma, with blastoid

cells infiltrating solid organs and bone marrow. B cells isolated from transgenic mice exhibited elevated NF-κB and JNK activity compared to controls. This phenotype was abrogated by intercross with either $Bcl10^{-/-}$ or $MALT1^{-/-}$ mice demonstrating that disruption of the CBM complex resolves aberrant NF-κB activation[27]. While this study showed that a single mutation in CARD11 can yield a disease phenotype mirroring lymphoma, whether other CARD11 mutants - that result in a spectrum of NF-κB activity[19]- will behave similarly is unknown. Also, as these animals succumbed to disease immediately post-birth, this model was unable to provide insight into how aCARD11 mutants impact a GC response.

As the activating, somatic mutations in CARD11 that lead to DLBCL are predicted to occur during the B cell GC response, GC-specific analyses are likely to improve understanding of DLBCL biology. To evaluate the impact of aCARD11 on the GC response, we developed a transgenic model allowing inducible expression of aCARD11 (mouse CARD11-L251P) that mimics an analogous mutation identified in human DLBCL (L244P)[19]. This construct was introduced in association with a downstream T2A-linked GFP marker into the endogenous *Rosa26* locus. Crossing this strain to various B cell-intrinsic Cre-bearing strains gives rise to GFP^+ cells co-expressing aCARD11. Importantly, this model was designed to facilitate aCARD11 expression levels similar to that observed in heterozygotes that develop DLBCL. Further, this specific mutant activates NF-κB to a lesser extent than the previously modeled L225LI mutation[19, 27] and was anticipated to permit a relatively normal B cell developmental program wherein animals would establish a mature peripheral B cell compartment. Using several B cell intrinsic models, we assessed both how this mutation modulates B cell development and, most importantly, its impact within a GC response. Our findings indicate that cells expressing aCARD11 display enhanced NF-κB and mTORC1 signaling, significantly altered GC kinetics, cell fate determination and class switch recombination (CSR) during the primary response to T-dependent (TD) antigens.

Materials & Methods

Mice

1x-Flag tagged murine CARD11-L251P was knocked into the ROSA26 locus, with an upstream loxp-flanked 3x-stop codon and a downstream self-cleaving T2A linked GFP reporter. These mice are called

activated Card11 (aCard11) mice throughout the paper. The aCard11 mice were maintained by crossing to C57BL/6 mice and have been backcrossed 5 times. aCard11 mice were crossed to Mb1-Cre[50] and Cγ1-Cre[51] mice, which are on a fully C57BL/6 background. Mice were bred and maintained in the specific pathogen-free animal facility of Seattle Children's Research Institute and handled according to Institutional Animal Care and Use Committee-approved protocols. $Mb1^{Cre}$ mice were provided by M. Reth (Max Planck Institute of Immunobiology, Freiburg, Germany).

Immunizations

12- to 15-week old mice were i.p. immunized with 200ul of 20% by volume sheep red blood cells (SRBCs – Colorado Serum Co.) diluted in 1x PBS and sacrificed 5, 7, 10, and 21 days post immunization. 12- to 23- week old mice were i.p. immunized with 50 ug of NP-CGG (Ratio>40, Biosearch Technologies) precipitated in alum and sacrificed at 12 days post immunization.

Reagents and antibodies

LIVE/DEAD Fixable Near-IR Dead Cell Stain Kit (Invitrogen) was used according to manufacturers, instructions. Anti-murine antibodies used in the study include: eBioscience - CD38 (90), Bcl-6 (BCL-DWN), AID (mAID-2), IRF4 (3E4), IgM (II/41), CD8 (53-6.7), Gr-1/Ly-6G (RB6-8C5), SA-e450; Southern Biotech - IgD (11-26), BP-1 (FG35.4), λ (JC5-1); Biolegend - B220 (RA3-6B2), CD19 (6D5), CD24 (M1/69), CD21 (7E9 & 7G6), CD23 (B3B4), BP-1 (6C3), CD4 (GK1.5); BD Biosciences - CD43 (S7), CD21 (7G6) CD19 (1D3), CD138 (281-2), CD95/Fas (Jo2), IgG1 (A85-1), κ (187.1), CXCR4 (2B11), CD86 (GL1), CD11b (M1/70), CD5 (53-7.3), Blimp1 (5E7), SA-PE.; Life technologies - CD3 (500A2), SA-AF700, SA-APC; Vector labs - PNA; Cell Signaling technology - FOXO1 (C29H4), p4E-BP1 (Thr37/46, 236B4), p-S6 (Ser235/236, D57.2.2E). IKK-2 inhibitor MLN120B (Sigma Aldrich).

All flow cytometric, EdU, BrdU, and phospho-flow data were collected on an LSRII (BD) and analyzed using FlowJo software (Tree Star).

Spleen immunofluorescence staining

Mouse spleens were embedded in OCT compound and frozen over dry ice. 10 μm sections were cut on a cryostat, mounted on Superfrost Excell slides (Fisher), and fixed in -20℃ acetone for 20 minutes. After

rehydration in staining buffer (PBS, 1% goat serum, 1% BSA, 0.1% Tween-20), slides were stained with: B220-PE (RA3-6B2, BD biosciences), CD3-APC (Life Technologies, 500A2) and PNA-FITC (Vector labs). Images were acquired and analyzed using a Leica DM6000B microscope at 10x magnification, Leica DFL300 FX camera, and Leica Application Suite Advanced Fluorescence software. Analysis performed using ImageJ software.

Flow Cytometric Analysis

Single-cell suspensions for spleen, bone marrow (BM), and peritoneal fluid (PF) were obtained as previously described[52] and incubated with fluorescence-labeled Abs for 15 min at 4°C. Transcription factor labeling was performed using the True-Nuclear Transcription Factor Buffer Set (Biolegend). Surface Abs were stained for 20 min at 4°C followed by incubation with a transcription factor fixation/permeabilization solution (TrueNuclear) 35 mins at RT. Transcription factor Abs were then stained for 35 min at RT in a permeabilization buffer. For intracellular staining, cells were first fixed for 30min at 4°C with fix/perm solution (BD), followed by staining with intracellular Abs for 30min at 4°C in fix/perm buffer (BD).

Cell cycle analysis using in vivo EdU labeling

5-ethynyl-2'-deoxyuridine (EdU, Thermo Fisher) was dissolved in sterile 1x PBS or DMSO and 1mg in a volume of 100ul was injected i.p. 1 hr prior to sacrifice. EdU detection was performed with the Click-iT Plus EdU Pacific Blue and Alexa647 Flow Cytometry Assay Kits (Thermo Fisher). Cells are stained for surface markers for 15min at 4°C, followed by fixation and incubation with the Click-iT Plus reaction cocktail according to manufacturer's instructions.

Cell cycle analysis using in vivo BrdU labeling.

For in vivo labeling of cycling cells, mice were i.p. injected with 1 mg in a volume of 100ul BrdU 24 hrs prior to sacrifice. Both spleens and BM were collected, and cells were surface stained, fixed and permeabilized, and treated with DNase for 1 h at 37°C and stained with anti-BrdU FITC (BD Biosciences) immediately before FACS analysis.

Phospho-flow analysis

1e6 cells were fixed with Cytofix/Cytoperm solution (BD biosciences) for 20 min at RT in the dark. Cells were resuspended in 90% methanol and stored at -20 ℃ for a minimum of 30 mins. Cells were stained with surface and phospho-site antibodies for 45 min at RT in the dark. For phosphorylation site staining in the DZ and LZ: cells were fixed as described above, then permeabilized in 90% methanol for 30mins at -20ºC, followed by incubation with antibodies for surface markers for 45 min at RT in the dark, and a subsequent 45 min incubation with streptavidin and phosphor-site antibodies at RT in the dark.

ELISA

96 well Nunc-Immuno MaxiSorp plates (Thermo Fisher) were pre-coated overnight at 4℃ with 2ug/ml anti-IgM, anti-IgG, anti-IgG1, and anti-IgG2C (Southern Biotech), or 50µg/mL NP(5)-BSA and NP(30)-BSA (Biosearch Technologies). Plates were blocked for 1hr with 2% BSA in PBS before addition of diluted serum (1:6250, 1:31250, 1:156250) for 2hrs at RT or overnight at 4℃. Specific antibodies were detected using goat anti-mouse IgM-, IgG, IgG1-, IgG3, or rat-anti IgG2C-horseradish peroxidase (1:2,000 dilution; Southern Biotech), and peroxidase reactions were developed using OptEIA TMB substrate (BD biosciences) and stopped with sulfuric acid. Absorbance at 450 nm was read using a SpectraMax 190 microplate reader (Molecular Devices). 450 nm absorbance was corrected by subtraction of 570nm absorbance.

Immunoblot analysis

Primary murine naïve B cells were purified by CD43 microbead depletion (Miltenyi Biotec). For analysis of immunized animals, total B lineage cells were isolated with Pan B Cell Isolation Kit II (StemCell). Cell pellets were lysed in 1x RIPA lysis buffer (1% NP40, 0.25% sodium deoxycholate, 0.1% SDS, 150mM NaCl, 20mM HEPES pH 7.5, 1mM β-glycerophosphate, 1mM NaF, 10mM Na-pyrophosphate, 1mM Na-orthovanadate, & Pierce protease inhibitor tablet) on ice for 10 min. Lysates were centrifuged at 17,000 for 20min at 4℃, and supernatant was collected. Protein concentration of cleared supernatants was determined by bicinchoninic acid (BCA) analysis. performed. 15 ug of sample were run on 4-12% Bis-Tris

NuPAGE gels (Invitrogen) in 1x MOPs Buffer (Invitrogen). Protein was transferred onto nitrocellulose in 1x Transfer Buffer (Invitrogen) with 10% methanol. Non-specific binding was by incubation with Odyssey LI-COR Blocking Buffer. All primary antibodies were incubated for a minimum of 12hrs at 4°C except actin, which was incubated for 1hr at RT. Primary anti-mouse antibodies used for immunoblot analysis included: Cell Signaling technology - CARD11 (1D12), HSP90, p-p65 (Ser536, 93H1), p65 (C-20), FOXO1 (D7C1H), p-S6 (Ser235/236), S6 (54D2), IκBα (5A5); Santa Cruz Biotechnology – p65; Sigma - actin (Rb polyclonal). Secondary antibodies were incubated with membranes at 1:10,000 in 1x TBST for 30 min at RT in the dark. Membranes were imaged with Odyssey Infrared Imaging System (LI-COR Biotechnology, Lincoln, NE). Immunoblot quantification was performed using ImageJ software.

Guassia Luciferase & Cell Titer Glo assay

$0.1x10^6$ transduced OCI-Ly7 cells in 100ul media (IMDM+10%FBS+BME) were cultured under the following conditions: DMSO 1:1000, MLN120B (60nM, 600nM and 1uM), or 50nM Rapamycin. After 16hrs, 20µL of culture supernatant was transferred into a 96 well opaque plate (Corning) with 10µL Gluc reagent cocktail (1:100 of BioLux GLuc Substrate diluted into BioLux GLuc assay buffer, New England BioLabs) added and incubated for 45s at room temperature before luminescence was recorded. The remaining 80µL culture volume was transferred to an opaque 96 well-flat bottom plate with 10µL Cell Titer Glo reagent (Promega). Cells were incubated with cell titer glo for 15 mins at RT in the dark before luminescence was recorded.

Single-cell RNA sequencing

Single-cell suspensions were prepared from spleens harvested from mice 5dpi with SRBCs. B lineage cells were enriched using the EasySep Mouse B Cell Isolation Kit (StemCell). Single-cell cDNA libraries were generated using the Chromium product suite by 10x Genomics[53] and sequenced using an Illumina NextSeq 500. Cell Ranger (by 10x Genomics) was used for sample demultiplexing, barcode processing, and single-cell 3' gene counting, revealing a total cell count of n=1954. Monocle 2 was used for downstream analysis as described previously[54] and in the Monocle vignette. Only cells with a total unique molecular identifier (UMI) count of between 600 and 12500 were included in the analysis

(n=1945). Cells were clustered using t-SNE, and the major cell types were identified using canonical marker genes. Non-B cell clusters were completely removed and, in addition, only CD79a-positive cells were retained for downstream analysis (n=1581). Clustering of B cells only was again performed using t-SNE. Differential gene expression analysis between WT and aCard111 cells was performed using the differential-GeneTest function included within Monocle.

Statistical analysis.

Unpaired, two-tailed Student's *t* tests and 2-way ANOVA were applied to determine the statistical significance of the differences between groups of mice. Paired, two-tailed Student's *t* tests were applied to determine the statistical significance of the differences between the cell lines expressing WT or L251P-CARD11. The p-values were considered significant when $P < 0.05$ (*), $P < 0.01$ (**), and $P < 0.001$ (***). 2-way ANOVA $P<0.05$ is *, $P<0.005$ is **, $P<0.0005$ is ***.

Results

aCARD11 promotes follicular over marginal zone B cell development and alters the B1 compartment

To better understand how aCARD11 impacts B cell biology we developed an inducible model for expressing CARD11 with a L251P coding change (equivalent to human CARD11-L244P)[19] with a cis-linked GFP reporter knocked-into the endogenous *Rosa26* locus (Fig. 2-1A). For the initial characterization of B cell maturation, ROSA-aCard11 animals were crossed to the Mb1-Cre strain (referred to as "Mb1-aCard11")[50], which initiates Cre recombinase expression at the BM pro-B cell stage. Importantly, total CARD11 protein levels, in naïve splenic B cells in Mb1-aCard11 mice, were minimally changed relative to control animals (Fig. 2-1B&C). While unlikely, inefficient cleavage of the T2A fusion protein could impact mutant CARD11 protein levels and contribute to our observations of no difference in total CARD11 protein. Alternatively, the mutant CARD11 protein may be expressed at lower levels than the endogenous, wildtype protein, as it has been shown that activated forms of CARD11 have decreased stability at steady state[55]. GFP expression was detected in pro-B cells ($B220^+IgM^-CD43^+$; ~30-50%) and in all later developmental stages (Fig. 2-S1A&B; >90% GFP^+ starting at the small pre-B cell stage). There

was no significant impact of aCARD11 on B cell subsets in the bone marrow (Fig. 2-S1D). GFP expression in the periphery was restricted to cells of the B lineage (Fig. 2-S1A&C).

Despite expression of aCARD11 in all peripheral B cells, we did not observe striking differences in spleen weight or in absolute counts or frequency within the T or myeloid compartments (Fig. 2-S1E-H). Characterization of splenic B cells revealed a slight increase in total cell numbers (Fig. 2-S1H), decreased spontaneous GC B cells (Fig. 2-S1I) increased follicular mature (FM) B cells (percentage and absolute B cell counts) and a decreased percentage of marginal zone (MZ) B cells (Fig. 2-1D-F). There was also no significant B cell expansion evident in the spleens of older animals (>30 wks, data not shown). Characterization of B cell subsets in the peritoneal cavity revealed near absence of B1a B cells ($CD19^+CD11b^+CD5^+$) and marked reduction of B1b B cells ($CD19^+CD11b^+CD5^-$) (Fig. 2-1G-I). Mb1-aCard11 animals also exhibited decreased total IgM with a trend towards decreased total IgG, despite equivalent levels of IgG1 and IgG2c (Fig. 2-1J-K, & Fig. 2-S1J-K). The decrease in basal IgM production likely reflected absence of the B1a compartment, a major source of natural IgM[56]. Together, these data demonstrate establishment of a murine model, expressing an inducible, oncogenic CARD11 variant at near endogenous levels, leading to modest changes in B2 B cell development and marked reduction in B1 B cell compartment in the absence of immunization.

aCARD11 promotes more rapid formation and contraction of the GC response

Previous work showed that overexpression of aCARD11 variants in mature mouse B cells promoted plasmacytic differentiation in response to self-antigen exposure[25]. However, the impact of activating mutations on a GC reaction has not been assessed. To determine how aCARD11 impacts the response to TD antigens, we first immunized control and aCard11 mice with sheep red blood cells (SRBC) and evaluated the kinetics of the GC response. We hypothesized that aCARD11 would result in a larger and more prolonged GC response due to increased NF-κB signaling. Contrary to this prediction, we observed an altered kinetic in immunized Mb1-aCard11 vs. control mice, with the GC response reaching an earlier peak (Fig. 2-2A-C, Day 5 post immunization) followed by GC contraction as early as Day 7 (Fig. 2-2B&C). In contrast, the GC response in control animals peaked between Days 7- 10.

Consistent with our flow-based data, immunofluorescence studies revealed larger and more abundant GCs in the spleen at Day 5 in immunized Mb1-aCard11 mice (Fig. 2-2D&E, Fig. 2-S1L). Correlating with the more rapid GC contraction in Mb1-aCard11 mice, we observed an earlier expansion of the splenic plasma cell (PC; $B220^{-}CD138^{+}$) compartment at Day 7 relative to controls (Fig. 2-2F-H). Further, in contrast to controls, the splenic PC compartment was nearly absent by Day 10 in Mb1-aCard11, without evidence for increased PC migration to the bone marrow (data not shown). While serum IgM antibody titers increased with a similar kinetic post-immunization in Mb1-aCard11 and control animals, total IgM levels were reduced at baseline (Fig. 2-1J & 2-2I) and remained lower at all time points compared to controls (Fig. 2-2I). In contrast, total IgG, IgG1 and IgG2C levels were not significantly different in Mb1-aCard11 vs. control animals (Fig. 2-2J-K, and data not shown). Together, these findings support a model wherein aCARD11 enhances GC generation and coordinately promotes terminal differentiation into short-lived PCs.

GC B cell intrinsic aCARD11 expression is sufficient to alter the kinetics of the GC response

The altered kinetics of TD GC response in Mb1-aCard11 mice might be caused by the increased development of FM B cells and/or pre-activation of B cells in this strain. To specifically assess the impact of aCARD11 within an ongoing GC response, we crossed ROSA-aCard11 mice to the Cγ1-Cre strain. In the resulting model (Cγ1-aCard11), Cre expression is induced by transcription of the IgG1 constant region gene (Cγ1)[51], limiting transgene expression to a subset of B cells that have class-switched. Cγ1-aCard11 mice lacked GFP expression within the splenic non-GC B cells (Fig. 2-3A). Unlike Mb1-aCard11 animals, Cγ1-aCard11 mice show no difference in peritoneal B cell subsets (Fig. 2-S2A-C) and have comparable serum IgM and IgG titers at baseline (Fig. 2-S2D&E). Upon immunization with SRBC, GFP expression was readily detected in splenic GC B cells and PCs (PCs) (Fig. 2-3A, left and right panels, respectively), consistent with Cγ1-Cre induction in response to immunization. Immunization with SRBC led to robust GC response in both control and Cγ1-aCard11 mice. However, at Day 7, Cγ1-aCard11 mice exhibited a more rapid contraction of the GC response relative to that observed in controls (Fig. 2-3B). In parallel with more rapid GC contraction, we observed an increase in the PC compartment at Day 7 post-

immunization in Cγ1-aCard11 relative to control mice (Fig. 2-3C). While these findings mirrored the rapid contraction of the GC and earlier PC production present in Mb1-aCard11 mice, the Cγ1-aCard11 model did not reproduce the early peak in the GC; likely due to the requirement for class switching to trigger initial aCARD11 expression.

To determine whether the PCs generated in aCard11 mice were capable of producing antigen-specific antibodies, we immunized Cγ1-aCard11 and control mice with the TD antigen NP-CGG in order to track the NP-specific antibody response. Despite the absence of GC B cells at 12 dpi, Cγ1-aCard11 mice exhibited increased serum titers for both high- and low-affinity NP-specific total IgG and IgG1 (Fig. 2-3D&E). Together, these data suggest that aCARD11 promotes rapid terminal differentiation of B cells into PCs, including antigen-specific PCs, following antigen encounter. These findings also demonstrate that GC B cell intrinsic expression of aCARD11 is sufficient to alter the kinetic of the GC response to TD antigens.

aCARD11 enhances cycling in vivo and skews GC polarization

We next tested whether the earlier peak of the GC response in Mb1-aCard11 animals reflected enhanced cycling driven by aCARD11. Previous studies have shown that activating mutations in CARD11 enhance proliferation *in vitro*[22] and can switch the response to self-antigen recognition *in vivo* from antigen-induced cell death to proliferation[25]. To determine whether GC B cells expressing aCARD11 exhibit higher rates of proliferation, we immunized control and Mb1-aCard11 mice with SRBC and, at one hour prior to sacrifice at the peak of the GC response (Day 5 post immunization), mice were injected intraperitoneally with the thymidine analog, ethynyl deoxyuridine (EdU). We observed a significant increase in the frequency of EdU^+ cells within both the GC and PC compartments in Mb1-aCard11 compared to control mice (Fig. 2-4A-C). In contrast, we observed no difference in EdU incorporation in pro/pre B cells (IgM^-B220^+, Fig. 2-S3A&B) and no difference in EdU incorporation in non-GC B cells (Fig. 2-S3C, $B220^+CD95^-CD38^+$). Thus, the increased cycling observed in aCARD11 GCs and PCs is unlikely the result of changes prior to immunization or GC entry. Together, these data demonstrate that aCARD11 significantly enhances both GC B cell and plasmablast proliferation.

Next, we assessed whether the enhanced cell cycling in aCARD11 GC B cells correlated with alterations in the polarization of the GC response. The GC is polarized into two zones: light zone (LZ) and dark zone (DZ). The DZ is the proliferative compartment within the GC[1]. Using the SRBC immunization model, we observed ~2:1 ratio of DZ ($CD86^{lo}CXCR4^{hi}$) to LZ ($CD86^{hi}CXCR4^{lo}$) GC B cells in control mice at Day 5 post immunization. In Mb1-aCard11 mice, GC B cells exhibited exaggerated DZ skewing yielding an ~3:1 DZ to LZ ratio (Fig. 2-4D&E). One possible explanation for this finding includes an increase in naïve B cells that enter the GC response (perhaps due to a lower activation threshold). In contrast to this idea, however, we also observed an increased frequency of $BrdU^+$ GC B cells (bromodeoxyuridine, Fig. 2-S3D) and exaggerated DZ skewing (~3:1 ratio –Fig. 2-S3E) in the Cγ1-aCard11. We queried whether the enhanced cycling we observed was restricted to the DZ, as that could account for the exaggerated skewing. Rather than a majority of EdU^+ cells restricted to the DZ, we observed enhanced cycling in both DZ and LZ cells at similar proportions within Mb1-aCard11 mice compared to controls (Fig. 2-4F&G). This finding implies that aCARD11 causes dysregulated cycling throughout the GC.

We also assessed the transcriptional program of GC B cells in the Mb1-aCard11 model. Activation induced cytidine deaminase (AID) promotes both SHM and CSR in GC B cells and DZ B cells have increased AID expression compared to LZ B cells[57]. Mb1-aCard11 GC B cells ($B220^+CD95^{hi}PNA^{hi}$) expressed greater levels of AID compared to control GC B cells at the peak of the GC response (Fig. 2-4H&I), consistent with skewing of the GC towards a DZ phenotype. AID expression is regulated by FOXO1, a critical transcriptional regulator of the DZ program. FOXO1 deletion in GC B cells results in a loss of the DZ[5]. Surprisingly, we observed decreased expression of FOXO1 within total GC B cells ($B220^+CD95^{hi}PNA^{hi}$) in Mb1-aCard11 mice at the peak of the GC response (Fig. 2-S3F&G). Decreased FOXO1 may indicate enhanced PI3K signaling since Akt, downstream of PI3K, phosphorylates FOXO1 resulting in nuclear export and increased proteasomal degradation[58]. However, GC B cell restricted expression of constitutively active PI3K results in a loss of the DZ, reminiscent of GC B cell intrinsic deletion of FOXO1[5, 39]. In summary, expression of aCARD11 in GC B cells increases their proliferation and promotes a DZ phenotype.

GC B cells expressing aCARD11 demonstrate elevated mTORC1 signaling

GC-specific, hyper-activation of mechanistic target of rapamycin (mTOR) results in DZ skewing and larger GC cell size[59], reminiscent of the phenotype in the Mb1- and Cγ1-aCard11 models. mTORC1 signaling, triggered in response to positive selection within the LZ, yields increased biomass that permits GC B cells to undergo subsequent rounds of proliferation within the DZ. mTORC1 hyperactivation has also been shown to drive plasma cell development when TSC1 is deleted in mature B cells[60]. GC B cells are more metabolically active, correlating with increased mTORC1 activity, cell size, glucose uptake, and mitochondrial biomass[61]. Using forward scatter (FSC) as a measure of cell size, we observed a significant increase in the size of GC B cells and PCs in both Mb1-aCard11 (Fig. 2-5A) and Cγ1-aCard11 (Fig. 2-S4A&C) mice compared to controls (at Day 5 post-immunization with SRBC). Further dissection of the GC into DZ vs LZ cells showed that aCARD11 expressing cells in the DZ trend towards a larger FSC than their control counterparts while LZ cells are significantly larger than control LZ cells (Fig. 2-5B & Fig. 2-S4B).

To explicitly determine if mTORC1 signaling is increased in this strain, we quantified phosphorylation of ribosomal protein S6 and eukaryotic translation initiation factor 4E-binding protein 1 (4E-BP1), major downstream targets of the mTORC1 pathway[62]. Using flow cytometry, we observed a significant increase in pS6 and p4E-BP1 in GC B cells ($B220^{+}CD95^{hi}CD38^{-}$) in Mb1-aCard11 mice compared to controls (Fig. 2-5C-F). Immunoblotting of total splenic B cells (including naïve and GC B cells, plasmablasts and PCs) from immunized mice further supported our findings, with evidence for increased pS6 in Mb1-aCard11 mice (Fig. 2-S4D&E). As anticipated, we also observed a trend towards a decrease in total basal IκBα in unimmunized Mb1-aCard11 B cells compared to controls ($Mb1^{Cre/+}$, Fig. 2-S4D&E), consistent with enhanced NF-κB activation[19]. Segregation of GC B cells into DZ vs LZ cells, demonstrated increased pS6 and p4E-BP1 in both populations in Mb1-aCard11 mice compared to controls (Fig. 2-5G-J). Thus, the enhanced mTORC1 signature observed is not solely due to increased DZ skewing in Mb1-aCard11 mice. The increased pS6 and p4E-BP1 in the aCard11 GC B cells is potentially a result of their increased biomass. However, it remains unclear whether the increased biomass precedes elevated mTORC1 signaling, or, conversely, is a result of enhanced mTORC1

signaling. Together, these data indicate that aCARD11 expression enhances NF-κB signals and, directly or indirectly, potentiates mTORC1 signaling, in response to TD antigens.

Cells overexpressing aCARD11 manifest an NF-κB -independent elevation in mTORC1 signaling

To further assess the impact of aCARD11 on signaling, we next analyzed basal signaling differences in a GC B cell like (GCB)-DLBCL line, OCI-Ly7, whose survival is not dependent on CARD11. This GCB-DLBCL line was transduced with lentiviral vectors expressing either flag-tagged wildtype (WT) CARD11 or CARD11-L251P and a cis-linked GFP marker (Fig. 2-6A). Using cells closely matched for GFP expression and viral copy number, we observed increased pS6 in aCARD11 expressing cells (Fig. 2-6B&C). Of note, consistent with increased turnover of aCARD11[55], CARD11 protein levels were significantly reduced in CARD11-L251P transduced samples (data not shown). Consistent with this finding, aCARD11 cells exhibited enhanced NF-κB signaling as assessed using an NF-κB reporter and by immunoblotting, demonstrating increased phospho-p65 and decreased total IκBα (Fig. 2-6B-D). To determine whether the enhanced mTORC1 signaling characteristic of CARD11-L251P expressing cells is dependent on NF-κB signaling, CARD11-L251P expressing cells were treated with the IKK-2 inhibitor, MLN120B[63]. While MLN120B treatment significantly reduced NF-κB signaling, measured by diminished NF-κB driven luciferase production (Fig. 2-6D), we observed no difference in pS6 levels post treatment (Fig. 2-6E), unlike treatment with rapamycin. Our findings demonstrate that enhanced mTORC1 signaling in CARD11-L251P expressing cells is NF-κB -independent, however, whether mTORC1 signaling is directly or indirectly driven by oncogenic CARD11 remains unclear.

Activation of mTORC1 requires mTORC1 recruitment to the lysosome, which is induced by amino acid sensing. Patients with hypomorphic, dominant-negative mutations in CARD11 display decreased pS6, as well as diminished expression of amino acid transporters[14]. CD98 is a heterodimer comprised of a heavy chain (*Slc3a2*) covalently linked to one of several light chains (e.g. LAT1/*Slc7a5* or LAT2/*Slc7a8*), that function as amino acid transporters[64]. Aside from amino acid transport, CD98 plays a role in cell adhesion, growth and survival[65]. To determine whether CD98 expression is altered in aCARD11 expressing cells, we analyzed GC B cells in control and Mb1-aCard11 mice at 5 days post immunization with SRBCs. We observed a significant increase in surface CD98 expression on aCard11

GC B cells compared to controls (Fig. 2-6F&G). Analysis of DZ and LZ cells demonstrated that the DZ displays greater expression of CD98 (Fig. 2-6F&G). Increased expression of CD98 in DZ cells in Mb1-aCard11 mice may support the observed increase in cycling, allowing GC B cells to better compete in the setting of limited nutrient availability. However, our data cannot distinguish whether the increase in CD98 facilitates or merely reflects the observed exaggerated DZ skewing.

aCARD11 signaling likely enhances class switch recombination

Pharmacological inhibition and murine models of B cell intrinsic deletion of *Rictor* or *Raptor*, demonstrate the importance of the mTORC1/pS6 axis in promoting class switch recombination (CSR). Treatment of B cells with ATP-competitive mTOR kinase inhibitors (TOR-KIs) that targeted both mTORC1/2, or conditional deletion of Rictor, a key component of the mTORC2 complex, resulted in enhanced CSR. In contrast, inhibition of mTORC1 by rapamycin or B cell specific deletion of Raptor, required for mTORC1 function, reduced CSR and plasmablast formation[66]. Mass-cytometry (CyTOF) has demonstrated that GC B cells with the highest levels of pS6 also express the highest levels of IgG1[61]. These data support a model wherein cells with increased mTORC1 activity are selected to undergo CSR. Our findings indicate that aCARD11 alters the kinetic of the GC response and GC B cells expressing aCARD11 display enhanced mTORC1 signaling. We used single-cell RNA-sequencing (scRNA-seq) to interrogate the impact of aCARD11 on the transcriptome of B cells in response to immunization. Total B cells and PCs were isolated from Mb1-aCard11 and control ($Mb1^{Cre/+}$) mice at Day 5 post-immunization with SRBCs, and processed for scRNA-seq using the Chromium product suite by 10x Genomics[53]. Cell Ranger (10x Genomics) and Monocle 2[54] were used for data analysis. We obtained single-cell expression profiles for a total of 1954 cells. Unsupervised clustering was performed to identify and remove non-B lineage cells (Fig. 2-S5A), as well as to separate B cells into non-activated vs GC B cells and plasmablasts (PBs, Fig. 2-7A). The GC cluster was characterized by high transcript levels of AID (AICDA –Fig. 2-S5B) and genes associated with cell cycle progression and DNA-repair pathways previously shown to be upregulated in GC B cells[1]. The plasmablast cluster was characterized by high transcript levels of Xbp1 (Fig. 2-5C), a transcription factor specifically upregulated in antibody-secreting cells (ASCs)[67]. Consistent with our flow and immunohistochemistry findings, Mb1-aCard11 mice were

found to have increased GC and plasmablast compartments (Fig. 2-7B). Differential gene expression analysis between control and aCARD11 cells revealed membrane-bound and secreted BCR isotypes amongst the most significantly differentially expressed genes within the GC and PB compartments. The GC B cells in the aCARD11 samples showed an increase in membrane-bound total IgG transcripts with a concomitant decrease in membrane-bound IgM, compared with controls (Fig. 2-7C-top &D). Similarly, within the plasmablast cluster, aCARD11 cells exhibited increased secreted IgG transcripts and decreased secreted IgM compared to control cells (Fig. 2-7C-bottom &E). aCARD11 GC B cells also showed increased secreted IgG transcript levels, suggesting that they are on their way to becoming plasmablasts, as well as decreased membrane bound IgM in the plasmablast compartment (Fig. 2-S5D&E).

To determine if CSR is altered at the protein level, we also performed FACS analysis of PCs at Day 5 post-immunization in Mb1-aCard11 and control mice to assess intracellular Ig levels and the antibody isotype being produced. Compared with control cells, PCs in Mb1-aCard11 mice exhibited an increased proportion of in $IgM^{-}IgG1^{-}$ PCs ($B220^{-}CD138^{+}$) following immunization (Fig. 2-S5F&G). These "double-negative" PCs have likely switched to an IgG isotype other than IgG1, as there is a significant decrease in $IgG1^{+}$ PCs as well (Fig. 2-5F&G). These findings, while not definitive, are consistent with a model whereby aCARD11 expression increases CSR during a TD immune response.

Discussion

CARD11 plays a pivotal role in B and T cell function through regulation of the antigen receptor (AgR)-NF-κB signaling axis. Expanding work has identified both germline and somatic, loss-of function (LOF) and gain-of-function (GOF) variants in *CARD11*, providing insight into human immune development and function. Germline GOF CARD11 mutations lead to an immune dysregulation disorder referred to as B cell expansion with NF-κB and T cell anergy (BENTA)[22, 68]. These patients have defects in humoral responses to some vaccines, with decreased switched memory B cells and T cell hyperresponsiveness. In contrast, somatic CARD11 GOF mutations are enriched in ABC-DLBCL, a post-GC malignancy exhibiting mutated Ig V genes and a gene expression signature that includes plasmablast genes[10].

Previous murine models of *Card11* GOF variants utilized pan-B lineage transgenic expression[27] or lentiviral expression and adoptive transfer[25] to assess the impact on developing and mature B cells, but did not assess the role of these variants in TD immune responses. In this study, we characterized the impact of an activating mutation in CARD11 on B cell development and, most notably, within the GC response. We show that B cell intrinsic expression of aCARD11 markedly alters the innate B cell compartment while exerting only limited impact on the naïve B2 B cell compartments. B cell-intrinsic aCARD11 expression substantially impacts GC dynamics leading to more rapid GC formation and resolution with enhanced terminal differentiation. aCARD11 expressing GC B cells exhibit increased cycling and DZ skewing. Surprisingly, in addition to increased NF-κB signals, aCARD11 GC B cells exhibit enhanced mTORC1 signaling. Consistent with these findings, a DLBCL cell line overexpressing CARD11-L251P demonstrated enhanced NF-κB and mTORC1 signaling in the absence of stimulation. Thus, aCARD11 potentially modulates multiple critical signaling pathways that uniquely alter the GC response.

Expression of aCARD11 during B cell development exerted only minimal impact on BM and splenic B2 B cell development but lead to an unexpected impact on the innate B cell compartment. aCARD11 expression had no appreciable impact on BM B cell development or the number or proportion of splenic transitional B cells. Mb1-aCard11 mice, however, exhibited a modest increase in the proportion and number of FM B cells, a change that accounted for a moderate increase in total B2 cell numbers. In parallel, these animals exhibited a decreased frequency of MZ B cells. BENTA patients exhibit polyclonal expansion of immature, transitional, and naïve mature B cells[23]. In contrast, aCARD11 expression led to loss of the peritoneal B1 compartment with near absence of the B1a B cell subset and marked reduction in B1b B cell numbers. Loss of these innate-like B cell populations correlated with decreased serum IgM in unimmunized Mb1-aCard11 mice. While not answered in our studies, a range of mechanisms might account for these findings. One possibility is that aCARD11 promotes terminal differentiation of B1 B cells, similar to the enhanced PC response observed following TD immunization (see below). However, the combined reduction of both B1 B cells and IgM argues against this idea. Alternatively, aCARD11 signals may impact B lineage fate at an early stage of B1 B cell development or limit resting and/or

activated B1 cell survival. Notably, previous studies in *Card11*$^{-/-}$ and *Bcl10*$^{-/-}$ mice[8, 69] reported defects in both the MZ and B1 compartments, suggesting that signals mediated by the CBM complex are required for development and/or maintenance of these populations. The parallel findings in *Card11* loss- vs gain-of-function mice, suggest that precise tuning of one or more CARD11 dependent signals (NF-κB , JNK and/or mTORC1; see also below) is required for B1 development or maintenance and that perturbation in either direction promotes loss of innate B cells. Of note, consistent with our data, IgM levels are consistently reduced in human subjects with BENTA[22, 68]. BENTA patients exhibit impaired responses to T-independent polysaccharide vaccines, and low serum titers to some T-cell dependent viral vaccines have been observed in some patients[23]. These defects in T-independent humoral responses parallel our findings of diminished innate B cell populations and decreased IgM titers in the Mb1-aCard11 mice. The similarities between our mouse model and the BENTA phenotype may indicate that aCARD11 expression would yield dampened T-independent humoral responses in our mouse model, and will be a focus of future studies. While the B1 B cell compartment has not been evaluated in BENTA, this may be a fruitful area for future study. Defining CARD11-dependent signals essential for the B1 development or survival is likely to provide insight into the regulation of this important population.

Using two distinct, inducible B cell-intrinsic models, we show that expression of the CARD11-L251P is sufficient to alter GC dynamics. Upon immunization, aCARD11 expression promoted both accelerated GC formation and resolution. At the peak of the GC response, aCard11 mice exhibited exaggerated DZ skewing compared to controls. This change correlated with enhanced cycling and increased AID expression, increased cell biomass, enhanced pS6 and p4E-BP1 levels, and decreased FOXO1 levels illustrating a unique impact of aCARD11 on B cell intrinsic signaling. Importantly, nearly all of these observations were recapitulated in a model where aCARD11 expression was restricted to GC B cells (Cγ1-Cre), indicating that these changes are not due to a developmental impact of aCARD11 in the Mb1-cre model. GOF mutations in *CARD11* yield a spectrum of NF-κB activation[19] that support survival, proliferation, and terminal differentiation. In contrast to previous work using retroviral overexpression of aCARD11 mutants in primary murine B cells[25], CARD11 expression was comparable to endogenous levels in our knock-in model. Further, while CARD11-L251P mediates less robust constitutive NF-κB

activation compared to the L225LI mutation modeled in previous studies[19, 25, 27], our combined data demonstrate that B cell intrinsic, endogenous level CARD11-L251P expression (as would occur following mutation in somatic cells) is sufficient to drive enhanced cycling of GC DZ cells.

In addition to its impact on DZ cells, aCARD11 expressing LZ cells are likely more responsive to AgR- and, potentially, to costimulatory or cytokine signals that mediate activation and promote differentiation, GC exit and GC dissolution. NF-κB signaling in B cells promotes IRF4 and Blimp1 expression leading to terminal differentiation. Consistent with this idea, both B cell-intrinsic GC models revealed a major impact on the rate of PC generation in response to immunization. Cγ1-aCard11 and Mb1-aCard11 animals exhibited a ~6- and 8-fold increase in splenic PCs, respectively. PCs in the Mb1-aCard11 model exhibited enhanced cycling and cell biomass was increased in both models at the peak of the GC response. Cγ1-aCard11 animals also exhibited an increase in antigen-specific IgG and IgG1 at 12 days post-immunization. These observations are consistent with previous work showing that GOF mutations in *CARD11* promote proliferation and plasmacytic differentiation[25]. Similarly, expression of CARD11-L225LI, using a similar Rosa26 transgenic model[27], lead to diffuse organ infiltration of plasmacytic cells and early mortality. In contrast to aCARD11, B cells expressing constitutively active IKKβ exhibit increased proliferation *in vitro* but fail to persist *in vivo* in the presence of self-antigen. Similarly, GC B cell-restricted expression of constitutively active IKK2 (IKK^{CA})[70] did not significantly alter the GC response, antibody levels or PC formation. The phenotypic differences observed across the aCARD11 vs. the IKK^{CA} models supports the idea that aCARD11 can influence B cell fate via both NF-κB -dependent and -independent signals.

Consistent with the role for aCARD11 in enhanced NF-κB signaling[19, 25, 27], CARD11-L251P expressing murine B cells (Mb1-aCard11 model) and DLBCL lines exhibited reduced IκBα levels. Importantly, in the context of the GC, we demonstrate that cells expressing aCARD11 have additional alterations in signals critical for GC function including, most notably, mTORC1. Our findings demonstrate that CARD11-L251P may directly, or indirectly, promote enhanced mTORC1 signaling as indicated by increased DZ skewing, biomass and pS6 and p4E-BP1 levels in murine GC B cells and elevated basal pS6 in a CARD11-L251P expressing GCB-DLBCL cell line. mTORC1 signals play a critical role in GC

biology. B cell intrinsic deletion of Raptor, a key adaptor for the mTORC1 complex, blocks PC differentiation and antibody secretion[71]. Similarly, hypomorphic mTOR variants inhibit humoral responses to antigen[72]. Raptor deletion at the peak of the GC, or treatment with rapamycin after GC initiation, results in premature collapse of the GC[71]. In contrast, hyperactive mTORC1 skews GC B cells towards a DZ phenotype[59]. In adoptive transfer models, however, mTORC1 hyperactive GC B cells are outcompeted at later time-points demonstrating the importance of coordinate regulation of this pathway. We specifically observed increased cell biomass and pS6 and p4E-BP1 levels were in aCARD11 GC B cells and plasma cells following immunization (and not in non-GC B cells). The GC comprises a hypoxic, nutrient deprived microenvironment due, in part, to the rapid proliferation of activated B cells[61, 73]. The altered GC response in the animal models described here suggests that aCARD11 may be particularly effective in promoting GC expansion in this “stressful” environment. While not tested here, aCARD11 may also facilitate this process by lowering the BCR activation threshold, allowing for a more efficient positive selection by T follicular helper cells or FDC-delivered antigen in the LZ. In this context, aCARD11 expressing B cells might also gain increased sensitivity to co-receptor signals and amino acid sensing pathways that mediate mTORC1 activation.

How CARD11 links AgR signaling to mTORC1 remains unclear. Our findings suggest there is a link between CARD11 and mTORC1 signaling in GC B cells, an idea that is consistent with, and expands upon, earlier *in vitro* studies in T cell lines and primary T cells. Studies in $CD4^+$ T cells support the idea that IKK activity is not required for CARD11-dependent mTORC1 induction[16, 74]. Work using CARD11-deficient Jurkat T cells and mouse $CD4^+$ T cells reported decreased pS6 levels in response to CD3/CD28 stimulation[16]. One model proposes that CARD11 complexes with MALT1 to activate mTORC1, independent of Bcl10. Consistent with this idea, the paracaspase activity of MALT1 was required for mTORC1 induction whereas blocking Bcl-10 or IKK2 had no impact on pS6 levels after CD3/CD28 stimulation. In contrast, another study showed a partial, impairment in mTORC1 in Bcl10-deficient naïve $CD4^+$ T cells after TCR/CD28 stimulation[74] perhaps reflecting differences in culture or stimulation conditions[75]. Our studies of CARD11-L251P expressing DLBCL cell lines support a model in which mTORC1 signaling is independent of NF-κB signaling. It has been postulated that CARD11 modulates a

novel signaling-axis involved in amino acid sensing that cooperates with PI3K/AKT to activate mTORC1. Diminished pS6 correlates with decreased expression of ASCT2 and CD98 in $CD4^{+}$T cells from patients with dominant negative CARD11 mutations[14]. Conversely, our data suggest that aCARD11 enhances this signaling-axis and plays a pivotal role in B cells, particularly during a GC response. While *Slc1a5*$^{-/-}$ ($ASCT2^{-/-}$) mice do not exhibit defects in TD GC responses[76], B cell intrinsic deletion of CD98 heavy chain (*Slc3a5*$^{flox/flox}$*CD19*$^{Cre/+}$) impairs antibody responses and plasma cell formation[64]. CD98 functions in both integrin signaling and amino acid transport[77, 78]. However, the impact these distinct functions *in vivo* has not been deconvoluted. CD98 (*Slc3a2-Slc7a5 heterodimer*) acts as a bidirectional transporter which exports intracellular L-glutamine in exchange for the import of L-leucine and activates mTORC1[77]. CD98 is upregulated upon B cell activation and confers a selective advantage to GC B cells[64]. The increase in CD98 expression on aCARD11 GC B cells suggests that they are likely more responsive to amino acid sensing, resulting in heightened mTORC1 signals. Alternatively, aCARD11 expression could sensitize cells to integrin-mediated signals, which would support enhanced cycling and survival. Thus, while the precise link(s) between CARD11 and mTORC1 in B cells remains to be elucidated, our data in association with previous findings in T cells, strongly supports a model in which altered mTORC1 signaling, due to enhanced amino acid sensing and/or NF-κB -independent mTORC1 activation downstream of CARD11, functions in conjunction with enhanced NF-κB signals to alter the GC response.

Multiple types of B cell malignancies that arise from GC and post-GC B cells exhibit GOF mutations in CARD11 including diffuse large-, marginal zone-, mantle cell- and follicular-B cell lymphomas and, less commonly, also Waldenstrom macroglobulinemia, lymphoplasmacytic lymphoma, and primary central nervous system lymphoma[10, 23, 79-81]. aCARD11 GC B cells exhibited increased AID expression and increased expression of switched transcripts and an increase in the secreted form of switched transcripts within plasmablasts by ssRNA-seq analysis. While Mb1-aCard11 and control mice displayed equivalent IgG and IgG1 levels after SRBC immunization, PCs in aCARD11 animals were predominantly $IgM^{-}IgG1^{-}$ at day 5 post-immunization, consistent with increased class switching. Previous work indicates that CSR to IgG1 drives GC B cells towards a plasma cell fate[82], suggesting that enhanced class switching in aCARD11 expressing cells may similarly increase plasma cell differentiation. Both enhanced CSR and plasma cell differentiation may be due to enhanced mTORC1 signaling in aCARD11 expressing

GC B, as mTORC1 promotes both CSR and plasma cell differentiation[66, 83]. These events likely function in concert with additional mutations acquired during the GC response to promote lymphomagenesis in GC-derived B cells. ABC-DLBCLs express high levels of AID and heavily mutated IgH genes and a requirement for AID activity during oncogenesis has been demonstrated in multiple models[84, 85]. In our aCard11 mice, overcoming the premature collapse of the GC may be required to allow additional oncogenic hits to be acquired, promoting lymphomagenesis. DLBCLs exhibit inactivation of *BLIMP1/PRDM1* at levels >50%[86], thus modeling aCARD11 signaling in the context of a block in terminal differentiation to study the impact of these coordinating oncogenic events in promoting lymphomagenesis is a line of inquiry we are currently pursuing.

In summary, we demonstrate that aCARD11 expression markedly alters GC dynamics and cell fate decisions. Disease-associated, activating CARD11 mutations have previously been shown to exhibit a spectrum of NF-κB activation. Our data build upon those findings indicating that aCARD11 may potentiate mTORC1 signaling. Many ABC-DLBCLs (~50%) are refractory to current therapeutic regimens and it has been shown that follicular lymphomas[87] and mantle cell lymphomas expressing aCARD11 are resistant to ibrutinib treatment[81, 88]. Our combined findings suggest that aCARD11 contributes to resistance in aggressive lymphomas via enhancement of these distinct signaling programs and that mTORC1 inhibitors should be explored as a potential treatment option in tumors expressing aCARD11.

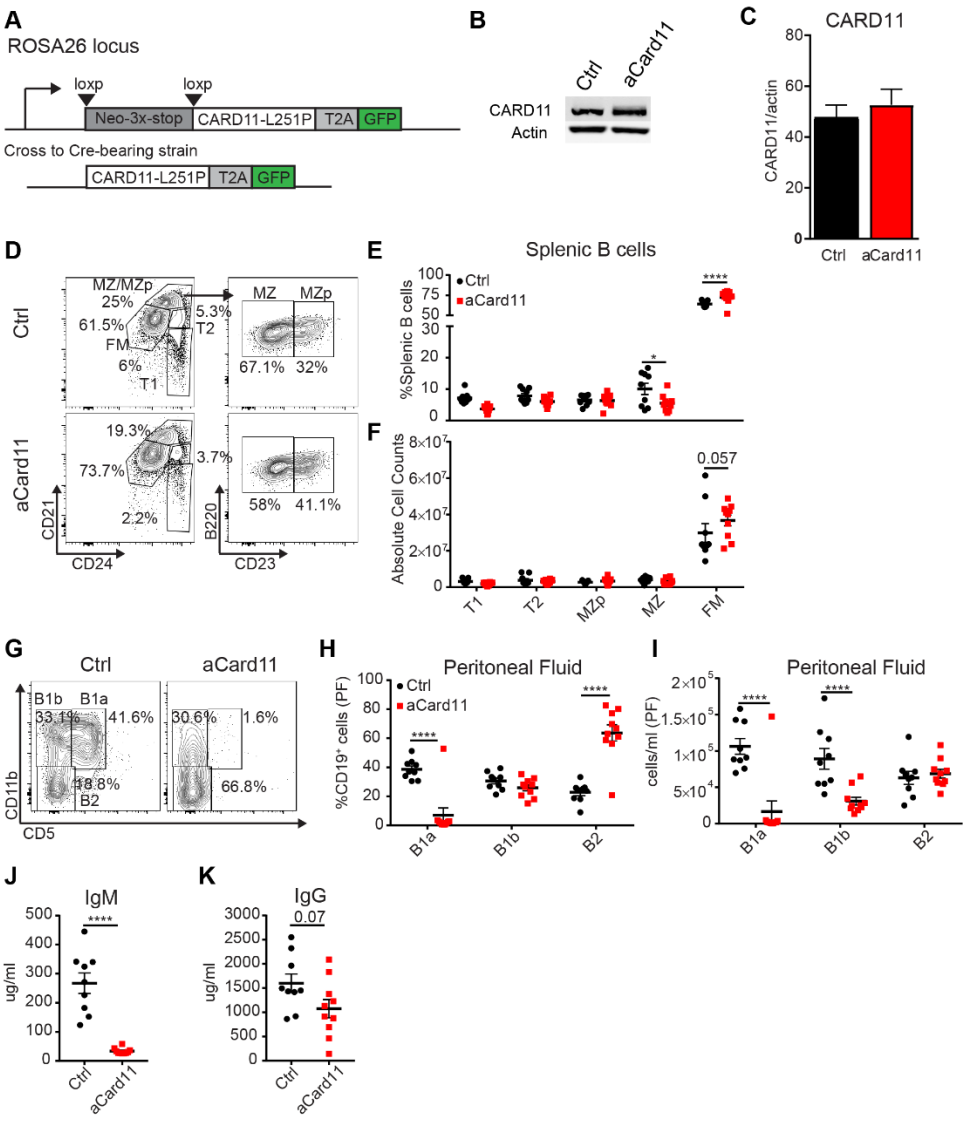

Figure 1-2. B lineage aCARD11 expression leads to modest alterations in mature B2 B cells but near absence of B1 B cells. A. Schematic showing activated mouse CARD11 (CARD11-L251P) with a self-cleaving T2A-linked GFP reporter in the *Rosa26* locus. **B.** Representative immunoblot of CARD11 levels in naïve B cells in Ctrl and Mb1-Cre-aCard11 mice. **C**. Quantification of CARD11 levels showing data from 2 independent experiments with N=5 Ctrls & 7 Mb1-aCard11 mice. **D**. Representative flow plots of splenic B cell subsets with gating schema to identify B cell subsets: early transitional, T1 ($B220^{+}CD24^{+}CD21^{lo}$), late transitional, T2 ($B220^{+}CD24^{+}CD21^{int}$), marginal zone precursor, MZp ($B220^{+}CD24^{+}CD21^{hi}CD23^{+}$), marginal zone, MZ ($B220^{+}CD24^{+}CD21^{hi}CD23^{-}$), and follicular mature, FM ($B220^{+}CD24^{int}CD21^{int}$) B cells. **E**. Frequency and **F**. Absolute number of B cell subsets. Black: Ctrl mice - animals lacking expression of the aCard11 transgene. Red: Mb1-aCard11 mice - homozygous for the aCard11 transgene and heterozygous for Mb1-Cre. **G**. Representative flow plots of B cell subsets in peritoneal fluid: B1a ($CD19^{+}CD11b^{+}CD5^{+}$), B1b ($CD19^{+}CD11b^{+}CD5^{-}$), and B2 ($CD19^{+}CD11b^{-}CD5^{-}$). **H**. Frequency and **I**. Absolute number of peritoneal B cell subsets (per mL of peritoneal fluid). Significance defined as P≤ 0.05 by 2-way ANOVA. **J**. IgM and **K.** IgG serum titers. J-K: Significance defined as P≤ 0.05 by unpaired t-test. D-K: Data from 2 independent experiments: N=9 Ctrl mice, N=10 Mb1-aCard11 mice at ~12 wks of age.

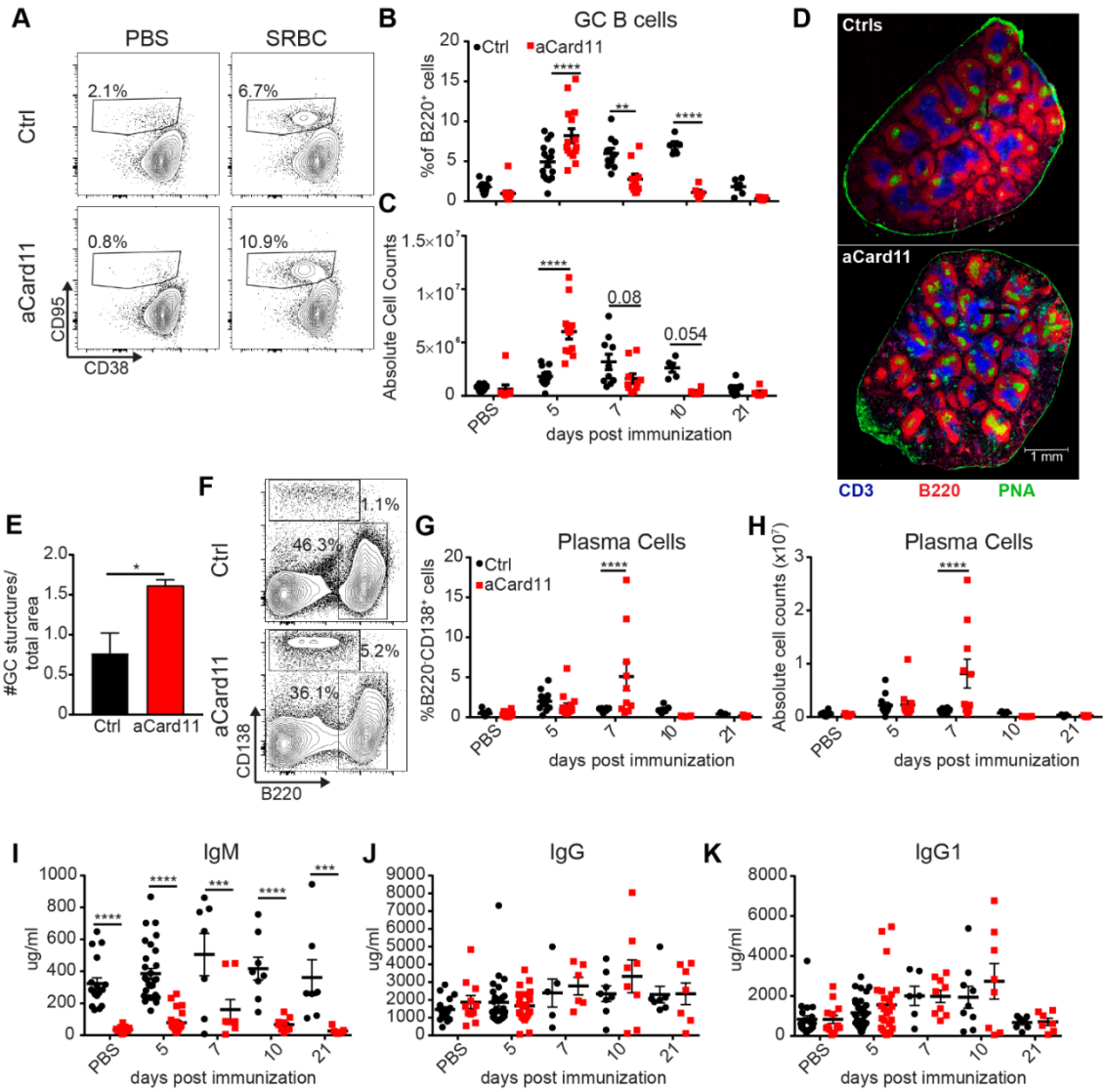

Figure 2-2. B cell intrinsic aCARD11 expression alters the kinetics of the GC response. Ctrl (Cre-negative littermates & $Mb1^{Cre/+}$ mice) and Mb1-aCard11 mice (homozygous for aCard11 transgene) were immunized as indicated with either PBS or sheep red blood cells (SRBC). **A**. Representative flow plots of splenic GC ($B220^{+}CD95^{hi}CD38^{lo}$) B cells at 5 days post immunization (dpi). Top panels: Ctrl, bottom panels: Mb1-aCard11 mice. **B**. Frequency and **C**. Absolute number of GC B cells post immunization at indicated time points. **D**. Representative splenic tissue sections in Ctrl (littermate controls) and Mb1-aCard11 mice at 5dpi. Blue: anti-CD3, Red: anti-B220, and Green: PNA. **E**. Number of germinal centers (PNA^{+} foci) normalized to total area (mm^2) of splenic tissue section. **F**. Representative flow plots of PCs ($B220^{-}CD138^{+}$) at 5dpi. Top panel: Ctrl, bottom panel: Mb1-aCard11 mice. E&F: Data representative of 5 ctrl and 5 Mb1-aCard11 mice 5dpi with SRBCs from 3 independent experiments. **G**. Frequency and **H**. Absolute number of PCs post immunization. **I**. IgM, **J.** IgG, **K**. IgG1 serum titers at Days 5, 7, 10, and 21 post-immunization. Significance defined as P≤ 0.05 by 2-way ANOVA. Data shown in A-C&F-K include: PBS immunization: 13 ctrls, 12 Mb1-aCard11; SRBC immunization – Day 5: 15 ctrls, 15 Mb1-aCard11; Day 7: 10 ctrls, 10 Mb1-aCard11; Day 10: 5 ctrls, 6 Mb1-aCard11; Day 21: 7 ctrls, 7 Mb1-aCard11. Data for each timepoint is representative of at least 2 independent experiments.

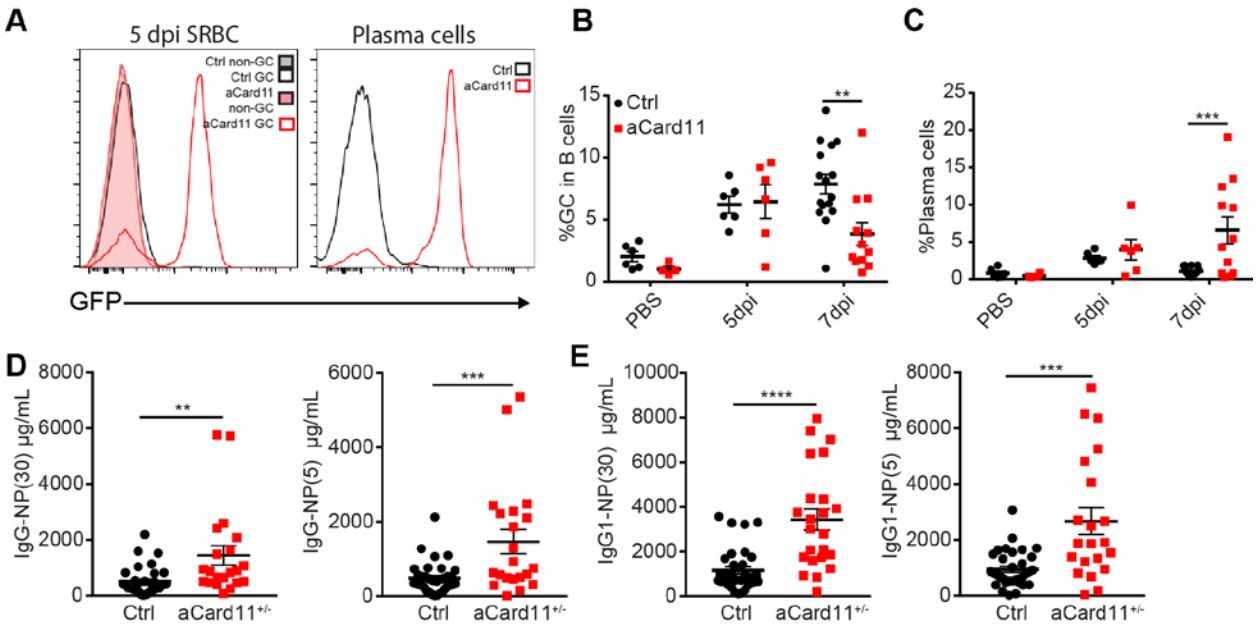

Figure 2-3. GC B cell intrinsic aCARD11 expression induces rapid GC peak and contraction with increased terminal differentiation. A. (Right panel) GFP expression in ctrl (Cre-negative littermates) and aCard11$^{+/+}$ mice crossed to the Cγ1-Cre strain showing non-GC (B220^{+}CD95^{lo}CD38^{hi}) and GC (B220^{+}CD95^{hi}CD38^{lo}) B cells at day 5 post-immunization with SRBC. *Left panel:* filled histogram: non-GC (grey=Ctrl, pink= Cγ1-aCard11), open histogram: GC (Black=Ctrl, red= Cγ1-aCard11). *Right panel*: GFP expression in PCs (B220^{-}CD138^{+}). **B.** Percentage of splenic GC B cells in PBS controls and at Days 5 and 7 post-immunization with SRBC (P=0.001 at 7dpi). **C.** Percentage of splenic PCs post-immunization (P<0.001 at 7dpi). To measure antigen-specific antibody response, Cγ1-aCard11$^{+/-}$ and control mice (Cre-negative littermates & Cγ1$^{Cre/+}$) were injected with PBS or 50ug NP-CGG injected i.p. **D.** Low- (NP-30) and high-affinity (NP-5) NP-specific IgG serum titers. **E.** Low- and high-affinity NP-specific IgG1 serum titers. D-E: Serum titers 12 days post immunization. For panels B-E, each timepoint represents at least two independent experiments with significance defined as P<0.05 using 2-way ANOVA. P<0.05.

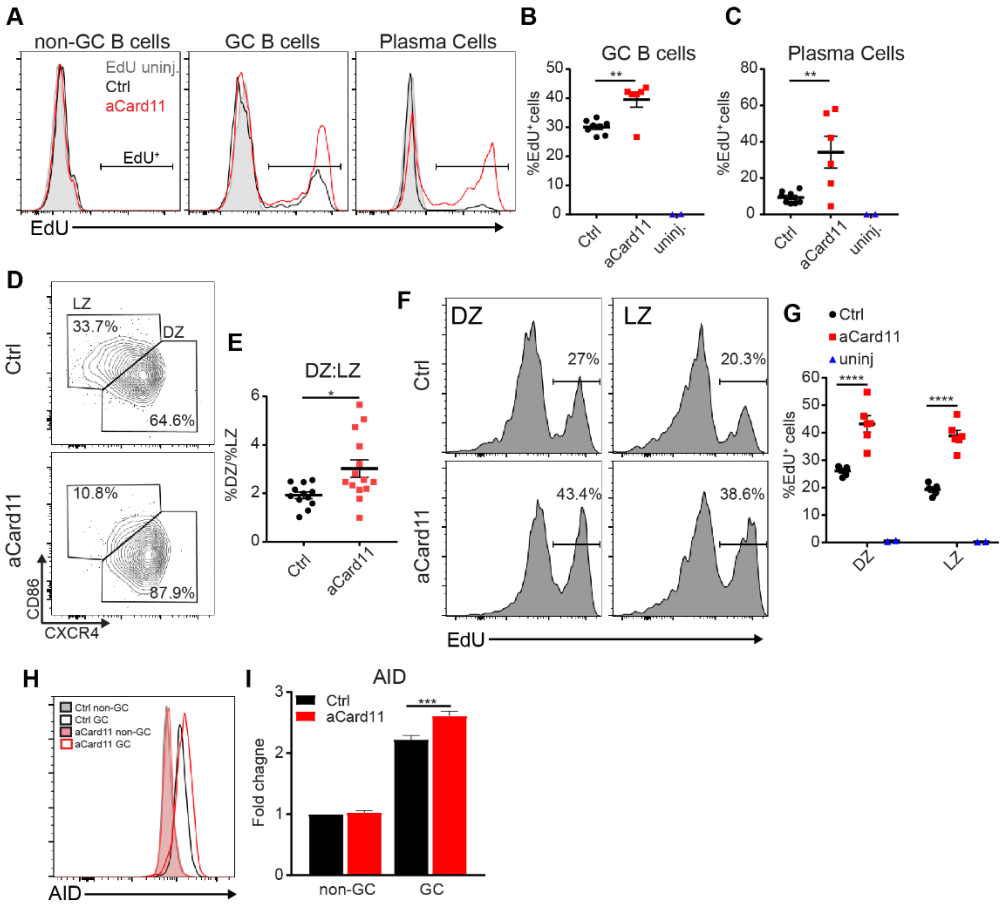

Figure 2-4. aCARD11 promotes GC B cell cycling and DZ skewing. A-C & F-G. Ctrl and Mb1-aCard11 mice were immunized with SRBC and sacrificed on day 5 post-immunization for analysis of B cell populations. In A-C, 1mg EdU was injected i.p. at 1hr prior to sacrifice. **A.** Representative histograms showing the relative proportion of EdU$^+$ cells in the non-GC (B220$^+$CD95^{lo}CD38^{hi}), GC (B220$^+$CD95^{hi}CD38^{lo}), and PC (B220$^-$CD138$^+$) compartments. **B.** Percent EdU$^+$ cells in GC B cells (P=0.002). **C.** Percent EdU$^+$ cells in PCs (P=0.007). Blue triangles: control animals without EdU labeling, 1 per experiment. A-C: Data representative of two independent experiments using 8 Ctrls and 6 Mb1-aCard11 (EdU injected) and 2 untreated animals, significance defined as P<0.05 using student's unpaired t-test. **D.** Representative flow plots of DZ (CXCR4$^+$CD86$^-$) vs LZ (CXCR4$^-$CD86$^+$) GC B cells at 5dpi. **E.** Ratio of DZ to LZ cells within the GC at 5dpi (P=0.013). D-E: Data is representative of 3 independent experiments, with 13 Ctrl and 14 Mb1-aCard11 mice, significance defined as P<0.05 using student's unpaired t-test. **F.** Representative histograms showing the relative proportion of EdU$^+$ cells in DZ (left, CD19$^+$CD95^{hi}CD38^{lo}CXCR4$^+$CD86$^-$) and LZ (right, CD19$^+$CD95^{hi}CD38^{lo}CXCR4$^-$CD86$^+$) GC B cells in littermate controls (top) and Mb1-aCard11 (bottom) mice. **G.** Percent EdU$^+$ cells in the DZ and LZ within the germinal center B cell population. Black circles: littermate controls, red squares: Mb1-aCard11, & blue triangles: animals without EdU labeling (1 per experiment). F&G: Data representative of 2 independent experiments with 5 Ctrls and 6 Mb1-aCard11 (EdU injected) and 2 untreated animals, significance defined as P<0.05 using 2-way ANOVA. **H.** AID expression in non-GC (B220$^+$CD95$^-$PNA$^-$) and GC (B220$^+$CD95$^+$PNA$^+$) B cells at 5dpi. *Filled histograms*: non-GC B cells - grey=Ctrl and pink=aCard11. *Open histograms*: GC B cells - black=Ctrl and red=aCard11. **I.** Fold change in median fluorescence intensity for AID over ctrl non-GC B cells (P<0.001). H-I: Data representative of 3 independent experiments with 13 Ctrl and 13 Mb1-aCard11 mice, significance defined as P<0.05 using 2-way ANOVA.

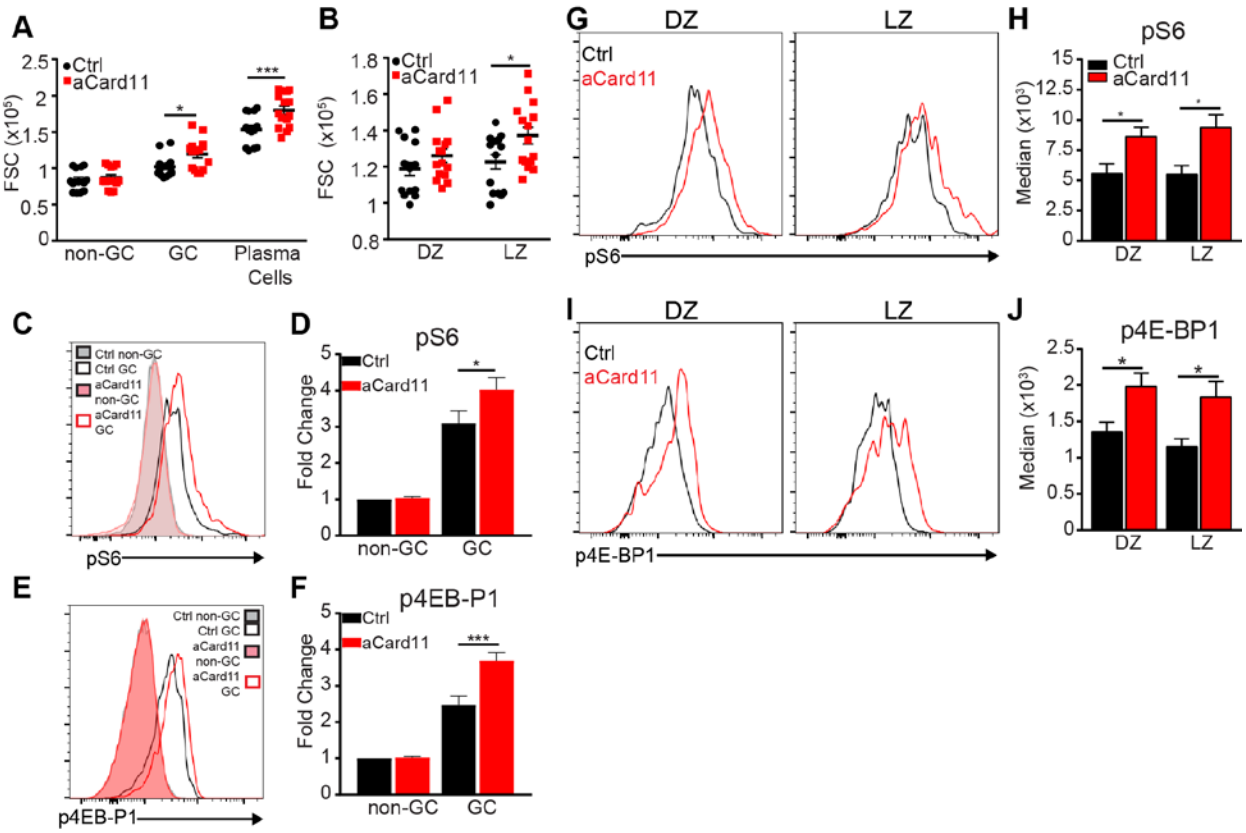

Figure 2-5. GC B cells expressing aCARD11 exhibit increased mTORC1 signaling. Ctrl and Mb1-aCard11 mice were immunized with SRBC and sacrificed on Day 5 post-immunization for analysis of B cell populations. **A**. Median forward scatter (FSC-A) of non-GC B cells ($B220^{+}CD95^{lo}CD38^{hi}$), GC B cells ($B220^{+}CD95^{hi}CD38^{lo}$) and PCs ($B220^{-}CD138^{+}$). **B**. Median forward scatter (FSC-A) of DZ ($CXCR4^{+}CD86^{-}$) and LZ ($CXCR4^{-}CD86^{+}$) GC B cells. C-D are representative of 4 independent experiments, statistics calculated by 2-way ANOVA. **C**. pS6 in non-GC ($B220^{+}CD95^{lo}CD38^{hi}$) and GC ($B220^{+}CD95^{hi}CD38^{lo}$) B cells. Filled histograms: non-GC B cells (Grey=Ctrl & pink=aCard11). Open histograms: GC B cells (black=Ctrl & red=aCard11). **D**. Fold change in pS6 median expression normalized to average pS6 median in Ctrl non-GC B cells. Data representative of 2 independent experiments, N=8 Ctrl and N=8 Mb1-aCard11 mice. Significance defined as $P<0.05$ by 2-way ANOVA, $P=0.044$. **E**. p4E-BP1 in non-GC and GC B cells. Filled histograms: non-GC B cells (Grey=Ctrl & pink=aCARD11). Open histograms: GC B cells (black=Ctrl & red=aCARD11). **F.** Fold change in p4E-BP1 median expression normalized to average p4E-BP1 median in Ctrl non-GC B cells. Data representative of 2 independent experiments, N=7 Ctrl and N=6 Mb1-aCard11 mice. Significance defined as $P<0.05$ by 2-way ANOVA, $P<0.001$. G. Representative histogram overlays pS6 within the DZ (left, $CD19^{+}CD95^{hi}CD38^{lo}CXCR4^{+}CD86^{-}$) and LZ (right, $CD19^{+}CD95^{hi}CD38^{lo}CXCR4^{-}CD86^{+}$) in Ctrl (black) and Mb1-aCard11 (red) mice. H. Median fluorescence intensity of pS6 in DZ and LZ cells in Ctrls and Mb1-aCard11 mice. I. Representative histogram overlays of p4E-BP1 in DZ and LZ in Ctrl (black) and Mb1-aCard11 (red) mice. J. Median fluorescence intensity of p4E-BP1 in DZ and LZ cells in Ctrls and Mb1-aCard11 mice. G-J: Data representative of 2 independent experiments with 5 Ctrls and 7 Mb1-aCard11 mice. Significance defined as $P<0.05$ by 2-way ANOVA.

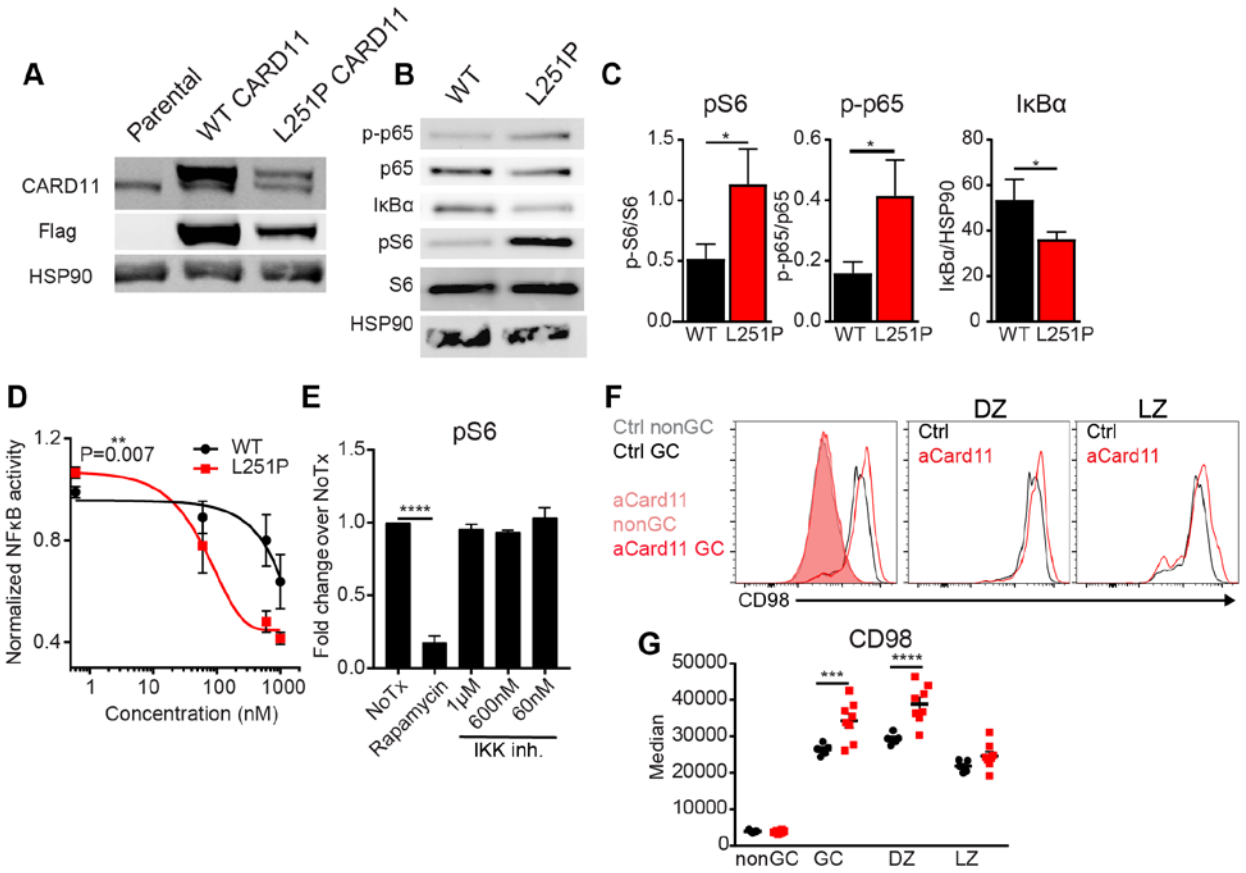

Figure 2-6. DLBCL B cells expressing aCARD11 exhibit increased pS6 independent of NFkB signaling. The GCB-DLBCL line, OCI-Ly7, was transduced with lentiviral vectors encoding murine, flag-tagged WT CARD11 or CARD11- L251P and a cis-linked GFP reporter. **A.** Immunoblot showing expression of flag-tagged CARD11 in transduced cell populations. **B.** Representative immunoblot of basal signaling in WT or CARD11-L251P cells. **C.** (Right) Quantification of signaling using imageJ of pS6 normalized to total S6 (P=0.017), p-p65 normalized to total p65 (P=0.031), and total IkBa normalized to HSP90 (P=0.041). Combined data from 3 experiments; significance defined as P<0.05 using student's paired t-test. Data in A-C are representative of 7 biological replicates. **D**. NF-κB activity (luciferase) normalized to viability (Cell Titer Glo) after treatment with different doses of IKK-2 inhibitor for 16hrs. Area under the curve is significantly different between WT and CARD11-L251P, calculated by student's paired t-test. Data represents 3 independent experiments. **E.** Fold change in pS6 median fluorescent intensity of CARD11-L251P expressing OCI-Ly7 cells normalized to untreated cells. Data representative of 3-independent experiments with 3 biological replicates. Significance defined as P<0.05 by One-way ANOVA. **F**. Representative histogram overlays of CD98 expression on (*left*) non-GC B cells (filled histograms – grey: Ctrl, pink: Mb1-aCard11, $CD19^{+}CD95^{lo}CD38^{hi}$) and GC B cells (open histograms – black: Ctrl, red: Mb1-aCard11, $CD19^{+}CD95^{hi}CD38^{lo}$); (*middle*) DZ ($CD19^{+}CD95^{hi}CD38^{lo}CXCR4^{+}CD86^{-}$) and (*right*) LZ (right, $CD19^{+}CD95^{hi}CD38^{lo}CXCR4^{-}CD86^{+}$) GC B cells in Ctrl (black) and Mb1-aCard11 (red) mice. **G**. MFI of CD98 on non-GC, GC, DZ and LZ cells in Ctrls and Mb1-aCard11 mice. F-G: Data representative of 2 independent experiments with 5 Ctrls and 7 Mb1-aCard11 mice. Significance defined as P<0.05 by 2-way ANOVA.

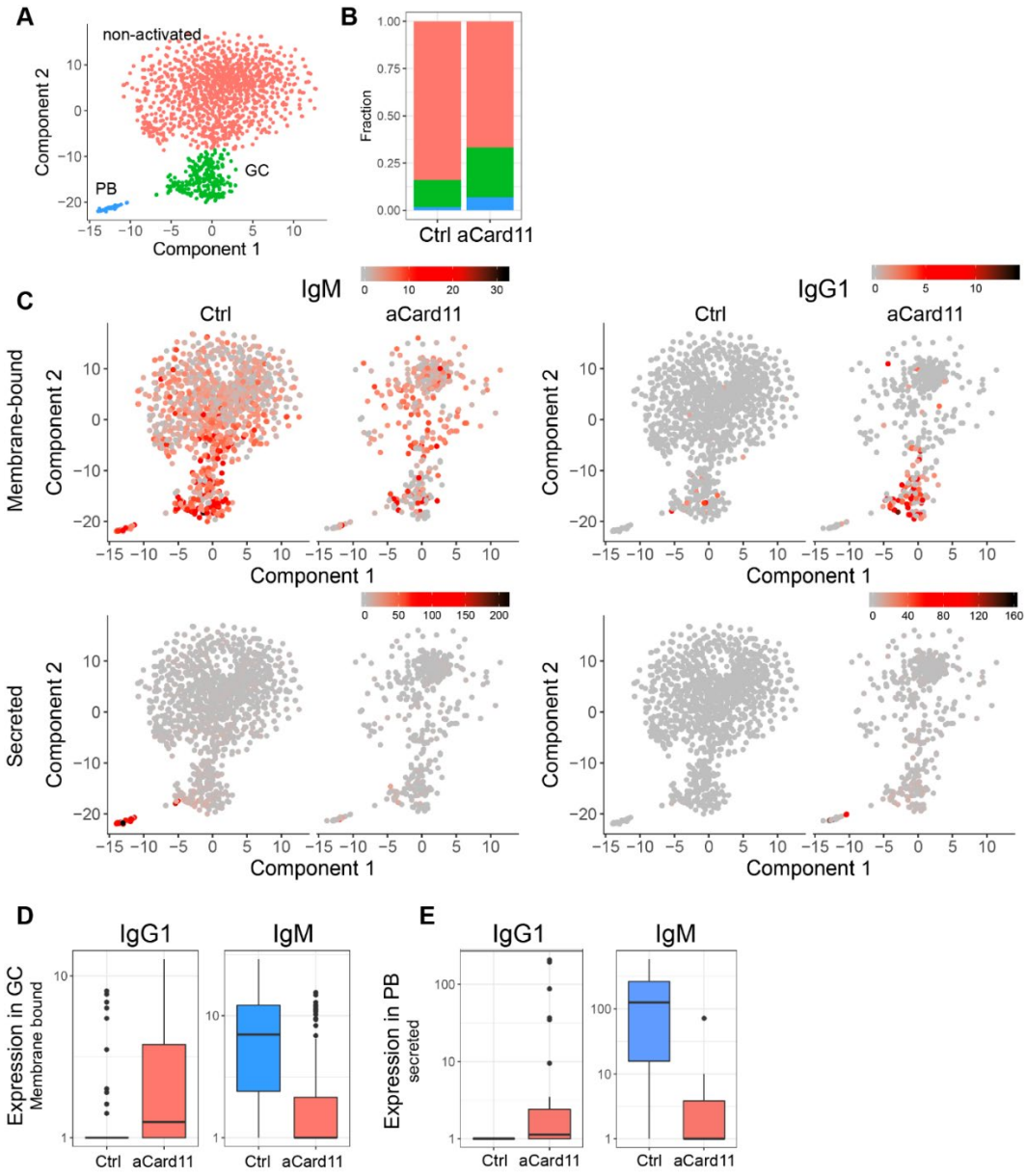

Figure 2-7. aCARD11 promotes Ig class-switching in GC B cells and generation of IgG1 secreting PCs. Ctrl ($Mb1^{Cre/+}$) and Mb1-aCARD11 mice were immunized with SRBC and sacrificed on Day 5 post-immunization for scRNA sequence analysis (see methods). **A.** A t-SNE plot of 1581 single B cells reveals 3 clusters: Red – non-activated, green – GC, and blue – plasmablasts. **B.** Fraction of B cell clusters in A within Ctrl and Mb1-aCard11 samples. **C.** t-SNE plots of B cells (as shown in A) illustrating gene expression – left: Ctrl cells, right: Mb1-aCard11. Depicted are transcript levels of membrane bound IgM (*upper left*), secreted IgM (*lower left*), membrane bound IgG1 (*upper right*), and secreted IgG1 (*lower right*). **D.** Expression levels of membrane bound IgG (*left*, $P=3.1x10^{-39}$) and IgM (*right*, $P=1.6x10^{-74}$) transcripts in GC B cells. **E.** Expression levels of secreted IgG (*left,* $P=2.4x10^{-58}$) and IgM (*right*, $P=1.7x10^{-143}$) transcripts in GC B cells. D-E: Ctrl in blue, Mb1-aCard11 in red. D-E: P values were calculated using the likelihood ratio test included within Monocle's differential-GeneTest function. Showing data from 1 of 2 representative experiments.

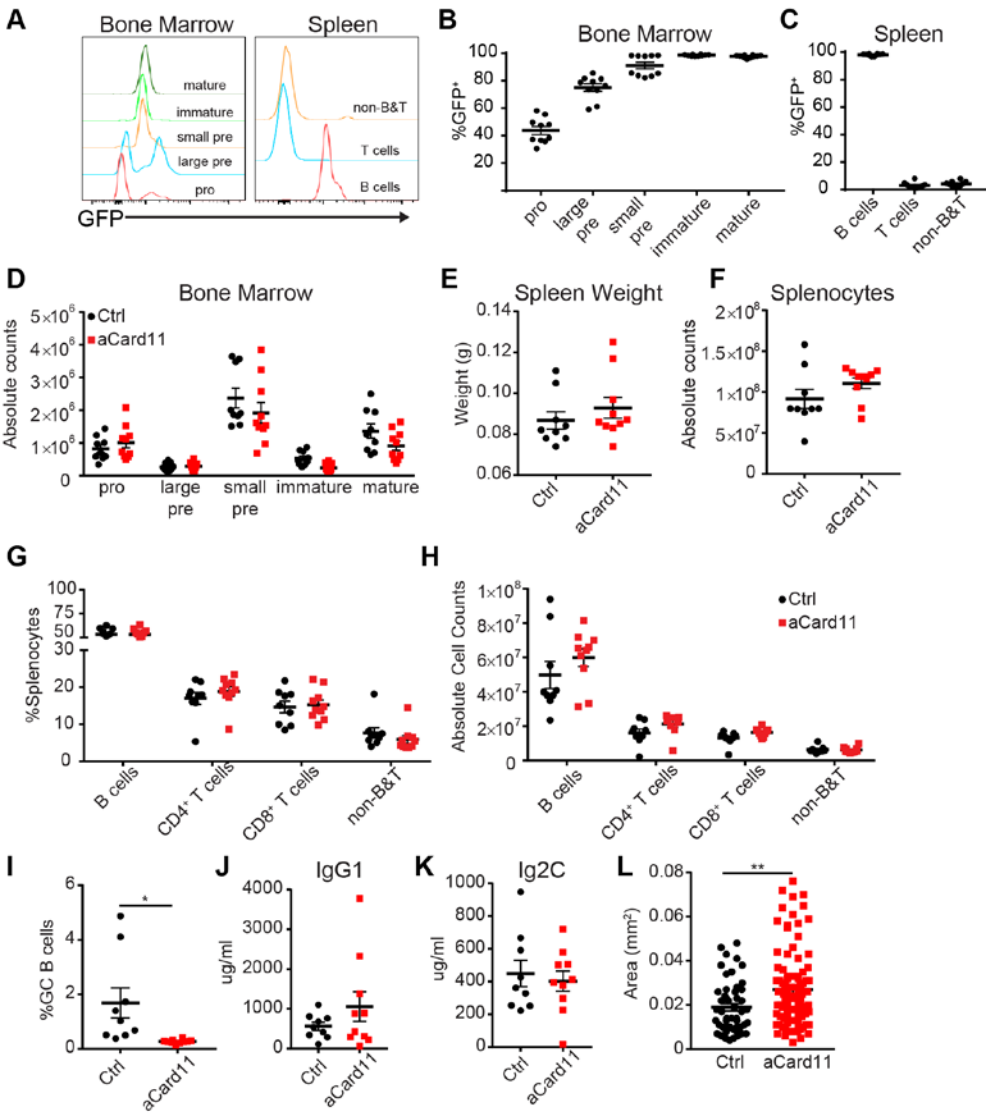

Figure 2-S1. Mb1-aCard11 mice have mild splenomegaly with unaltered bone marrow B cell development. A. Representative histograms of GFP expression in B cell subsets in the BM (right panel) and spleen (left panel) of Mb1-Cre-aCard11 mice. B. Frequency of GFP$^+$ cells in BM B cell subsets. **C.** Frequency of GFP$^+$ cells in splenic B cells (B220$^+$), T cells (CD3$^+$), and non-B&T (B220$^-$CD3$^-$). **D.** Absolute cell counts of BM B cell subsets from 1 leg (per animal) in ctrl and Mb1-Cre-aCard11 mice: pro (B220$^+$IgM$^-$CD43$^+$), large pre (B220$^+$IgM$^-$CD43$^-$SSC^{hi}), small pre (B220$^+$IgM$^-$CD43$^-$SS^{lo}), immature (B220$^+$IgM$^+$IgD$^-$), and mature (B220$^+$IgM$^+$IgD$^+$). **E.** Spleen weight. **F.** Total splenocytes. **G.** Frequency of splenic B cells (B220$^+$), CD4$^+$ T cells (CD3$^+$CD4$^+$), CD8$^+$ T cells (CD3$^+$CD8$^+$) and non-B&T cells (B220$^-$CD3$^-$). **H.** Absolute cell counts of splenic subsets. **I.** Frequency of spontaneous GC B cells (B220$^+$CD95^{hi}CD38^{lo}). **J.** IgG1 serum titers. **K.** IgG2c serum titers. I-K: Significance defined as P<0.05 by student's unpaired t-test. A-K: data representative of 2 independent experiments with 9 Ctrls and N=10 aCard11 mice all ~12 wks of age. **L.** Area (mm^2) of individual germinal centers (PNA$^+$ foci) in splenic tissues sections from Ctrl (littermate controls) and Mb1-aCard11 mice at 5dpi with SRBCs. Area measured by ImageJ, with significance defined as P<0.05 by unpaired t-test. Data representative of 3 independent experiments with 5 Ctrls and 5 Mb1-aCard11 mice.

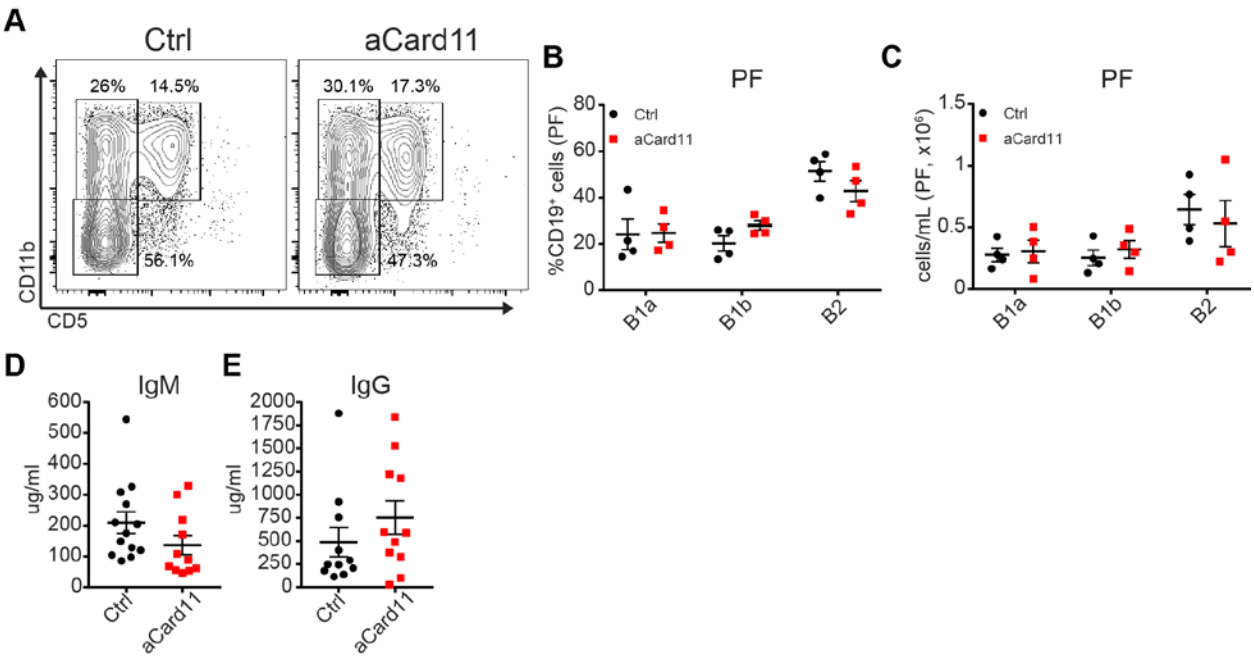

Figure 2-S 2. Cγ1-aCard11 mice have normal peritoneal B cells and serum Ig titers. A. Representative flow plots of B cell subsets in peritoneal fluid: B1a ($CD19^+CD11b^+CD5^+$), B1b ($CD19^+CD11b^+CD5^-$), and B2 ($CD19^+CD11b^-CD5^-$). *Left*: Ctrl (Cre-negative littermate control), and *right*: aCard11 (Cγ1-aCard11). **B**. Frequency and **C**. Absolute number of peritoneal B cell subsets (per mL of peritoneal fluid). **D**. IgM serum titers. **E.** IgG serum titers. A-C: data representative of 2 independent experiments with 4 Ctrls (aCard11) and 4 aCard11 (Cγ1-aCard11) mice all ~12-15 wks of age. Significance defined as P≤ 0.05 by 2-way ANOVA. D&E: Data representative of 3 independent experiments with 8 Ctrls and 8 Cγ1-aCard11 mice 11-15 wks of age. Significance defined as P≤ 0.05 by unpaired student's t-test.

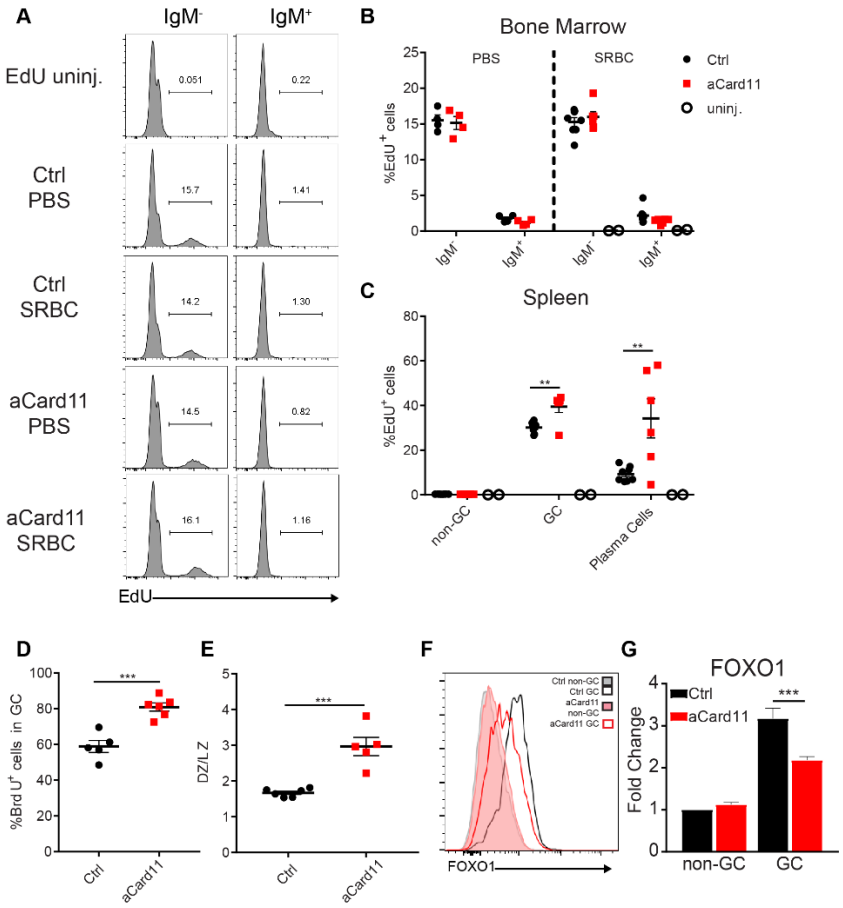

Figure 2-S 3. aCARD11 enhances cycling of GC B cells and PCs, with no impact on cycling in the bone marrow. A-C. Ctrl and Mb1-aCard11 mice were immunized with SRBC and sacrificed on day 5 post-immunization for analysis of B cell populations. In A-C, 1mg EdU was injected i.p. 1hr prior to sacrifice. **A.** Representative histograms showing the relative proportion of EdU$^+$ cells in pro/pre B cells (left column - B220$^+$IgM$^-$) and immature/mature B cells (right column - B220$^+$IgM$^+$) in the BM. **B.** Percent EdU$^+$ cells in pro/pre and immature/mature B cells in the BM from PBS and SRBC immunized mice at 5dpi. **C.** Percent EdU$^+$ cells in non-GC (B220$^+$CD95^{lo}CD38^{hi}), GC (B220$^+$CD95^{hi}CD38^{lo}), and PC (B220$^-$CD138$^+$) compartments. Significance defined as P<0.05 by student's unpaired t-test. A-C: Data representative of two independent experiments using 8 Ctrls (black circles) and 6 Mb1-aCard11 (red squares) (EdU injected), and 2 untreated animals (open circles). **D-E.** Ctrl and Cγ1-aCard11 mice were immunized with SRBC and sacrificed on day 5 post-immunization for analysis of B cell populations. 1mg of BrdU was injected ip 24hrs prior to sacrifice. **D**. Percent BrdU$^+$ cells in GC (B220$^+$CD95^{hi}CD38^{lo}) at 5dpi with SRBCs. **E.** Ratio of DZ to LZ cells within the germinal center at 5dpi (as defined in Fig 4). D&E: Data representative of N=5 Ctrls (black) vs N=6 Cγ1-aCard11 (red) from 2 independent experiments, significance defined as P<0.05 by student's unpaired t-test. **F.** Representative histogram of total FOXO1 protein in non-GC (B220$^+$CD95$^-$PNA$^-$) and GC (B220$^+$CD95^{hi}PNA^{hi}) B cells. Filled histograms: non-GC B cells (Grey=Ctrl and pink=aCard11). Open histograms: GC B cells (black=Ctrl and red=aCARD11). **G**. Fold change in FOXO1 median expression normalized to average FOXO1 expression in Ctrl non-GC B cells. Data in A-B representative of 2 independent experiments, N=8 Ctrl and N=8 Mb1-aCard11 mice. Significance defined as P<0.05 using 2-way ANOVA, P<0.001.

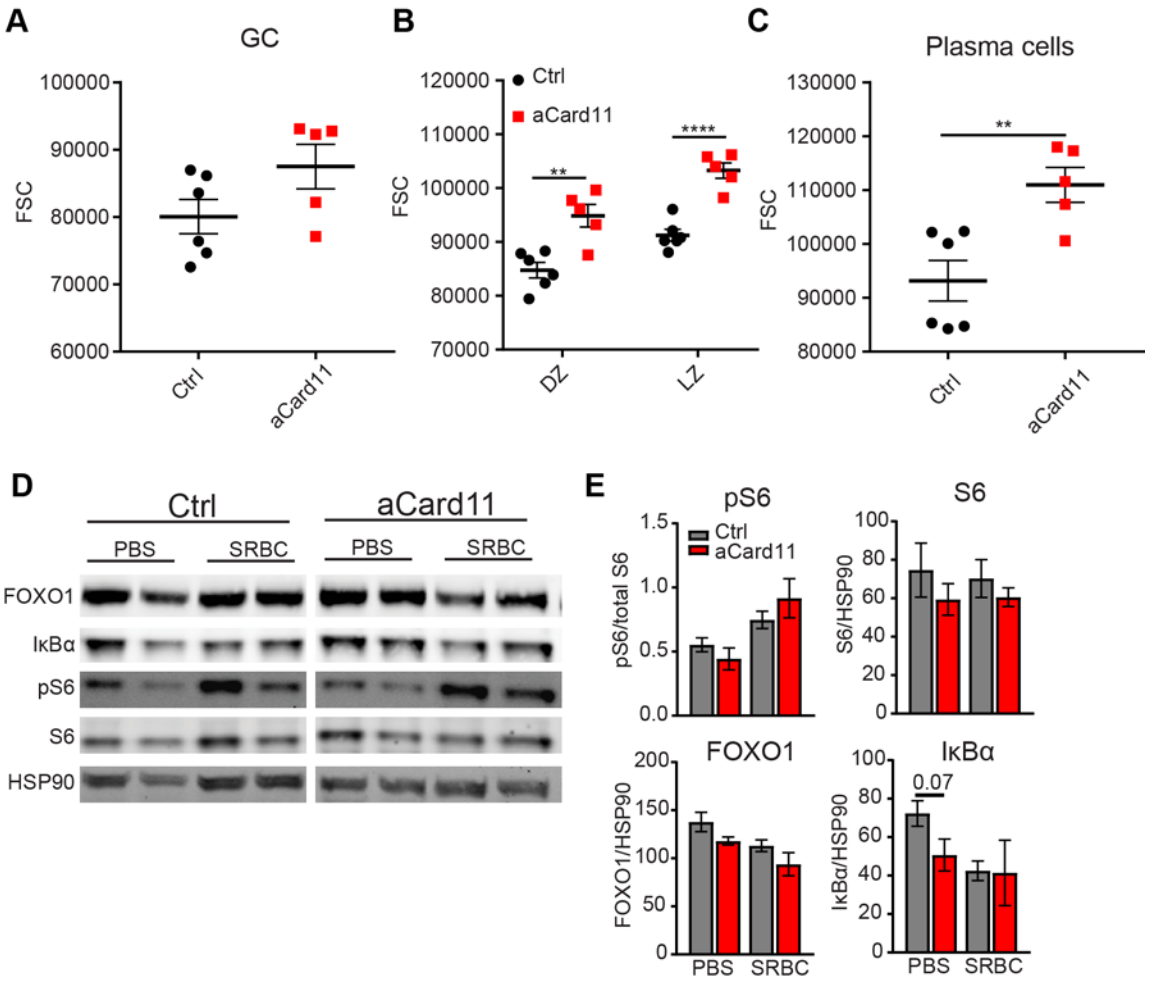

Figure 2-S 4. aCARD11 enhances cell biomass and mTORC1 signaling. A-C. Ctrl and Cγ1-aCard11 mice were immunized with SRBC and sacrificed on day 5 post-immunization for analysis of B cell populations. **A**. Median forward scatter (FSC) of GC B cells ($B220^{+}CD95^{hi}CD38^{lo}$). **B**. Median forward scatter (FSC) of DZ ($CXCR4^{+}CD86^{-}$) and LZ ($CXCR4^{-}CD86^{+}$) GC B cells (as defined in A). **C**. Median forward scatter (FSC) of PCs ($B220^{-}CD138^{+}$). A-C are derived from 2 independent experiments, significance defined as $P<0.05$ by student's unpaired t-test. **D-E**. Ctrl and Mb1-aCard11 mice were immunized with SRBC and sacrificed on day 5 for western blot analysis of splenic B cell populations. **D.** Representative immunoblot using purified splenic B cells and plasma cells derived from PBS or SRBC immunized mice at 5dpi. Each lane depicts protein data from an individual control or aCard11 animal immunized with PBS or SRBC as indicated. Graphs to the right indicate quantification of data from 2 independent experiments, with 6 Ctrl and 5 Mb1-aCard11 mice for PBS and 5 Ctrl and 4 Mb1-aCard11 mice for SRBC. **E**. Quantification of immunoblots using ImageJ: pS6 normalized to total S6, total S6 normalized to HSP90, FOXO1 normalized to HSP90, and total IkBa normalized to HSP90. Significance defined as $P<0.05$ by student's unpaired t-test.

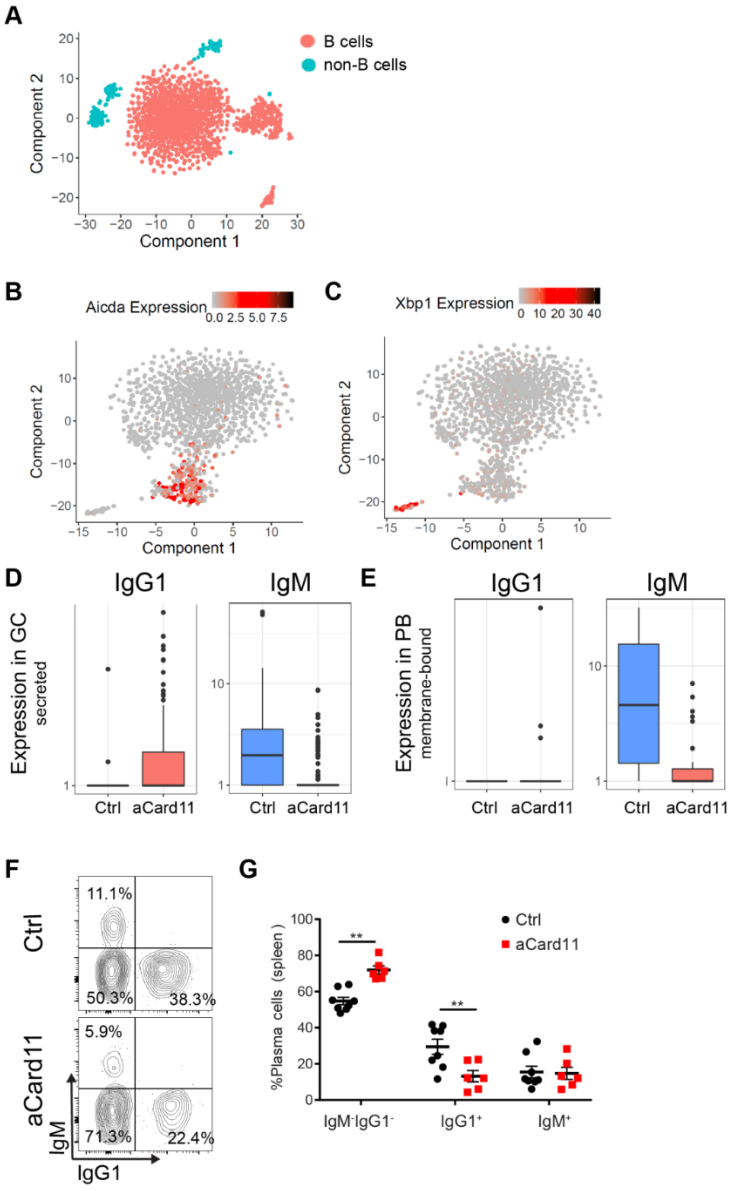

Figure 2-S5. aCard11 enhances CSR. Ctrl ($Mb1^{Cre/+}$) and Mb1-aCARD11 mice were immunized with SRBC and sacrificed on Day 5 post-immunization for scRNA sequence analysis. **A.** t-SNE plot of 1954 total cells: non-B cells in blue and B cells in pink. **B.** t-SNE plot of B cell clusters illustrating expression of AICD primarily in the GC cluster. **C.** t-SNE plot illustrating that XBP1 expression is primarily found in the PB cluster. **D.** Expression levels of secreted IgG1 (*left,* P=1.4x10^{-28}) and IgM (*right*, 3.8x10^{-36}) transcripts in GC B cells. **E**. Expression levels of membrane bound IgG1 (*left*) and IgM (*right,* 2x10^{-24}) transcripts in PBs. D-E: Showing data from 1 of 2 representative experiments. Ctrl in blue, Mb1-aCard11 in red. D-E: P values were calculated using the likelihood ratio test included within Monocle's differential-GeneTest function. **F.** Representative flow plots of cytoplasmic BCR isotype of PCs ($B220^{-}CD138^{+}$). *Top panels*: Ctrl; *bottom panels*: Mb1-aCard11 from SRBC immunized animals. **G.** Percent of $IgM^{-}IgG1^{-}$, $IgG1^{+}$, and IgM^{+} cells within the PC compartment in Ctrl (*black*) vs Mb1-aCard11 (*red*) mice. Statistical significance defined as P<0.05 calculated by 2-way ANOVA. F-G: data representative of 2 independent experiments with 8 Ctrl and 6 Mb1-aCard11 mice.

Chapter 3

Activated PIK3CD drives innate B cell expansion yet limits B cell intrinsic immune responses

Introduction

Phosphatidylinositol 3-kinase (PI3K) signaling plays a critical role at several stages of B cell development. While deletion of either PIK3CD (p110δ) or PIK3R1 (p85) in mice limits central B cell development, mature B cell development is also altered, resulting in development of fewer B1 and marginal zone (MZ) B cells[29]. These cellular defects contribute to decreased immunoglobulin production, weak responses to TI antigens and lack of response to TD antigens in mice[29, 32] or humans deficient in either PIK3CD[33] or PIK3R1[34]. Conversely, B cell-specific activation of class 1A PI3Ks, as assessed using genetic models of PI3K hyper-activity, also leads to defects in both TI and TD responses. For example, deficiency of either the PI3K phosphatases, INPP5D[36, 37] or PTEN[38], or forced expression of membrane-tethered PIK3CA[39], results in loss of B cell class-switch recombination and maturation in response to TD antigens.

As suggested from the data in mice, primary immunodeficiency in humans can be caused by germline mutations in PIK3CD (p110δ) or PIK3R1 (p85) that increase class 1A PI3K signaling. Patients with activating mutations in either gene present with complex immune phenotypes that include susceptibility to bacterial and viral respiratory infections, B cell lymphopenia, effector-memory T cell hyperplasia and senescence, antibody dysregulation (increased IgM and decreased IgG2)[42-44] and acquisition of B cell lymphoma. The cell intrinsic roles for B and T cells in this newly identified immune dysregulation disease, called Activated Phosphoinositide 3-kinase-d Syndrome (APDS), have not been carefully elucidated. Here, we report an inducible murine model of APDS driven by a common activating mutation in PIK3CD (hE1021K, mE1020K). Our data show that many aspects of the APDS clinical phenotype can be explained by B cell-intrinsic, activated PI3KD-driven signaling. Dysregulated PI3K signals in B cells leads to defects in immature B cell development, preferential expansion of innate-like B cells, increases in natural IgM and a naive B cell compartment that lacks the capacity to respond appropriately to immune challenge.

Materials and Methods

Mice

$Mb1^{Cre/+}$, $CD21^{Cre/+}$, $AID^{Cre/Cre}$, μMT mice were bred and maintained in the specific pathogen-free animal facility of Seattle Children's Research Institute and handled according to Institutional Animal Care and Use Committee-approved protocols. aPIK3CD mice were generated by knockin of mutant exon 24 bearing E1020K in 3'→5' orientation downstream of endogenous exon 24, flanked by loxp sites as shown in Supp Fig 1A. The targeting vector also included a neo-cassette flanked by frt sites in the endogenous PIK3CD locus that was removed by intercross with Flp-strain mice (ACTB:FLPe B6J mice, Jackson labs) following germline transmission. aPIK3CD mice were subsequently crossed to various B cell specific cre-bearing strains as described to induce excision of endogenous exon 24 and expression of mutant exon 24, via cre-mediated double-stranded breaks at the indicated Loxp and mLoxp sites, resulted in fixing the inversion in place as previously described (Fig. 3-S1A)[89]. $Mb1^{Cre}$ mice were provided by M. Reth (Max Planck Institute of Immunobiology, Freiburg, Germany). All aPIK3CD mice in this study are heterozygous for the E1020K mutation and all control (Ctrl) animals are cre-negative littermates.

Immunization

16-30-week old mice were i.p. immunized with 50 ug of NP-Ficoll (Biosearch technologies) in 200ul. For virus-like particle (VLP) immunization, mice 12-18 weeks of age were injected i.p. with 2ug/250ul VLPs or 250ul 1x PBS. For Pneumovax23 (Merck) injection, mice were injected with 0.125ug/200ul i.p. per mouse or 200ul 1x PBS.

Droplet digital PCR assay

ddPCR assays were performed in a total volume of 25 μL. Each reaction contained 50 ng of gDNA with a final 1X ddPCR Supermix for probes (Bio-Rad), 900nM of primers and 250 nM of each reference (labeled with HEX) and junction (labeled with FAM) probes. Droplets containing this reaction mix were generated (Bio-Rad QX200 ddPCR droplet generator) and amplified by PCR with the following thermocycler conditions: one cycle of 95°C for 10 min; 40 cycles of 95°C for 30 s, 60°C for 30 s, and 72°C for 30 s; one cycle of 98°C for 10 min; followed by holding at 12°C. Amplified samples were analyzed on the

QX200 Droplet Reader (Bio-Rad) using the QuantaSoftTM software (Bio-Rad). To calculate flipping frequency, HEX-positive droplets of junction probe were divided by FAM-positive droplets of reference probe. The same threshold was applied to all samples for each probe to define the positive droplets.

PI3K-Fw: AACCCGTACCCAACAAACAT;

PI3K-Rev: GCTAACGAAGAGAGGGACAC;

Reference probe: HEX-CCTGCGGCTACTGACACGAC-BHQ1;

Knock-in/junction probe: FAM-ACCTCAGGGAGGGACAGAATGGACCCC-BHQ1.

Reagents

LIVE/DEAD Fixable Near-IR Dead Cell Stain Kit (Invitrogen) was used according to manufacturer's instructions. Alexa-Fluor 350 carboxylic acid, succinyl ester (Invitrogen) was used according to manufacturer's instructions. Anti-murine antibodies used in the study include: eBioscience - CD38 (90), IgM (II/41), CD8 (53-6.7), Gr-1/Ly-6G (RB6-8C5), SA-e450; Southern Biotech - IgD (11-26), BP-1 (FG35.4), λ (JC5-1); Biolegend - B220 (RA3-6B2), CD19 (6D5), CD24 (M1/69), CD21 (7E9 & 7G6), CD23 (B3B4), BP-1 (6C3), CD4 (GK1.5); BD Biosciences - CD43 (S7), CD21 (7G6), CD19 (1D3), CD138 (281-2), CD95/Fas (Jo2), IgG1 (A85-1), κ (187.1), CXCR4 (2B11), CD86 (GL1), CD11b (M1/70), CD5 (53-7.3), SA-PE.; Life Technologies - CD3 (500A2), SA-AF700, SA-APC; Vector labs - PNA.

Competitive chimera bone marrow transplantations

Bone marrow (BM) was harvested from donor WT (CD45.1) and Mb1-aPIK3CD (CD45.2), and single-cell suspensions were mixed at a 50:50 ratio for retro-orbital injection of 5×10^6 cells into lethally irradiated (900 cGy) μMT (CD45.1/CD45.2) recipients. Resulting BM chimeras were sacrificed 12–14 wk post-transplantation. Data are representative of 2 independent experiments.

Flow cytometric analysis

Single-cell suspensions from spleen, BM, and peritoneal fluid (PF) were obtained as previously described[(52)] and incubated with fluorescence-labeled Abs for 15 min at 4°C. For phospho-flow analysis,

1e6 cells were fixed with fix/perm solution (BD) for 20 min at RT in the dark. Cells were resuspended in 90% methanol and stored at -20 C for a minimum of 30 mins. Cells were washed with FACs buffer (1xPBS plus 2% FBS) twice and stained for surface and phospho-site antibodies for 45 min at RT in the dark. Data were collected on an LSRII (BD) and analyzed using FlowJo software (Tree Star).

Cell cycle analysis

For *in vivo* labeling of cycling cells, mice were intraperitoneally injected with 1 mg BrdU 24 h prior to sacrifice. Both spleen and BM were collected, and cells were surface stained, fixed, permeabilized, treated with DNase for 1 h at 37°C, and stained with anti-BrdU FITC (BrdU kit from BD Biosciences). Data were collected on an LSRII (BD) and analyzed using FlowJo software (Tree Star).

ELISA

To test total serum Ig titers, 96 well Nunc-Immuno MaxiSorp plates (Thermo Fisher) were pre-coated overnight at 4℃ with 2ug/ml anti-IgM, anti-IgG, anti-IgG1, anti-IgG2C, and anti-IgG3. For total Ig ELISAs, serum was diluted 1:6250, 1:31250, and 1:156250. Serum diluted at 1:200 was tested for reactivity to dsDNA (Sigma-Aldrich), sm-RNP (ATRO1-10; Arotech Diagnostics Limited) and malondialdehyde-modified low-density lipoprotein (MDA-LDL; 20P-MD L-105; Academy Biomedical) at 100 μg/ml. To detect NP-specific antibody levels in serum, 96 well Nunc-Immuno MaxiSorp plates were coated with NP(30)-BSA (50μg/mL; Biosearch technologies) overnight at 4℃. Serum was diluted 1:8000, 1:16000, 1:32000, and 1:64000. To test reactivity to VLP, plates were coated with 1 ug/mL Qb VLP antigen, and serum was 2x-serially diluted from 1:200-1:409600. To test reactivity to Pneumovax23, plates were coated with 10ug/ml Pneumovax, and serum was diluted 1:100. Plates were blocked for 1hr with 2% BSA in PBS before addition of diluted serum for 2hrs at RT or overnight at 4℃. Specific antibodies were detected using goat anti-mouse IgM-, IgG-, IgG1-, IgG3-, or rat anti-mouse IgG2C-horseradish peroxidase (1:2000 dilution; SouthernBiotech). Peroxidase reactions were developed using OptEIA TMB substrate (BD) and stopped with sulfuric acid. Absorbance at 450 nm was read using a SpectraMax 190 microplate reader

(Molecular Devices). For total Ig titers, 450 nm absorbance was corrected by subtraction of 570 nm absorbance. For antigen specific ELISAs 450 nm absorbance was reported.

Apoptosis assays

Total cells from spleen, BM, and PF were incubated with fluorescently labeled antibodies for 30 min at 4°C in staining buffer, followed by TUNEL-based apoptosis analysis. Cells were fixed overnight at 4°C in 2% PFA, permeabilized for 2 min on ice in perm solution (0.1% TritonX-100, 0.1% sodium citrate), and labeled according to the manufacturer's instructions (In Situ Cell Death Detection kit, Fluorescein; Sigma-Aldrich). Data was collected using an LSR II and analyzed using FlowJo software. For AnnexinV staining, total cells from spleen or PF were incubated with fluorescently labeled antibodies for 15 min at 4°C in staining buffer, followed by AnnexinV staining with dead cell apoptosis kit (Life Technologies). Cells were resuspended in 1x Annexin-binding buffer and stained with AnnexinV-488 for 15 min at RT in the dark. The reaction was quenched with 1x Annexin-binding buffer, and samples were run immediately on an LSRII (BD) and analyzed using FlowJo software (Tree Star).

Statistical analysis

Unpaired, two-tailed Student's t tests were applied to assess statistical significance of the differences between groups of mice. For experiments that have more than two groups, more than two treatments or more than two time-points, one- or two-way analysis of variance was used to assess group and treatment differences and the Bonferroni method was used to correct for multiple hypotheses in pairwise comparisons. The p-values were considered significant when $P < 0.05$ (*), $P < 0.01$ (**), and $P < 0.001$ (***).

Results

A cell intrinsic model for tissue-specific knock-in of activated PIK3CD

To understand how activating mutations in the catalytic subunit of PIK3CD impact the differentiation and homeostasis of immune cells, we generated an inducible mouse model of PIK3CD-E1020K (equivalent to hE1021K, hereafter referred to as 'aPIK3CD'). A targeting vector containing the

aPIK3CD mutation within exon 24 of the *Pik3cd* gene and relevant cre-lox sites was introduced by homologous recombination into the endogenous *Pik3cd* locus. The mutant exon was placed in the opposite orientation of transcription (3'→5') and downstream of the endogenous exon 24. Upon Cre-mediated excision, the endogenous exon 24 is excised and the mutant exon is flipped so that its transcription is subject to endogenous regulation (Fig. 3-S1A). Using droplet digital (dd)PCR with knock-in (junction)-specific probes, we confirmed the flipping efficiency in $CD21^{Cre/+}$aPIK3CD$^{+/-}$ to be ~50% and restricted to the B cell lineage, as expected in a heterozygote genotype (Fig. 3-S1B-D). These data demonstrate establishment of an efficient murine model that enables tissue-specific expression of aPIK3CD.

Expression of aPIK3CD in developing B cells leads to BM B lymphopenia

APDS patients exhibit peripheral B cell lymphopenia[42, 44, 45, 47]. Bone marrow (BM) B cell phenotyping in a limited number of APDS subjects has suggested that aPIK3CD may impact the pre-B-I stage leading to an increased proportion of apoptotic $CD19^{dim}$ B cell progenitors[47] or, similarly based on alternative surface markers, a proportional increase in $CD10^{hi}CD20^{neg}$ early B cell progenitors[48]. To better understand the consequences of hyperactive PI3K signaling during early B cell development, we crossed aPIK3CD animals to the Mb1-Cre strain to drive aPIK3CD expression beginning at the pro-B cell stage[50]. To minimize the indirect effects of long-term aPIK3CD expression, we focused our analyses on cohorts 11-13 weeks of age. Mb1-aPIK3CD mice displayed diminished frequency and ~50% reduction in the absolute number of bone marrow (BM) B cells (Fig. 3-1A&B, Fig. 3-S1G). Detailed characterization of the BM B cell compartment demonstrated an increased proportion of pro-B cells ($B220^{+}IgM^{-}CD43^{+}$) and a decreased frequency of mature recirculating B cells ($B220^{+}IgM^{+}IgD^{+}$, Fig. 3-1C & Fig. 3-S1G). By absolute cell counts we observed a reduction in the number of small pre- and mature recirculating B cells (Fig. 3-1D; Fig. 3-S1G). Thus, while previous human studies were unable to assess total BM B progenitor cell numbers, consistent with phenotypic data from APDS subjects, B cell intrinsic aPIK3CD expression restricts BM B lymphopoiesis with its major impact at the pre-B stage leading to a proportional increase in pro-B cells and reduction in the absolute number of pre-B, immature and recirculating B cells.

aPIK3CD expression promotes expansion of peripheral innate B cell compartments

We next evaluated the impact of aPIK3CD on peripheral B cell development. In the peritoneum, Mb1-aPIK3CD mice displayed increases in both the proportion and absolute number of B1a B cells (Fig. 3-1E&F, Fig. 3-S1H) and a proportional reduction in the frequency, but not the number, of B1b and B2 B cells. In the spleen, Mb1-aPIK3CD mice exhibited an increased proportion of MZ B cells and a decrease in the proportion of follicular mature (FM) B cells with a similar trend in cell numbers (Fig. 3-1G&H, Fig. 3-S1I). As anticipated based upon biochemical analysis of primary T and B cells in APDS subjects[44, 45, 47], all splenic B cells subsets displayed increased phosphorylation of ribosomal protein S6 (pS6; Ser235/236) compared to controls (Fig. 3-S1E&F). Thus, despite a reduction in BM B cell development, B cell intrinsic aPIK3CD expression is sufficient to drive expansion of both the B1a and MZ B cell compartments.

aPIK3CD B cells exhibit differential selection within the immature vs. MZ and B1a compartments

To precisely assess the specific stages of B cell development wherein cells expressing aPIK3CD exhibit altered competitive selection, we performed BM chimera studies using mixed populations of wildtype (WT, CD45.1$^+$) and Mb1-aPIK3CD (aPIK3CD, CD45.2$^+$) BM transplanted into congenically marked, B cell deficient, μMT recipients (CD45.1$^+$/CD45.2$^+$). Recipient mice were characterized 12 weeks post-transfer to interrogate chimerism within B cell developmental stages. Within the BM, relative to aPIK3CD cells, WT B cells were enriched at the immature stage (B220$^+$IgM$^+$IgD$^-$), an advantage that remained despite skewing the input BM ratio to 2:1 in favor of aPIK3CD B cells (Fig. 3-2A-B). As the absolute number of immature B cells is primarily dependent upon clonal expansion of pre-B cells, this reduced competitive fitness likely reflects the diminished small pre-B cell compartment (Fig. 3-1D) observed under homeostatic conditions.

Similar to our observations in the periphery of Mb1-aPIK3CD mice, despite their being at a disadvantage prior to egress from the BM, aPIK3CD B cells outcompeted WT cells within the B1a (Fig. 3-2C&D) and MZ compartments (Fig. 3-2E&F). In addition to the impact on the B1a cells, we observed

skewing in favor of aPIK3CD B1b B cells, suggesting that aPIK3CD globally promotes B1 B cell fitness and enhances the activated B1a $CD5^+$ phenotype.

To determine whether aPIK3CD alters innate B cell populations independently of early B lineage commitment, we crossed aPIK3CD mice to the CD21-Cre strain. In this model, aPIK3CD is first expressed at the splenic T1 stage and to a somewhat lesser degree in peritoneal B cells[90]. CD21-aPIK3CD displayed an expansion of innate B cells, including an increased frequency of B1a cells, with a trend towards increased numbers (Fig. 3-2G&H), and significant increases in MZ B cell numbers with a concomitant decrease in FM B cells (Fig. 3-2I&J). While chimeric studies suggested a trend for increased proportion of aPIK3CD transitional B cells (Fig. 3-2E&F), absolute numbers of T1/T2 and MZp B cells were unchanged in CD21-aPIK3CD mice. Thus, restricting aPIK3CD expression to peripheral B cell stages is sufficient to drive expansion of innate B cell populations.

aPIK3CD does not alter cycling but differentially impacts immature vs. innate B cell survival.

To clarify how aPIK3CD leads to reduced BM B cells and higher B1a and MZ B cell numbers, we quantified its effects on cell proliferation and survival. To measure proliferation, Mb1-aPIK3CD and control mice were injected 24 hours prior to sacrifice with BrdU, a thymidine analog incorporated into DNA during S phase. We observed no difference in $BrdU^+$ BM B cell subsets in Mb1-aPIK3CD vs. Ctrl mice (Fig. 3-3A, Fig. 3-S2A). In the periphery, aPIK3CD B1a B cells exhibited decreased proliferation and B1b cells showed a similar trend (Fig. 3-3B). Peritoneal B2 (Fig. 3-3B) and splenic B cell subsets including MZ B cells (Fig. 3-3C) showed no differences in cycling in Mb1-aPIK3CD mice compared to controls.

Because there is no evidence of altered cycling under homeostatic conditions, we postulated that the reduction in immature B cells and/or expansion of innate B cells reflected differences in cell survival. Analysis of WT vs. aPIK3CD B cells in the chimeric setting demonstrated an increased frequency of aPIK3CD expressing immature B cells undergoing apoptosis ($TUNEL^+$, Fig. 3-3D, Fig. 3-S2B). Under homeostatic conditions, removing the impact of hyperactive PI3K signaling in the BM, we observed decreased $TUNEL^+$ B1a B cells in CD21-aPIK3CD mice (Fig. 3-3E) and similar trends in MZ precursor

(MZp) and MZ B cells (data not shown). In the chimeric setting, we observed a decreased proportion of apoptotic aPIK3CD MZ B cells (Fig. 3-3F). Consistent with these data, MZ B cells and peritoneal B cells exhibited decreased Annexin V staining, an alternative measure of apoptosis (Fig. 3-S2C-F). Together, these data show that B cell intrinsic aPIK3CD expression promotes innate B cell survival without altering proliferation. Conversely, aPIK3CD expression limits survival of immature B cells, and may be selected against, without impacting proliferation.

aPIK3CD expression drives plasma cell formation that correlates with elevated natural IgM

To assess the impact of aPIK3CD on immunoglobulin production and terminal differentiation, we quantified plasma cell (PC) numbers and antibody isotypes. We observed a significant increase in frequency and number of splenic PCs ($B220^{-}CD138^{+}$) in the absence of immunization (Fig. 3-4A&B). In chimeras, we found that aPIK3CD B cells out-competed WT B cells in the germinal center (GC) ($B220^{+}CD95^{hi}CD38^{lo}$) and PC compartments (Fig. 3-4C&D, Fig. 3-S3A), supporting the idea that hyperactive PI3K signaling enhances terminal differentiation.

To further investigate the functional impact of alterations in PC, B1a and MZ B cells we quantified serum antibody. Mb1-aPIK3CD exhibited a ~3-fold increase in both IgM and IgG3 (Fig. 3-4E). Restricting expression of aPIK3CD to peripheral B cells also resulted in an increase in serum IgM and IgG3 (Fig. 3-4G). B1 B cells are the major source of IgM and IgG3 natural antibodies that recognize self- and non-self/microbial antigens[91]. Many natural antibodies recognize oxidation-specific epitopes on lipids and apoptotic cells. We found that MDA-LDL and phosphorylcholine (PC) reactive IgM were increased (Fig. 3-4F), and reactivity to nuclear antigens was reduced (Fig. 3-S3B&C) in Mb1-aPIK3CD compared to control animals. Restriction of aPIK3CD expression to peripheral B cells led to a similar phenotype (Fig. 3-4H). These findings suggest that hyperactive PI3K enhances the formation of PCs, that are derived, at least in part, by activation of innate B cells leading to increased serum levels of natural antibodies.

While B1a B cells have been proposed to generate natural IgM in murine models [92-95], analysis of BM IgM^{+} PCs and peritoneal cell transfer studies suggest that an early B1 progenitor may preferentially

seed the natural IgM$^+$ PC compartment[96]. To test this idea, we quantified B1 progenitors in the BM and observed significant increases in their number and proportion (Fig. 3-S3D-F) in aPIK3CD mice[97]. In future studies, aPIK3CD models could be used to define these progenitors and assess other B1 B cell functions, including generation of IL10 producing subsets.

B-intrinsic aPIK3CD expression blunts TI immune responses

The elevated IgM and innate B cell numbers in aPIK3CD mice suggested these mice might exhibit an increased TI immune response. To test this hypothesis, we immunized Mb1-aPIK3CD and control mice with the TI antigen, NP-Ficoll. Despite increased basal NP-specific IgM, seven days post immunization Mb1-aPIK3CD mice had reduced NP-specific IgM compared to controls (Fig. 3-5A&B). The fold change in antigen-specific IgM was also reduced (~1.4 fold vs ~6.5 fold in controls). Mb1-aPIK3CD mice also exhibited decreased NP-specific IgG3 at baseline and post-immunization (Fig. 3-S3G&H). Notably, APDS patients suffer from recurrent sinopulmonary infections with encapsulated bacteria (*S. pneumonia* and *H. influenzae*) and exhibit diminished responses to polysaccharide-based vaccines[42, 44, 45]. To test whether aPIK3CD mice exhibit a defective response to polysaccharide antigens, we immunized control and Mb1-aPIK3CD mice with Pneumovax23 and measured antibody titers at 6 and 12 days post-immunization. Similar to alterations in mice immunized with NP-Ficoll, Mb1-aPIK3CD mice exhibited higher baseline levels of antigen-specific IgM (Fig. 3-S3I). While peak IgM antibody titers were similar to controls (Fig. 3-5C), the overall fold-induction of antigen-specific antibody was reduced ~1.5-2-fold in the Mb1-aPIK3CD mice (Fig. 3-5D). Thus, B cell intrinsic aPIK3CD expression blunts the capacity to mount a TI immune response.

B-intrinsic aPIK3CD expression skews GCs toward a light zone fate and limits Ig class-switching

Patients with APDS exhibit defects in circulating, class-switched memory B cells, normal or reduced serum IgG with preferential loss of IgG2[42, 44, 45, 47]. Lymph node biopsies have revealed either increased or decreased GC B cell follicles with normal or reduced IgG positive cells[43, 44, 98]. IgG and IgA transcripts exhibit minimal differences in AID targeting and SHM[47] and *in vitro* studies of primary B cells from APDS patients revealed either normal or reduced production of class-switched antibodies[98, 99]. Together, these previous observations suggest that aPIK3CD expression may inhibit class-switch recombination in human B cells. Similarly, alternative mouse models of GC-restricted hyperactive PI3K signaling exhibit defective class-switch recombination[5, 39]. To directly assess how aPIK3CD impacts a TD immune response, we challenged mice with virus-like-particles (VLPs) containing a TLR7 ligand. To eliminate any impact of aPIK3CD on B cell development or BCR repertoire, we performed studies using the AID-Cre strain. In this model, aPIK3CD expression is induced upon transcription of AID, which is most highly expressed in GC B cells[57]. At 14 days post VLP immunization, we observed no differences in the frequency of total or VLP-specific GC B cells (Fig. 3-5 E-G). GC B cell intrinsic deletion of FOXO1[5] or constitutive activation of PI3K (p110α)[39] results in a reduction of the GC dark zone (DZ) compartment. Consistent with these previous findings, GC B cells in AID-aPIK3CD mice demonstrated skewing towards a light zone (LZ; $CXCR4^{-}CD86^{+}$) phenotype (Fig. 3-5H&I). To determine how aPIK3CD impacts the production of antigen-specific antibodies we measured VLP-specific serum titers. At 14 days post immunization, AID-aPIK3CD mice exhibited a heightened VLP-specific IgM response compared to control animals (Fig. 3-5J). In contrast, AID-aPIK3CD mice generated a blunted class-switched response with reduced levels of VLP-specific total IgG and IgG2c, the dominant isotype triggered in response to VLP immunization (Fig. 3-5K&L). To assess the impact of aPIK3CD when expressed in all peripheral B cell populations, we performed identical immunization studies using CD21-aPIK3CD mice (Fig. 3-S3J-O). In this setting, we also observed a modest increase in the proportion of GC B cells with reduced VLP-specificity, LZ skewing and reduced levels of VLP-specific total IgG and IgG2c in CD21-aPIK3CD compared to control animals. Thus, consistent with previous observations in APDS subjects and in alternative mouse models of activated PI3K, B cell intrinsic aPIK3CD promotes GC LZ cell skewing and limits, but does not eliminate, class-switch recombination of antigen-specific B cells.

Discussion:

PI3K is required for mature B cell homeostasis and survival[100]. Mouse models of LOF of PI3K and PI3K hyperactive, through deletion of negative regulators of PI3K, have demonstrated the profound impact PI3K signaling has on both B cell development and immune responses. Germline mutations impacting PI3K signaling support data generated from murine studies and expand upon the impact of GOF mutations in PI3K in driving immunodeficiencies. However, the individual contribution of dysregulated PI3K signaling within the B cell compartment, due to heterozygous, activating mutations in the endogenous *Pik3cd* locus had yet to be elucidated. In this study, we specifically interrogated the impact of B cell intrinsic PIK3CD-E1020K (hE1021K, aPIK3CD) on B cell development and their role during immune responses, both T-independent and -dependent. We show that aPIK3CD is detrimental within the BM niche, however, drives the expansion of innate B cell compartments in the periphery. Hyperactive PI3K signaling has no impact on cycling under homeostatic conditions but enhances survival of innate B cells. aPIK3CD drives increased plasma cell formation, yielding increased serum titers of T-independent isotypes IgM and IgG3, with increased production of natural antibodies. Upon immunization, aPIK3CD inhibits both T-independent and -dependent antigen-specific responses. These findings shed light on the role of B cells in APDS.

B cell lymphopenia in APDS subjects is associated with a proportional, but not a numerical, increase in circulating transitional B cells and a reduction in the number of mature and memory B cells[42, 44, 45, 47]. Mb1-aPIK3CD mice display B cell lymphopenia in the BM, and peripheral expansion of innate B cells that are known to depend on PI3K signaling under homeostatic conditions. We observed decreased recirculating, FM and peritoneal B2 B cells, supporting the idea that aPIK3CD leads to B cell lymphopenia, as observed in APDS subjects, via a combined impact on BM development and reduced fitness of mature B2 B cells. While we did not assess memory cells, our findings are consistent with these data where transitional B cell numbers were minimally impacted, while FM and recirculating B cells were numerically and proportionally reduced. Similarly, in the CD21-aPIK3CD mice where aPIK3CD expression is restricted to peripheral B cells, thus negating the impact of hyperactive PI3K signaling in the BM, we also found diminished proportions of peritoneal B2 B cells and decreased proportion and number of FM B

cells in the spleen. Whether this negative impact on B2 B cells in the periphery of the CD21-aPIK3CD is a result of preferential differentiation into innate B cells or due to lack of space for these cells in the peripheral tissues due to expansion of their innate counterparts in unclear.

Additional work is required to understand the contrasting impact of aPIK3CD in BM vs innate B cell development. Mice homozygous for catalytically inactive p110δ exhibit reduced numbers of BM pre-B and immature B cells[32], and deletion of both p110α and p110δ results in a more severe pre-B cell developmental arrest[35]. Conversely, B cell intrinsic Pdk1 deficiency also negatively impacts these BM B cell populations, with a near complete loss of recirculating and immature B cells due to a decreased frequency of pre-B cells[30]. Consistent with the idea that both reduced and enhanced PI3K activity may negatively impact BM B cell survival. Pten deletion in pre-B cells expressing oncogenic BCR-ABL1 drives rapid leukemic cell death. This leads to downregulation of IL-7R, CD19, and components of the pre-BCR and hyperactive Akt signaling; events that are countered by pharmacological inhibition of Akt[46]. Thus, together with these previous data, our findings imply that altered PI3K signals dysregulate the pre-B checkpoint, leading to increased cell death, possibly via dysregulation of Pax5 target gene expression[101]. In the periphery, loss of PIK3CD restricts both MZ and B1a B cell development. In contrast, increased PI3K activity limits BCR-mediated apoptosis in splenic B cells promoting survival and proliferation[40]. Additionally, PIK3CD is required for BAFF-R driven positive selection[102]. As BAFF signals preferentially regulate innate B cell populations including B1 and MZ B cells, aPIK3CD may augment this BCR-dependent program promoting innate cell expansion despite its negative impact on BM lymphopoiesis.

Mb1-aPIK3CD and CD21-aPIK3CD mice both have elevated serum IgM and IgG3 levels, with increased reactivity for natural antigens. Consistent with our findings in mice, APDS subjects exhibit increased circulating plasmablasts and elevated serum IgM[42, 44, 45, 47]; implying that expansion of innate B cells may account for the common hyper-IgM phenotype. Assessment of IgM specificities in APDS subjects may provide important insight into this question. T-independent immunization of Mb1-aPIK3CD mice demonstrated a defect in the T-independent response in these animals. While the precise mechanism responsible for this defective response remains to be determined, the increased number of innate B cells and elevated baseline levels of antigen-specific IgM suggest that AFCs derived from

antigen-triggered, aPIK3CD innate B cells exhibit reduced survival and/or other functional changes that limit sustained TI antibody production. Decreased survival of antigen specific AFCs may also contribute to the defects in TD responses we observed in our VLP immunization studies, however, this explanation does not explain the block in CSR[5, 39, 42].

In summary, we describe a robust, Cre-inducible model to assess lineage-specific impact of aPIK3CD expression. Using intercross with a series of B-lineage specific Cre-strains, we demonstrate that aPIK3CD expression in B cells is sufficient for several features of APDS including elevated IgM, reduced responses to both TI- and TD-antigens and discrete alterations in the BM and peripheral B cell compartments. Further, our data indicate that a subset of these clinical findings likely reflect alterations in innate B cell compartments that warrant direct assessment in patients. To date, no information is available regarding splenic MZ structures and, while all subjects in one study had an increased proportion of $CD5^{+}CD20^{+}$ B cells[44], direct assessment of candidate human B1 populations[103] in peripheral or, ideally, tissue compartments may be informative. Finally, a key finding in our study is that while the innate B cell compartment is increased in aPIK3CD animals, these cells are unable to manifest normal TI responses. This finding likely explains the near universal failure of APDS subjects to respond to the polyvalent pneumococcal vaccine and, at least in part, the recurrent sinopulmonary infections in these subjects with *Streptococcal pneumoniae.* Notably, a recent study using the oral PI3K-delta inhibitor, leniolisib in 6 APDS patients demonstrated improvement in disease features including reduction in serum IgM, normalization of the peripheral blood B cell phenotype and reduced adenopathy[49]. Together with our findings, these observations suggest that combining leniolisib with delivery of pneumococcal vaccine may provide improved protection from *S. pneumoniae* in these patients; an idea that could be initially assessed in the animal model described here. Finally, while aPIK3CD increases the risk for multiple forms of B cell lymphoma[104], PI3K-delta inhibitors may also increase the risk for genomic instability in malignant B cells[105], suggesting that long-term use of these agents may need to be carefully assessed in this context.

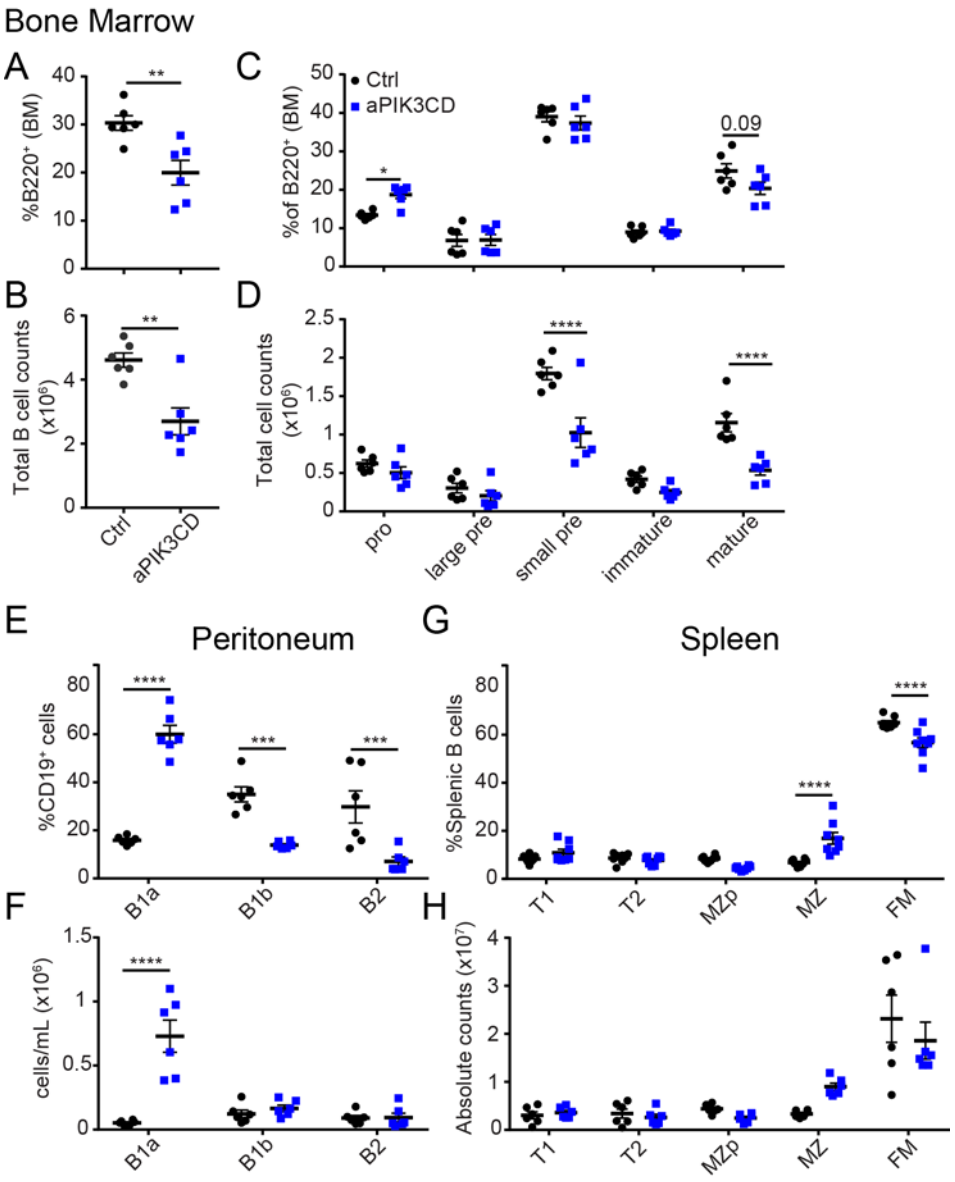

Figure 3-1. Mb1-aPIK3CD mice exhibit BM B lymphopenia and expanded peripheral, innate B cell compartments. A. Frequency and **B.** Absolute cell counts of bone marrow (BM) B cells ($B220^+$) in littermate control (Ctrl) and Mb1-aPIK3CD mice. Significance defined as $P<0.05$ by student's unpaired t-test. **C**. Frequency and **D.** Absolute cell counts of BM B cell subsets (as defined Figure 3-S1G). **E.** Frequency and **F**. Absolute number of peritoneal B cell subsets (see Figure 3-S1H). **G**. Frequency and **H**. Absolute number of splenic B cell subsets (see Figure 3-S1I). A-H: Black: Ctrl mice - animals expressing wildtype *Pik3cd*. Blue: aPIK3CD mice – mice expressing 1 copy of *Pik3cd-E1020K* (hE1021K) restricted to B cell lineage. C-H: Significance defined as $P\leq 0.05$ by 2-way ANOVA. A-F: data representative of 2 independent experiments with 6 Ctrls and 6 aPIK3CD mice all ~12 wks of age. G & H: data representative of 3 independent experiments with 6 Ctrls and 8 aPIK3CD mice all ~12 wks of age.

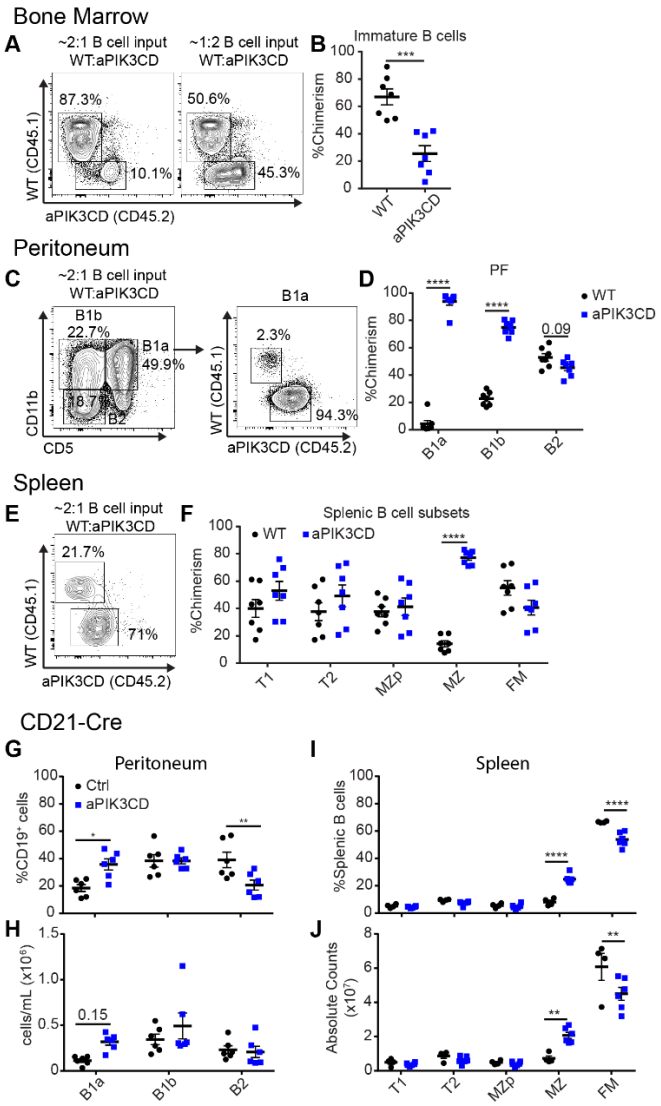

Figure 3-2. aPIK3CD B cells exhibit a competitive disadvantage in the BM but outcompete WT B cells in innate B cell compartments. A-F: WT (CD45.1$^+$) and Mb1-aPIK3CD (CD45.2$^+$) total BM was adoptively transferred into pre-conditioned (CD45.1$^+$/CD45.2$^+$) μMT recipient animals. Recipient animals were sacrificed 12 wks post-transfer. **A**. Representative flow plots of BM B cell chimerism at 12 wks post transfer with (*left panel*) showing experiment using 2:1 ratio of WT to Mb1-aPIK3CD input BM B cells and (*right panel*) showing 1:2 ratio of WT to Mb1-aPIK3CD input BM B cells. **B**. Immature BM B cell chimerism. Significance defined as P<0.05 by student's unpaired t-test. **C.** Representative flow plots of peritoneal B cell subsets (*left panel*) and B1a B cell chimerism (*right panel*) at 12 wks post-transfer of 2:1 ratio of WT to Mb1-aPIK3CD input BM B cells. **D**. Chimerism of peritoneal B cell subsets. **E.** Representative flow plots of splenic MZ B cell chimerism at 12 wks post-transfer of 2:1 ratio of WT to Mb1-aPIK3CD input BM B cells. **F**. Chimerism of splenic B cell subsets. **G-J**: aPIK3CD carrier animals were crossed to the CD21-Cre strain and characterized at ~12 wks of age. **G**. Frequency and **H**. absolute numbers of peritoneal B cell subsets. **I.** Frequency and **J.** absolute numbers of splenic B cell subsets. D, F, & G-J: Significance defined as P≤ 0.05 by 2-way ANOVA. A-B: data representative of two independent experiments with 7 recipients with input BM ratio as shown in A. C-F: data representative of two independent experiments with 7 recipients with 2:1 ratio of WT to Mb1-aPIK3CD input BM B cells. G-J: data representative of two independent experiments with 6 Ctrls and 6 CD21-aPIK3CD mice, 10-12 wks of age.

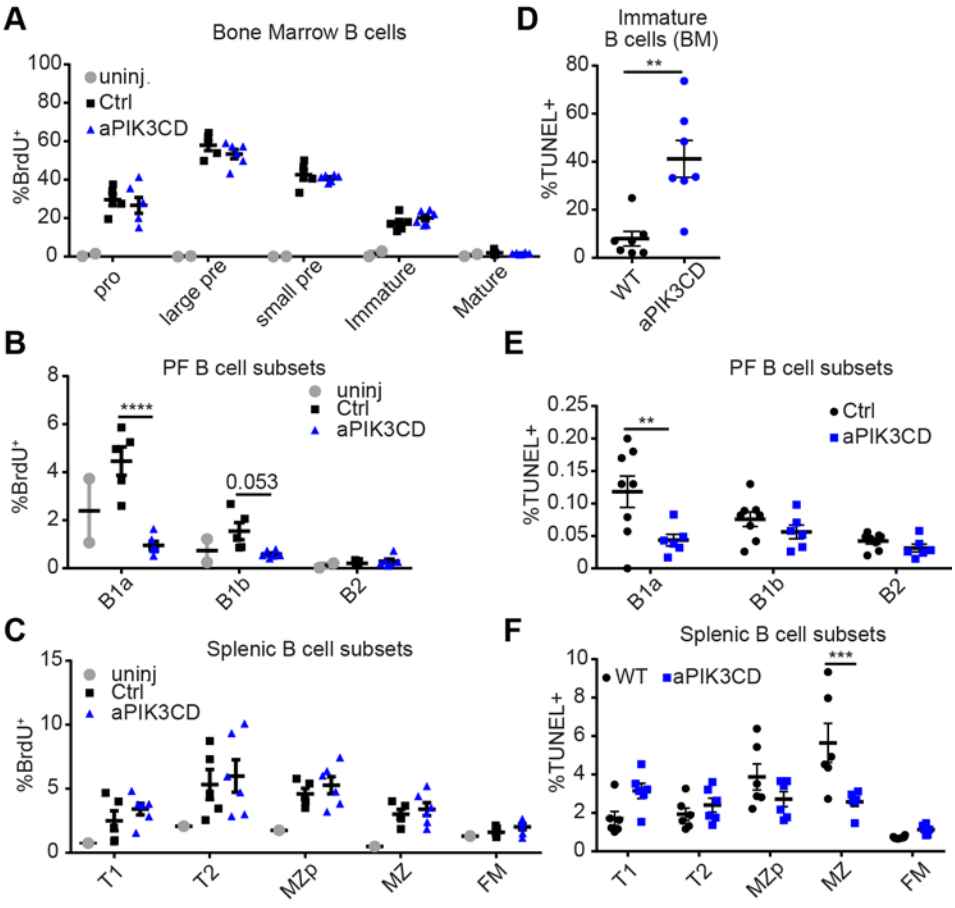

Figure 3-3. aPIK3CD does not alter B cell cycling but differentially impacts survival in immature vs. innate B cell subsets. A-C: Mb1-aPIK3CD and Ctrl mice were injected with 1 mg BrdU i.p. 24 hrs prior to sacrifice. **A**. Percent BrdU$^+$ cells in BM B cell subsets, **B**. percent BrdU$^+$ cells in peritoneal B cell subsets in, and **C**. percent BrdU$^+$ cells in splenic B cell subsets in Mb1-aPIK3CD and Ctrl mice. A-C: data representative of 2 independent experiments with 6 Ctrls and 6 Mb1-aPIK3CD mice injected with BrdU and 2 BrdU uninjected Ctrl mice (12-30 wks of age); significance defined as $P<0.05$ by 2-way ANOVA. **D**. Percent TUNEL$^+$ WT vs. Mb1-aPIK3CD BM immature B cells in μMT recipient animals (12 wks post-transfer with 2:1 and 1:2 ratio of WT to Mb1-aPIK3CD input BM B cells, see Figure 3-2A). Significance defined as $P<0.05$ by student's unpaired t-test. **E**. Percent TUNEL$^+$ cells in peritoneal B cell subsets in 8 Ctrl and 6 CD21-aPIK3CD mice, 12-19 wks of age. **F**. Percent TUNEL$^+$ WT vs. Mb1-aPIK3CD splenic B cell subsets in μMT recipient animals (12 post-transfer with same input as in D). D-F: data representative of 2 independent experiments. E-F: significance defined as $P<0.05$ by 2-way ANOVA.

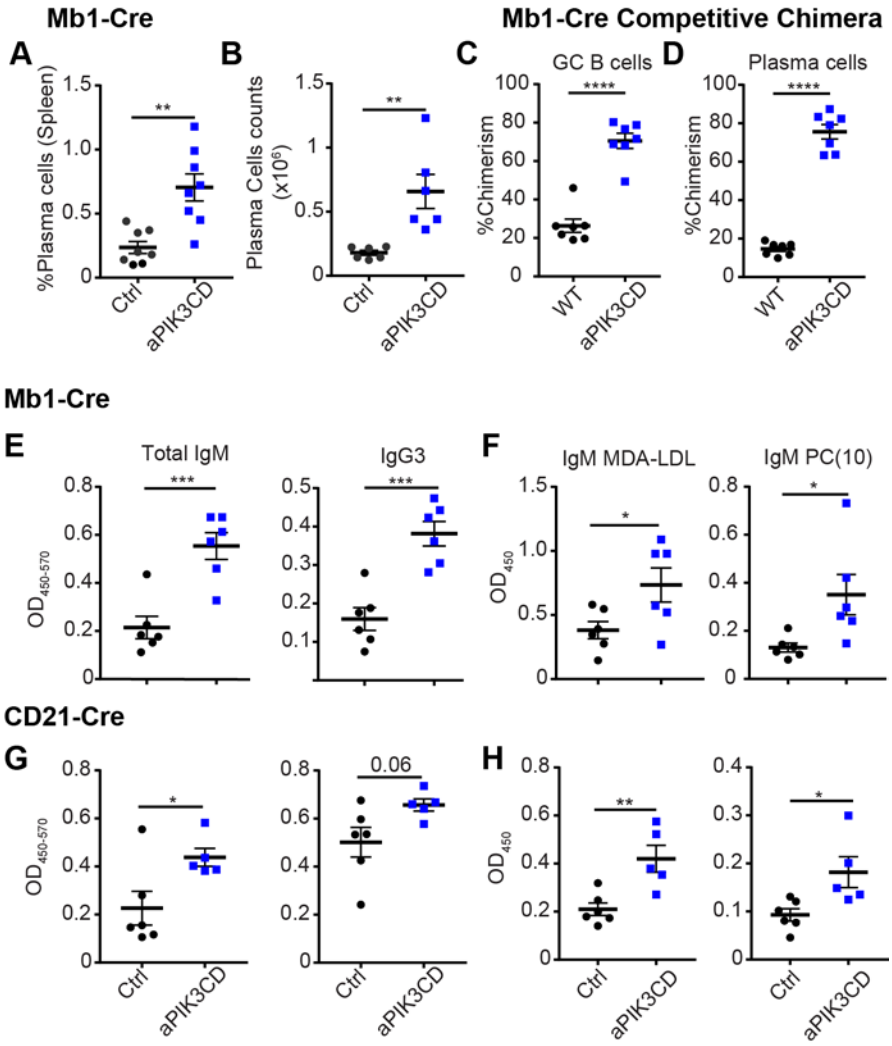

Figure 3-4. aPIK3CD enhances plasma cell differentiation and IgM and IgG3 production in the absence of immunization. A. Frequency and **B**. Absolute number of plasma cells (PCs, $B220^{-}CD138^{+}$) in the spleen of unimmunized Mb1-aPIK3CD and Ctrl mice. **C**. Chimerism of germinal center ($B220^{+}CD95^{hi}CD38^{lo}$) B cells and **D**. Plasma cells in the spleen of μMT recipient animals (12 wks post-transfer with 2:1 ratio of WT vs. Mb1-aPIK3CD input BM B cells). **E**. Optical density of serum IgM (*left panel*) and IgG3 (*right panel*) in Ctrl vs Mb1-aPIK3CD mice. **F.** Optical density of serum MDA-LDL- (l*eft panel*) and PC(10)-specific IgM (*right panel*) in Ctrl vs Mb1-aPIK3CD mice. **G.** Optical density of serum IgM (*left panel*) and IgG3 (*right panel*) in Ctrl vs CD21-aPIK3CD mice. **H.** Optical density of serum MDA-LDL-(*left panel*) and PC(10)- specific IgM (*right panel*) in Ctrl vs CD21-aPIK3CD mice . Significance defined as $P<0.05$ by unpaired student's t-test. A-B, E-F: data representative of 2 independent experiments with 6 Ctrls vs 6 Mb1-aPIK3CD mice. C-D: data representative of two independent experiments with 7 μMT recipient animals. G&H: data representative of 2-independent experiments with 6 Ctrls vs 6 CD21-aPIK3CD mice. Ctrls (controls) were cre-negative littermates at 18 wks of age.

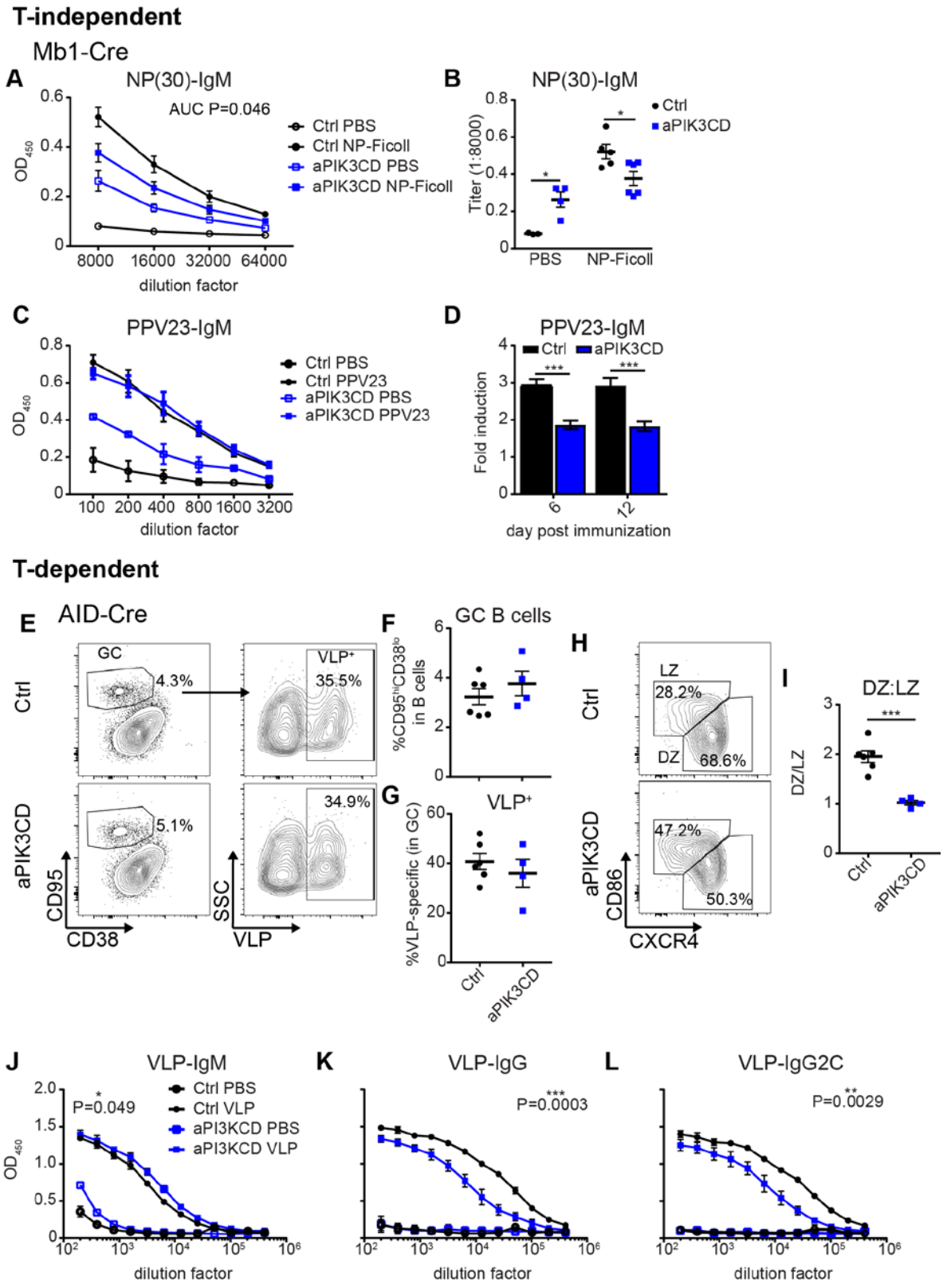

Figure 3-5. B cell intrinsic aPIK3CD expression limits both TI and TD humoral responses. A-B: Ctrl and Mb1-aPIK3CD mice were injected i.p. with 50ug NP-Ficoll or PBS and sacrificed 7 days post

immunization. **A**. Dilution curves of low affinity (NP-30) antigen-specific IgM in serum at 7 days post immunization. Significance defined as P<0.05 using student's t-test testing area under the curve (AUC) with baseline of 0.0415. Open black circles: Ctrl injected with PBS; filled black circles: Ctrl injected with NP-Ficoll; open blue squares: Mb1-aPIK3CD injected with PBS; filled blue squares: Mb1-aPIK3CD injected with NP-Ficoll. **B**. End-point titers of low affinity (NP-30) antigen-specific IgM at 1:8000 serum dilution. Significance defined as P<0.05 by student's t-test. A-B: data representative of 2 independent experiments with 3 Ctrl mice injected with PBS and 5 injected with NP-Ficoll, 4 Mb1-aPIK3CD injected with PBS and 6 injected with NP-Ficoll. **C-D:** Ctrl and Mb1-aPIK3CD mice were injected i.p. with 0.125ug Pneumovax23 or PBS. **C**. Dilution curves of Pneumovax23 (PPV23)-specific IgM in serum at 6 days post immunization. Black open circles: Ctrl PBS injected (N=2); Black filled circles: Ctrl PPV23 injected (N=7); Blue open squares: Mb1-aPIK3CD PBS injected (N=2); Blue filled squares: Mb1-aPIK3CD PPV23 injected (N=5). **D**. Fold induction of PPV23-IgM over baseline (Day 0) OD_{450} for day 6 and 12 post-immunization with PPV23. Black: Ctrl PPV23 injected mice, blue: Mb1-aPIK3CD PPV23 injected mice. Significance defined as P<0.05 by 2-way ANOVA. Data representative of 2 independent experiments with mice 19-21 weeks of age. **E-L:** Ctrl and AID-aPIK3CD mice were injected i.p. with PBS or 2ug of virus-like particles (VLPs) containing TLR7 ligand in 250ul and sacrificed 14 days post immunization. **E**. Representative flow plots of (*left*) GC B cells ($B220^{+}CD95^{hi}CD38^{lo}$) and (*right*) VLP-specific cells (VLP^{+}) within the GC at 14 days post immunization. *Top panels*: Ctrl; *bottom panels*: AID-aPIK3CD. **F**. Frequency of GC B cells and **G**. VLP-specific cells in GC at 14 days post immunization. *Black*: Ctrl, *blue*: AID-aPIK3CD. **H**. Representative flow plots of dark zone ($CXCR4^{+}CD86^{-}$) vs light zone ($CXCR4^{-}CD86^{+}$) GC B cells from (*top*) Ctrl and (*bottom*) AID-aPIK3CD mice at 14 days post immunization. **I**. Ratio of DZ:LZ within GC in Ctrl (black) vs AID-aPIK3CD (blue) mice. Significance defined as P<0.05 using student's t-test. Dilution curves of serum VLP-specific-**(J)** IgM, **(K).** IgG & **(L)** IgG2C. P-value calculated by student's t-test of area under the curve (AUC) (baseline of 0). E-L: data representative of 2 independent experiments with 6 Ctrl mice injected with VLPs and 2 injected with PBS, and 4 AID-aPIK3CD mice injected with VLPs and 2 injected with PBS 13-16 wks of age.

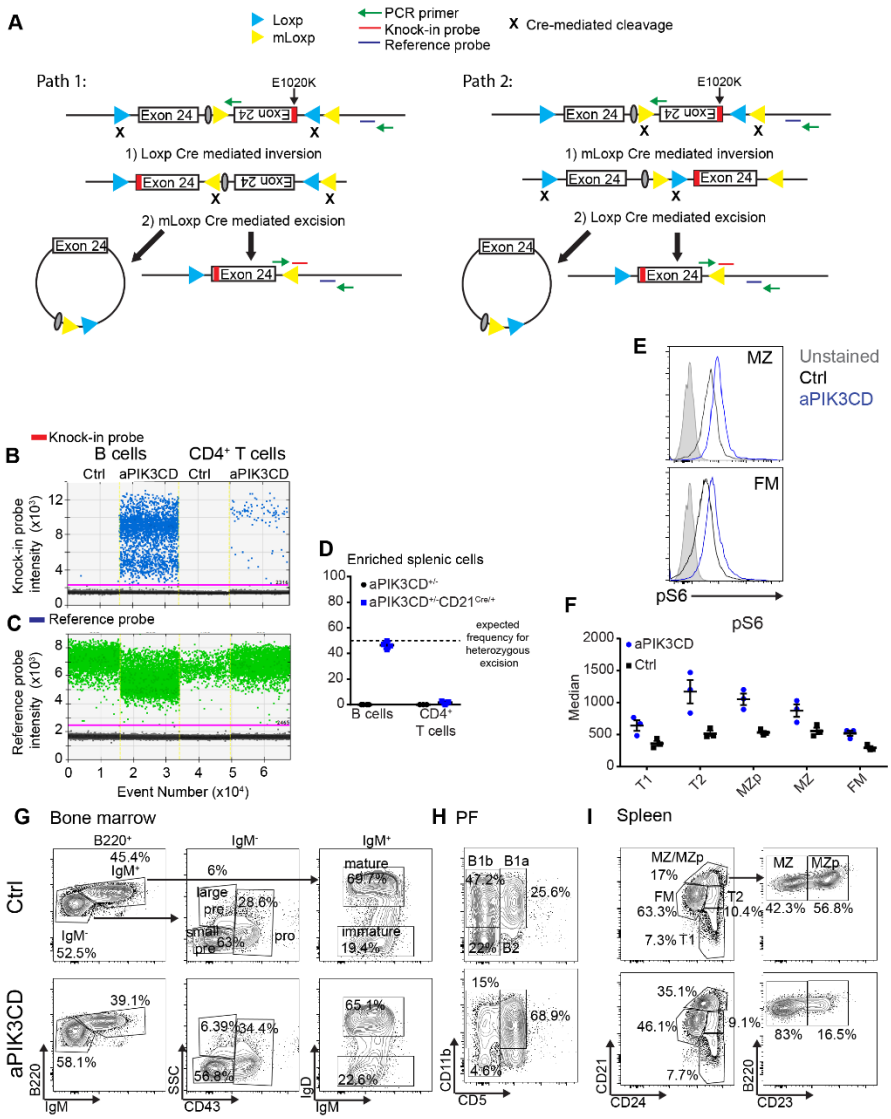

Figure 3-S1. Inducible PIK3CD-E1020K (aPIK3CD) murine model and representative gating strategies to identify B cell subsets in B-cell specific aPIK3CD models. A: Schematic of endogenous *Pik3cd* locus with Loxp-flanked endogenous exon 24 with a downstream mLoxp-flanked mutant exon 24 in the opposite orientation of transcription (3'→5'). Upon Cre mediated excision flipping/inversion of mutant exon24 and excision of endogenous exon 24 can occur by two paths: Path 1) *(left*) Cre-mediated cleavage at Loxp sites causes flipping/inversion of mutant and endogenous exon 24, followed by cre-mediated cleavage at mLoxp sites that results in excision of endogenous exon 24; Path 2) (*right*) Cre-mediated cleavage at mLoxp sites causes flipping/inversion of mutant exon 24, followed by cre-mediated cleavage at Loxp sites leading to excision of endogenous exon 24. The end result of these events is fixed inversion of mutant exon 24 into the correct orientation for transcription to proceed (5'→3'). Yellow triangles: mutant mLoxp sites, blue triangles: Loxp sites. Green arrows indicate droplet digital (dd)PCR primer binding sites. Red line indicates knock-in ddPCR probe binding site. Blue line indicates reference ddPCR probe binding site. X indicates site of cre-mediated cleavage. **B-D**: B220^{+} splenic B and CD4^{+} T cells were purified by positive selection from 12-19 week old CD21$^{Cre/+}$aPIK3CD$^{+/-}$ and aPIK3CD$^{+/-}$ mice and used for ddPCR assay. **B-C**: Representative figures showing 1 dimensional amplitude ddPCR results for B cells and CD4^{+} T cells. Blue droplets in **B.** show binding to the knock-in junction probe. Green droplets in **C.** shows binding to the reference probe **D.** Frequency of knock-in probe binding normalized to reference probe binding. Expected frequency of an aPIK3CD heterozygote mouse is ~50% (dashed line)

in the presence of Cre. **E**. pS6 in unstimulated MZ (*top*) and FM (*bottom*) splenic B cells. *Filled grey histogram*: unstained control, *open histograms: black* – ctrl and *blue* – Mb1-aPIK3CD. **F**. Median fluorescence intensity of pS6 in splenic B cell subsets in Mb1-aPIK3CD and control mice. Data shown are representative of 1 of 2 independent experiments with 6 Ctrls and 6 Mb1-aPIK3CD mice. **G-I:** Representative flow cytometry-based gating strategies to identify B cell subsets in Mb1-aPIK3CD and control mice. **G.** Gating strategy for bone marrow B cell subsets. Total B cells ($B220^+$ cells) within the viable, lymphocyte gate (with doublets excluded) were gated as shown to identify: pro- ($B220^+IgM^-CD43^+$), large pre- ($B220^+IgM^-CD43^-SSC^{hi}$), small pre- ($B220^+IgM^-CD43^-SSC^{lo}$), immature ($B220^+IgM^+IgD^-$), and mature ($B220^+IgM^+IgD^+$) B cells. **H**. Gating strategy for B cell subsets in peritoneal fluid. Total B cells ($CD19^+$ cells) within the viable, lymphocyte gate (with doublets excluded) were next gated on total $CD19^+$cells and $CD11b^{hi}$ myeloid cells were excluded. B cell subsets were subsequently defined as: B1a ($CD19^+CD11b^+CD5^+$), B1b ($CD19^+CD11b^+CD5^-$), and B2 ($CD19^+CD11b^-CD5^-$) B cells. **I**. Gating strategy for splenic B cell subsets. Total B cells ($B220^+CD24^+$) within the viable, lymphocyte gate (with doublets excluded) were gated as shown to identify: early transitional, T1 ($B220^+CD24^+CD21^{lo}$), late transitional, T2 ($B220^+CD24^+CD21^{int}$), marginal zone precursor, MZp ($B220^+CD24^+CD21^{hi}CD23^+$), marginal zone, MZ ($B220^+CD24^+CD21^{hi}CD23^-$), and follicular mature, FM ($B220^+CD24^{int}CD21^{int}$) B cells. G-I: (top) Control and (bottom) aPIK3CD.

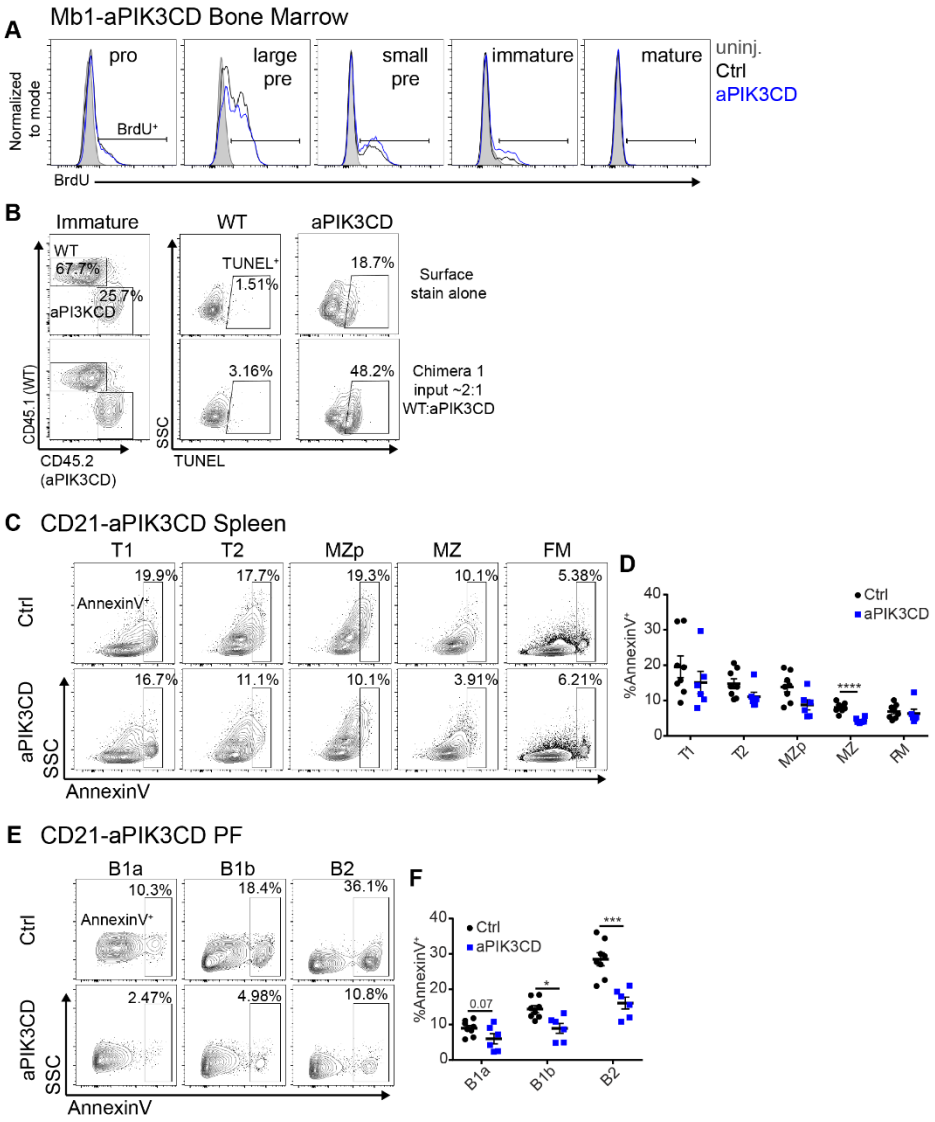

Figure 3-S2. Analysis of B cell cycling and survival in B-cell specific aPIK3CD models. A. Representative histogram overlays of BrdU$^+$ cells within each BM B cell subset showing uninjected control (grey filled histogram) and BrdU-labeled Ctrl (black open histogram) and Mb1-aPIK3CD (blue open histogram) cells. Data is representative of 2 independent experiments. **B**. Representative flow plots from competitive chimera animals assessing cell survival in immature BM B cells. Plots shown depict: L*eft panels,* the relative frequency of WT (CD45.1) vs. Mb1-aPIK3CD (CD45.2) immature BM B cells (B220$^+$IgM$^+$IgD$^-$); *Bottom, middle and right panels,* the frequency of apoptotic cells (TUNEL$^+$) within WT vs. Mb1-aPIK3CD immature B cells, respectively; and *Top, middle and right panels,* WT vs, Mb1-aPIK3CD immature B cells, respectively, not subjected to TUNEL staining shown as a negative control. **C**. Representative flow plots of apoptotic cells (AnnexinV$^+$) within splenic B cell subsets. **D.** Quantification of frequency of apoptotic cells (AnnexinV$^+$) within splenic B cell subsets. **E**. Representative flow plots of apoptotic cells (AnnexinV$^+$) within peritoneal B cell subsets. **F.** Quantification of frequency of apoptotic cells (AnnexinV$^+$) within splenic B cell subsets. C-F: Data representative of 2 independent experiments with 8 Ctrls and 6 CD21-aPIK3CD mice. C&E: (top panels) Ctrl and (bottom panels) CD21-aPIK3CD mice. Significance defined as P<0.05, calculated by unpaired student's t test.

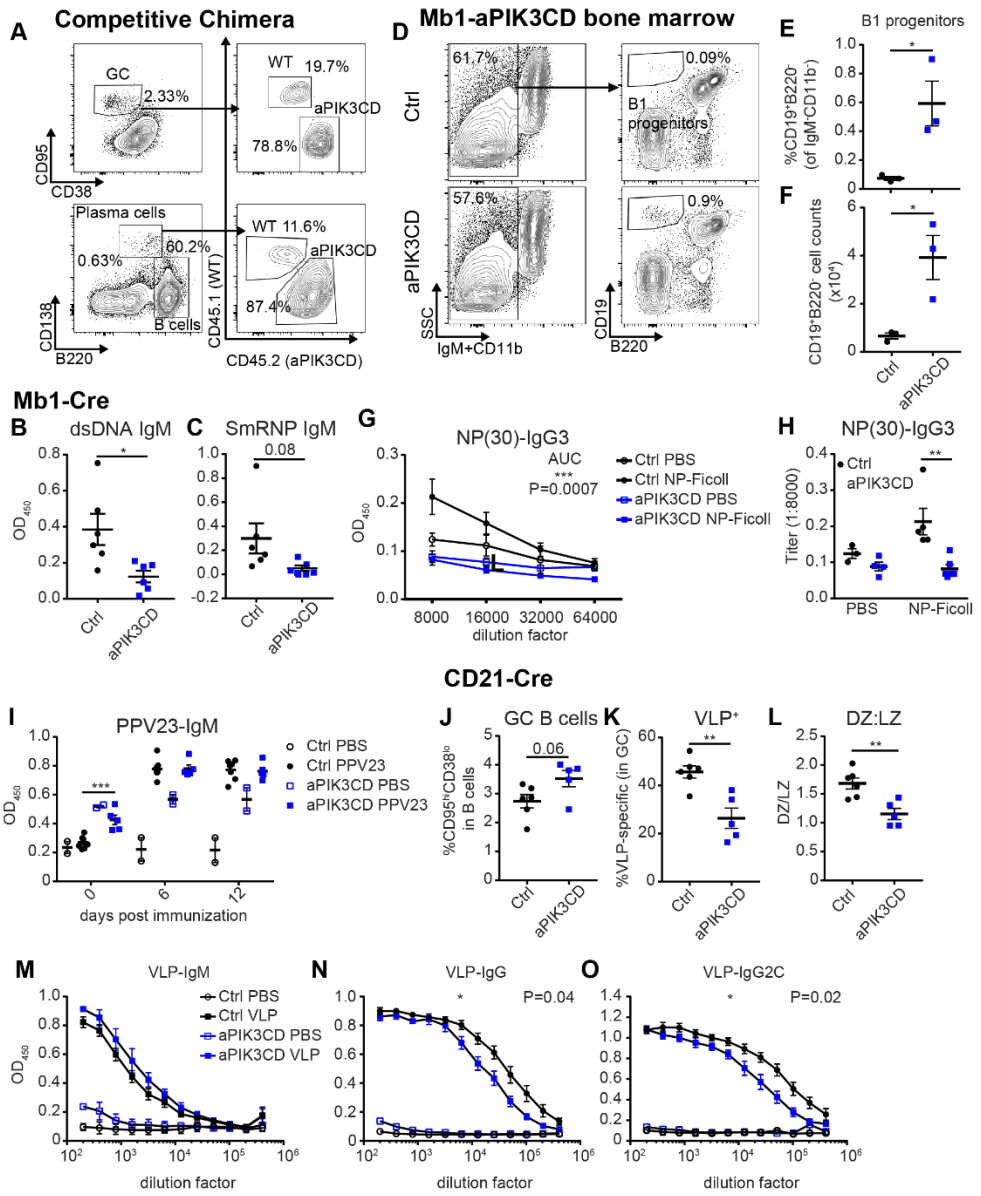

Figure 3-S3. Selection for GC, plasma B cells and B1 progenitors, natural IgM specificities, and TI-II IgG3 responses in B-cell specific aPIK3CD models. **A**. Representative flow plots of WT and aPIK3CD chimerism in (*top panels*) GC B cells ($B220^{+}CD95^{hi}CD38^{lo}$) and (*bottom panels*) plasma cells ($B220^{-}CD138^{+}$). Data representative of 2 independent experiments with 7 recipient animals (CD45.1/CD45.2) at 12 weeks post adoptive transfer of B cells at a 2:1 ratio of WT (CD45.1) to aPIK3CD (CD45.2) within donor BM. **B**. dsDNA reactive IgM and **C**. SmRNP reactive IgM optical density in Ctrl (black) and Mb1-aPIK3CD (blue) mice 12-13 weeks of age at 1:200 serum dilution. B-C: Data representative of 2 independent experiments with 6 Ctrls and 6 Mb1-a mice, significance defined as $P<0.05$ by unpaired student's t-test. **D**. Representative flow plots of B1 progenitors ($CD19^{+}B220^{-}CD11b^{-}IgM^{-}$) in BM of Ctrl (*top panels*) and Mb1-aPIK3CD (*bottom panels*) mice. **E**. Frequency of B1 progenitors in BM. **F**. Absolute cell counts of B1 progenitors in BM. D-F: data is representative of 1 experiment with 3 Ctrls (black) and 3 Mb1-a (blue) mice ~12 wks of age. Significance defined as $P<0.05$ by student's t-test. **G**. Serum dilution curves of antigen-specific (NP-30) IgG3 at 7 days post injection with PBS or NP-Ficoll. Unpaired student's t-test of area under the curve (AUC, baseline=0.0362), with significance defined as $P<0.05$. **H**. End-point titers of antigen-specific (NP-30) IgG3 of 1:8000 serum dilution at 7 days post

injection. Significance defined as P<0.05, calculated by 2-way ANOVA. D-E: Data representative of 2 independent experiments with 3 PBS and 5 NP-Ficoll injected Ctrls and 4 PBS and 6 NP-Ficoll injected Mb1-aPIK3CD mice. **I.** Optical density (OD_{450}) of Pneunovax23 (PPV23) reactive IgM in serum at day 0, 6, and 12 post immunization. Black open circles: Ctrl PBS injected (N=2); Black filled circles: Ctrl PPV23 injected (N=7); Blue open squares: Mb1-aPIK3CD PBS injected (N=2); Blue filled squares: Mb1-aPIK3CD PPV23 injected (N=5). **J-O**: Ctrl and CD21-aPIK3CD mice were injected i.p. with PBS or 2ug of virus-like particles (VLPs) containing TLR7 ligand in 250ul and sacrificed 14 days post immunization. **J**. Frequency of GC B cells and **K**. VLP-specific cells in GC, and **L**. DZ to LZ ratio within GC at 14 days post immunization. *Black*: Ctrl, *blue*: CD21-aPIK3CD. Significance defined as P<0.05 using student's t-test. Dilution curves of serum VLP-specific- **(M)** IgM, **(N).** IgG and **(O)** IgG2C. P-value calculated by student's t-test of area under the curve (AUC) (baseline of 0). I-L: data representative of 2 independent experiments with 6 Ctrl mice injected with VLPs and 5 CD21-aPIK3CD mice injected with VLPs 13-16 wks of age.

Chapter 4

Concluding Remarks

GOF mutations in signaling pathways downstream of the BCR are commonly found in malignancies, propagating the development and survival of malignant cells[10]. In the case of DLBCL, somatic mutations are the drivers of disease, however, the accumulation of multiple oncogenic events contribute to the pathology of disease. In this setting it is difficult to deconvolute the contributions of individual mutations in driving and or supporting malignant cells. Analysis of single mutants can help identify not only the initiating mutations that occur early in lymphomagenesis, but also gives us a better understanding of how a single mutant can perturb the immune response. We now appreciate that germline GOF mutations can also drive monogenic primary immunodeficiencies, such as BENTA and APDS. In both of these PIDs, heterozygous, dominant activating mutations result in both defective development and functionality of immune cells[24].

While patients with BENTA and APDS present with many shared clinical features (Table 1), the underlying mechanism for such features is distinct in each disease. BENTA patients display an expanded B cell compartment, whereas APDS patients are B cell lymphopenic. However, both groups have deficiencies in switched memory-B cells, have an increased proportion of transitional B cells in circulation and are at increased risk of developing B cell malignancies. The T cell compartment in these patients has been rendered non-functional: T cells in BENTA patients are anergic, and T cells in APDS patients are senescent. Murine models of lineage, restricted activated CARD11 and PI3K provides insight into how these GOF mutations contribute to disease.

Data from murine studies shows, activated CARD11 has a profound impact on innate B cell populations during B cell development, and significantly perturbs the T-dependent germinal center response. Mice expressing aCARD11 from early stages of B cell development (Mb1-Cre) show a complete loss of B1a B cells in the peritoneum, decreased B1 progenitors in the bone marrow (data not shown), and a diminished frequency of MZ B cells in the spleen. These animals also display diminished serum IgM titers, with a trend towards decreased IgG. BENTA patients present with decreased serum IgM

levels and IgG levels within the low-normal range, similar to our mouse model. BENTA patients fail to respond to polysaccharide-based vaccination strategies (T-independent vaccination), which normally drive T-independent antibody protection against infection. Because of this defect, BENTA patients suffer from recurrent sinopulmonary infections. Our murine data suggests that the innate B cell populations responsible for mounting T-independent responses are absent and/or diminished in BENTA patients. Alternatively, these populations may be present but impaired, however, our murine data suggests this is not the case. Difficulties in taking tissue samples that are representative of the spleen and pleural cavities, as well as a lack of well-defined markers for innate B cell populations in humans, are roadblocks in addressing the hypothesis that BENTA patients lack innate B cell populations. Whether treatment of these patients with NF-κB inhibitors would be able to correct the failure of BENTA patients to respond to T-independent vaccines is unknown. However, if the loss of innate B cell is due to a developmental defect, treatment with NF-κB inhibitors at or around the time of vaccination is unlikely to correct the failed T-independent response. Correcting the absence of B1 progenitors may be a more productive line of inquiry yet may be insufficient to correct the impact on immune function. Another avenue would be based on utilizing CRISPR technology to edit the mutated CARD11, reverting it back to wildtype, in hematopoietic stem cells for autologous transplantation.

APDS patients also fail to respond to T-independent vaccination and have recurrent sinopulmonary infections. APDS patients also suffer from progressive airway damage, most likely as a result of failure to clear infections, and exhibit hyper-IgM in serum, with decreased switched antibodies. Our murine data shows a significant increase in serum IgM titers, as well as heightened IgG3, when expressed in all B cells, and when restricted to peripheral B cells. Correlating with hyper IgM in both murine models, we also observed increased MZ and B1a compartments in both models as well. Of note, B1 progenitors were expanded in the Mb1-Cre model as well. Thus, aPIK3CD supports enhanced development of innate B cell populations during early stages of B cell development, however, hyperactivated PI3K signaling in the periphery is sufficient to drive the expansion of innate B cells. Despite having an expansion of innate B cells our aPIK3CD mice have impaired T-independent responses. Because we find expanded innate B cell populations in the CD21-Cre model, this points

towards a developmental defect not being the root cause of blunted T-independent responses. A recent publication showed inhibition of PI3K can partially restore functionality of B cells with *PIK3CD* GOF. Treatment of transitional B cells, from patients with *PIK3CD* GOF mutations, with the p110δ specific inhibitor, leniolisb, enhanced secretion of switched antibodies following *in vitro* stimulation[106]. PI3K inhibition may restore functionality of innate B cells as hyperactive PI3K may block terminal differentiation to antibody secreting cells (ASCs). The finding that *PIK3CD* GOF transitional B cells are unable to acquire or maintain a plasmablast phenotype and gene signature following *in vitro* stimulation, together with their decreased down-regulation of Pax5 support this hypothesis[106]. *PIK3CD* GOF transitional B cells were also found to have heightened expression of IL-10 by microarray[106], which acts as a growth/differentiation factor for human B cells[107]. The expanded innate B cells in our aPIK3CD mice potentially fail to terminally differentiate in response to T-independent immunization, and may rather form IL-10 secreting, suppressive B cells. If this is the case, this may be partially responsible for the recurrent sinopulmonary infections and failure to respond to T-independent vaccines. We are currently pursuing this line of inquiry in addition to studies involving treatment with leniolisib within the context of a T-independent immunization to determine whether we can restore responsiveness to this type of immunization.

Defects in the T cell compartments likely contribute to BENTA and APDS patients suffering from chronic viral infections. The T cells in BENTA patients are anergic, while in APDS the $CD8^+$ T cells are senescent and naïve $CD4^+$ T cells are decreased. However, the T-dependent response may be altered due to B cell intrinsic changes as well. Our mouse model of aCARD11 demonstrates how B cell intrinsic aCARD11 results in a premature peak of the GC response followed by rapid contraction. The premature collapse of the GC is accompanied by an expansion of what we hypothesize are short-lived plasma cells. Our mouse data, taken together with the observation that B cells from BENTA patients, while capable of becoming short-lived plasma cells, fail to terminally differentiate into long-lived plasma cells[23], supports the hypothesis that aCARD11 drives short-lived plasma cell formation. GC B cells from our aCARD11 mouse model demonstrate heightened mTORC1 signaling. It has been shown that GC B cells with hyperactive mTORC1 signaling are outcompeted by wildtype B cells overtime, demonstrating how

hyperactive mTORC1 signaling may be detrimental to a productive germinal center response[59]. The premature collapse of the GC in our activated CARD11 mouse model may be due to combined elevated NF-κB and mTORC1 signaling driving cells out of the GC. Dampening either signaling pathway, or both, may rescue the premature collapse of the GC or alternatively result in a more rapid collapse of the GC. The timing of such inhibition of either pathway will be difficult to elucidate as both pathways have been shown to be temporally regulated throughout the time a B cell is sequestered within the GC.

Our aPIK3CD mouse studies showed no such alteration in GC kinetic (data not shown), rather there was a clear block in formation of switched ASCs. Thus, the diminished switched-memory B cell population in APDS may be attributed to B cell intrinsic dysregulated signaling. Treatment with leniolisib is an attractive avenue for rescuing CSR in our mouse model, however it has been shown that the increase in AID after PI3K inhibition results in heightened genomic instability[105]. Though ~40-50% of DLBCL cases display activated PI3K/AKT/mTOR signaling[108] and ~20% of APDS patients develop lymphoma, continuous PI3K inhibition does not appear to be a viable treatment option. Our murine data implies that APDS patients are predisposed to lymphomagenesis due to increased survival rather than heightened proliferation of B cells. Thus, targeting pro-survival factors, such as Bcl-2, may be a better treatment option in the long-term, or dual targeting of both PI3K and Bcl-2 as well. However, we did not assess proliferation during an immune response, which could result in dysregulated cycling and promote lymphomagenesis.

Similar to APDS patients, GOF in CARD11 drives lymphoproliferation in the B cell compartment in BENTA patients predisposing them to lymphomagenesis. However, it is not thought that mutant CARD11 alone is sufficient to drive lymphomagenesis[22, 68], which is supported by our murine data. One BENTA patient that did go on to develop lymphoma was found to have acquired an additional oncogenic hit. We are currently studying a murine model of compound oncogenic hits, aCARD11 and Blimp1 deletion, which blocks terminal differentiation, to determine how aCARD11 collaborates with other oncogenic events to promote lymphomagenesis. The combined data from these studies demonstrates how the B cell lineage is impacted by dysregulated CARD11 and PI3K signaling and sheds light on

similarities and differences in clinical phenotypes of patients with GOF mutations in these signaling molecules.

References:

1. Mesin, L., J. Ersching, and G. D. Victora. 2016. Germinal Center B Cell Dynamics. *Immunity* 45: 471-482.
2. Shih, T. A., M. Roederer, and M. C. Nussenzweig. 2002. Role of antigen receptor affinity in T cell-independent antibody responses in vivo. *Nat Immunol* 3: 399-406.
3. Shih, T. A., E. Meffre, M. Roederer, and M. C. Nussenzweig. 2002. Role of BCR affinity in T cell dependent antibody responses in vivo. *Nat Immunol* 3: 570-575.
4. Obukhanych, T. V., and M. C. Nussenzweig. 2006. T-independent type II immune responses generate memory B cells. *J Exp Med* 203: 305-310.
5. Dominguez-Sola, D., J. Kung, A. B. Holmes, V. A. Wells, T. Mo, K. Basso, and R. Dalla-Favera. 2015. The FOXO1 Transcription Factor Instructs the Germinal Center Dark Zone Program. *Immunity* 43: 1064-1074.
6. Vallabhapurapu, S., and M. Karin. 2009. Regulation and function of NF-kappaB transcription factors in the immune system. *Annu Rev Immunol* 27: 693-733.
7. Shinohara, H., and T. Kurosaki. 2009. Comprehending the complex connection between PKCbeta, TAK1, and IKK in BCR signaling. *Immunol Rev* 232: 300-318.
8. Egawa, T., B. Albrecht, B. Favier, M. J. Sunshine, K. Mirchandani, W. O'Brien, M. Thome, and D. R. Littman. 2003. Requirement for CARMA1 in antigen receptor-induced NF-kappa B activation and lymphocyte proliferation. *Curr Biol* 13: 1252-1258.
9. Newton, K., and V. M. Dixit. 2003. Mice lacking the CARD of CARMA1 exhibit defective B lymphocyte development and impaired proliferation of their B and T lymphocytes. *Curr Biol* 13: 1247-1251.
10. Shaffer, A. L., R. M. Young, and L. M. Staudt. 2012. Pathogenesis of human B cell lymphomas. *Annu Rev Immunol* 30: 565-610.
11. Sommer, K., B. Guo, J. L. Pomerantz, A. D. Bandaranayake, M. E. Moreno-García, Y. L. Ovechkina, and D. J. Rawlings. 2005. Phosphorylation of the CARMA1 linker controls NF-kappaB activation. *Immunity* 23: 561-574.
12. Turvey, S. E., A. Durandy, A. Fischer, S. Y. Fung, R. S. Geha, A. Gewies, T. Giese, J. Greil, B. Keller, M. L. McKinnon, B. Neven, J. Rozmus, J. Ruland, A. L. Snow, P. Stepensky, and K. Warnatz. 2014. The CARD11-BCL10-MALT1 (CBM) signalosome complex: Stepping into the limelight of human primary immunodeficiency. *J Allergy Clin Immunol* 134: 276-284.
13. Greil, J., T. Rausch, T. Giese, O. R. Bandapalli, V. Daniel, I. Bekeredjian-Ding, A. M. Stütz, C. Drees, S. Roth, J. Ruland, J. O. Korbel, and A. E. Kulozik. 2013. Whole-exome sequencing links caspase recruitment domain 11 (CARD11) inactivation to severe combined immunodeficiency. *J Allergy Clin Immunol* 131: 1376-1383.e1373.
14. Ma, C. A., J. R. Stinson, Y. Zhang, J. K. Abbott, M. A. Weinreich, P. J. Hauk, P. R. Reynolds, J. J. Lyons, C. G. Nelson, E. Ruffo, B. Dorjbal, S. Glauzy, N. Yamakawa, S. Arjunaraja, K. Voss, J. Stoddard, J. Niemela, S. D. Rosenzweig, J. J. McElwee, T. DiMaggio, H. F. Matthews, N. Jones, K. D. Stone, A. Palma, M. Oleastro, E. Prieto, A. R. Bernasconi, G. Dubra, S. Danielian, J. Zaiat, M. A. Marti, B. Kim, M. A. Cooper, N. Romberg, E. Meffre, E. W. Gelfand, A. L. Snow, and J. D. Milner. 2017. Germline hypomorphic CARD11 mutations in severe atopic disease. *Nat Genet* 49: 1192-1201.
15. Altin, J. A., L. Tian, A. Liston, E. M. Bertram, C. C. Goodnow, and M. C. Cook. 2011. Decreased T-cell receptor signaling through CARD11 differentially compromises forkhead box protein 3-positive regulatory versus T(H)2 effector cells to cause allergy. *J Allergy Clin Immunol* 127: 1277-1285.e1275.

16. Hamilton, K. S., B. Phong, C. Corey, J. Cheng, B. Gorentla, X. Zhong, S. Shiva, and L. P. Kane. 2014. T cell receptor-dependent activation of mTOR signaling in T cells is mediated by Carma1 and MALT1, but not Bcl10. *Sci Signal* 7: ra55.
17. Küppers, R. 2005. Mechanisms of B-cell lymphoma pathogenesis. *Nat Rev Cancer* 5: 251-262.
18. Pasqualucci, L., and B. Zhang. 2016. Genetic drivers of NF-κB deregulation in diffuse large B-cell lymphoma. *Semin Cancer Biol* 39: 26-31.
19. Lenz, G., R. E. Davis, V. N. Ngo, L. Lam, T. C. George, G. W. Wright, S. S. Dave, H. Zhao, W. Xu, A. Rosenwald, G. Ott, H. K. Muller-Hermelink, R. D. Gascoyne, J. M. Connors, L. M. Rimsza, E. Campo, E. S. Jaffe, J. Delabie, E. B. Smeland, R. I. Fisher, W. C. Chan, and L. M. Staudt. 2008. Oncogenic CARD11 mutations in human diffuse large B cell lymphoma. *Science* 319: 1676-1679.
20. Staudt, L. M. 2010. Oncogenic activation of NF-kappaB. *Cold Spring Harb Perspect Biol* 2: a000109.
21. Ngo, V. N., R. E. Davis, L. Lamy, X. Yu, H. Zhao, G. Lenz, L. T. Lam, S. Dave, L. Yang, J. Powell, and L. M. Staudt. 2006. A loss-of-function RNA interference screen for molecular targets in cancer. *Nature* 441: 106-110.
22. Snow, A. L., W. Xiao, J. R. Stinson, W. Lu, B. Chaigne-Delalande, L. Zheng, S. Pittaluga, H. F. Matthews, R. Schmitz, S. Jhavar, S. Kuchen, L. Kardava, W. Wang, I. T. Lamborn, H. Jing, M. Raffeld, S. Moir, T. A. Fleisher, L. M. Staudt, H. C. Su, and M. J. Lenardo. 2012. Congenital B cell lymphocytosis explained by novel germline CARD11 mutations. *J Exp Med* 209: 2247-2261.
23. Arjunaraja, S., B. D. Nosé, G. Sukumar, N. M. Lott, C. L. Dalgard, and A. L. Snow. 2017. Intrinsic Plasma Cell Differentiation Defects in B Cell Expansion with NF-κB and T Cell Anergy Patient B Cells. *Front Immunol* 8: 913.
24. Arjunaraja, S., and A. L. Snow. 2015. Gain-of-function mutations and immunodeficiency: at a loss for proper tuning of lymphocyte signaling. *Curr Opin Allergy Clin Immunol* 15: 533-538.
25. Jeelall, Y. S., J. Q. Wang, H. D. Law, H. Domaschenz, H. K. Fung, A. Kallies, S. L. Nutt, C. C. Goodnow, and K. Horikawa. 2012. Human lymphoma mutations reveal CARD11 as the switch between self-antigen-induced B cell death or proliferation and autoantibody production. *J Exp Med* 209: 1907-1917.
26. Rui, L., R. Schmitz, M. Ceribelli, and L. M. Staudt. 2011. Malignant pirates of the immune system. *Nat Immunol* 12: 933-940.
27. Knies, N., B. Alankus, A. Weilemann, A. Tzankov, K. Brunner, T. Ruff, M. Kremer, U. B. Keller, G. Lenz, and J. Ruland. 2015. Lymphomagenic CARD11/BCL10/MALT1 signaling drives malignant B-cell proliferation via cooperative NF-κB and JNK activation. *Proc Natl Acad Sci U S A* 112: E7230-7238.
28. Marshall, A. J., H. Niiro, T. J. Yun, and E. A. Clark. 2000. Regulation of B-cell activation and differentiation by the phosphatidylinositol 3-kinase and phospholipase Cgamma pathway. *Immunol Rev* 176: 30-46.
29. Jou, S. T., N. Carpino, Y. Takahashi, R. Piekorz, J. R. Chao, D. Wang, and J. N. Ihle. 2002. Essential, nonredundant role for the phosphoinositide 3-kinase p110delta in signaling by the B-cell receptor complex. *Mol Cell Biol* 22: 8580-8591.
30. Baracho, G. V., M. H. Cato, Z. Zhu, O. R. Jaren, E. Hobeika, M. Reth, and R. C. Rickert. 2014. PDK1 regulates B cell differentiation and homeostasis. *Proc Natl Acad Sci U S A* 111: 9573-9578.
31. Clayton, E., G. Bardi, S. E. Bell, D. Chantry, C. P. Downes, A. Gray, L. A. Humphries, D. Rawlings, H. Reynolds, E. Vigorito, and M. Turner. 2002. A crucial role for the p110delta subunit of phosphatidylinositol 3-kinase in B cell development and activation. *J Exp Med* 196: 753-763.

32. Okkenhaug, K., A. Bilancio, G. Farjot, H. Priddle, S. Sancho, E. Peskett, W. Pearce, S. E. Meek, A. Salpekar, M. D. Waterfield, A. J. Smith, and B. Vanhaesebroeck. 2002. Impaired B and T cell antigen receptor signaling in p110delta PI 3-kinase mutant mice. *Science* 297: 1031-1034.
33. Zhang, K., A. Husami, R. Marsh, and M. B. Jordan. 2013. *Identification of a phosphoinositide 3 kinase (PI 3K p110? (PIK3CD) deficient individual*.
34. Conley, M. E., A. K. Dobbs, A. M. Quintana, A. Bosompem, Y. D. Wang, E. Coustan-Smith, A. M. Smith, E. E. Perez, and P. J. Murray. 2012. Agammaglobulinemia and absent B lineage cells in a patient lacking the p85α subunit of PI3K. *J Exp Med* 209: 463-470.
35. Ramadani, F., D. J. Bolland, F. Garcon, J. L. Emery, B. Vanhaesebroeck, A. E. Corcoran, and K. Okkenhaug. 2010. The PI3K isoforms p110alpha and p110delta are essential for pre-B cell receptor signaling and B cell development. *Sci Signal* 3: ra60.
36. Liu, Q., A. J. Oliveira-Dos-Santos, S. Mariathasan, D. Bouchard, J. Jones, R. Sarao, I. Kozieradzki, P. S. Ohashi, J. M. Penninger, and D. J. Dumont. 1998. The inositol polyphosphate 5-phosphatase ship is a crucial negative regulator of B cell antigen receptor signaling. *J Exp Med* 188: 1333-1342.
37. Okada, H., S. Bolland, A. Hashimoto, M. Kurosaki, Y. Kabuyama, M. Iino, J. V. Ravetch, and T. Kurosaki. 1998. Role of the inositol phosphatase SHIP in B cell receptor-induced Ca2+ oscillatory response. *J Immunol* 161: 5129-5132.
38. Browning, M. J., A. Chandra, V. Carbonaro, K. Okkenhaug, and J. Barwell. 2015. Cowden's syndrome with immunodeficiency. *J Med Genet* 52: 856-859.
39. Sander, S., V. T. Chu, T. Yasuda, A. Franklin, R. Graf, D. P. Calado, S. Li, K. Imami, M. Selbach, M. Di Virgilio, L. Bullinger, and K. Rajewsky. 2015. PI3 Kinase and FOXO1 Transcription Factor Activity Differentially Control B Cells in the Germinal Center Light and Dark Zones. *Immunity* 43: 1075-1086.
40. Cheng, S., C. Y. Hsia, B. Feng, M. L. Liou, X. Fang, P. P. Pandolfi, and H. C. Liou. 2009. BCR-mediated apoptosis associated with negative selection of immature B cells is selectively dependent on Pten. *Cell Res* 19: 196-207.
41. Anzelon, A. N., H. Wu, and R. C. Rickert. 2003. Pten inactivation alters peripheral B lymphocyte fate and reconstitutes CD19 function. *Nat Immunol* 4: 287-294.
42. Lucas, C. L., A. Chandra, S. Nejentsev, A. M. Condliffe, and K. Okkenhaug. 2016. PI3Kδ and primary immunodeficiencies. *Nat Rev Immunol* 16: 702-714.
43. Elkaim, E., B. Neven, J. Bruneau, K. Mitsui-Sekinaka, A. Stanislas, L. Heurtier, C. L. Lucas, H. Matthews, M. C. Deau, S. Sharapova, J. Curtis, J. Reichenbach, C. Glastre, D. A. Parry, G. Arumugakani, E. McDermott, S. S. Kilic, M. Yamashita, D. Moshous, H. Lamrini, B. Otremba, A. Gennery, T. Coulter, I. Quinti, J. L. Stephan, V. Lougaris, N. Brodszki, V. Barlogis, T. Asano, L. Galicier, D. Boutboul, S. Nonoyama, A. Cant, K. Imai, C. Picard, S. Nejentsev, T. J. Molina, M. Lenardo, S. Savic, M. Cavazzana, A. Fischer, A. Durandy, and S. Kracker. 2016. Clinical and immunologic phenotype associated with activated phosphoinositide 3-kinase δ syndrome 2: A cohort study. *J Allergy Clin Immunol* 138: 210-218.e219.
44. Lucas, C. L., H. S. Kuehn, F. Zhao, J. E. Niemela, E. K. Deenick, U. Palendira, D. T. Avery, L. Moens, J. L. Cannons, M. Biancalana, J. Stoddard, W. Ouyang, D. M. Frucht, V. K. Rao, T. P. Atkinson, A. Agharahimi, A. A. Hussey, L. R. Folio, K. N. Olivier, T. A. Fleisher, S. Pittaluga, S. M. Holland, J. I. Cohen, J. B. Oliveira, S. G. Tangye, P. L. Schwartzberg, M. J. Lenardo, and G. Uzel. 2014. Dominant-activating germline mutations in the gene encoding the PI(3)K catalytic subunit p110δ result in T cell senescence and human immunodeficiency. *Nat Immunol* 15: 88-97.
45. Angulo, I., O. Vadas, F. Garçon, E. Banham-Hall, V. Plagnol, T. R. Leahy, H. Baxendale, T. Coulter, J. Curtis, C. Wu, K. Blake-Palmer, O. Perisic, D. Smyth, M. Maes, C. Fiddler, J. Juss, D. Cilliers, G.

Markelj, A. Chandra, G. Farmer, A. Kielkowska, J. Clark, S. Kracker, M. Debré, C. Picard, I. Pellier, N. Jabado, J. A. Morris, G. Barcenas-Morales, A. Fischer, L. Stephens, P. Hawkins, J. C. Barrett, M. Abinun, M. Clatworthy, A. Durandy, R. Doffinger, E. R. Chilvers, A. J. Cant, D. Kumararatne, K. Okkenhaug, R. L. Williams, A. Condliffe, and S. Nejentsev. 2013. Phosphoinositide 3-kinase δ gene mutation predisposes to respiratory infection and airway damage. *Science* 342: 866-871.

46. Shojaee, S., L. N. Chan, M. Buchner, V. Cazzaniga, K. N. Cosgun, H. Geng, Y. H. Qiu, M. D. von Minden, T. Ernst, A. Hochhaus, G. Cazzaniga, A. Melnick, S. M. Kornblau, T. G. Graeber, H. Wu, H. Jumaa, and M. Müschen. 2016. PTEN opposes negative selection and enables oncogenic transformation of pre-B cells. *Nat Med* 22: 379-387.
47. Wentink, M., V. Dalm, A. C. Lankester, P. A. van Schouwenburg, L. Schölvinck, T. Kalina, R. Zachova, A. Sediva, A. Lambeck, I. Pico-Knijnenburg, J. J. van Dongen, M. Pac, E. Bernatowska, M. van Hagen, G. Driessen, and M. van der Burg. 2017. Genetic defects in PI3Kδ affect B-cell differentiation and maturation leading to hypogammaglobulineamia and recurrent infections. *Clin Immunol* 176: 77-86.
48. Dulau Florea, A. E., R. C. Braylan, K. T. Schafernak, K. W. Williams, J. Daub, R. K. Goyal, J. M. Puck, V. K. Rao, S. Pittaluga, S. M. Holland, G. Uzel, and K. R. Calvo. 2017. Abnormal B-cell maturation in the bone marrow of patients with germline mutations in PIK3CD. *J Allergy Clin Immunol* 139: 1032-1035.e1036.
49. Dornan, G. L., B. D. Siempelkamp, M. L. Jenkins, O. Vadas, C. L. Lucas, and J. E. Burke. 2017. Conformational disruption of PI3Kδ regulation by immunodeficiency mutations in. *Proc Natl Acad Sci U S A* 114: 1982-1987.
50. Hobeika, E., S. Thiemann, B. Storch, H. Jumaa, P. J. Nielsen, R. Pelanda, and M. Reth. 2006. Testing gene function early in the B cell lineage in mb1-cre mice. *Proc Natl Acad Sci U S A* 103: 13789-13794.
51. Casola, S., G. Cattoretti, N. Uyttersprot, S. B. Koralov, J. Seagal, J. Segal, Z. Hao, A. Waisman, A. Egert, D. Ghitza, and K. Rajewsky. 2006. Tracking germinal center B cells expressing germ-line immunoglobulin gamma1 transcripts by conditional gene targeting. *Proc Natl Acad Sci U S A* 103: 7396-7401.
52. Becker-Herman, S., A. Meyer-Bahlburg, M. A. Schwartz, S. W. Jackson, K. L. Hudkins, C. Liu, B. D. Sather, S. Khim, D. Liggitt, W. Song, G. J. Silverman, C. E. Alpers, and D. J. Rawlings. 2011. WASp-deficient B cells play a critical, cell-intrinsic role in triggering autoimmunity. *J Exp Med* 208: 2033-2042.
53. Zheng, G. X., J. M. Terry, P. Belgrader, P. Ryvkin, Z. W. Bent, R. Wilson, S. B. Ziraldo, T. D. Wheeler, G. P. McDermott, J. Zhu, M. T. Gregory, J. Shuga, L. Montesclaros, J. G. Underwood, D. A. Masquelier, S. Y. Nishimura, M. Schnall-Levin, P. W. Wyatt, C. M. Hindson, R. Bharadwaj, A. Wong, K. D. Ness, L. W. Beppu, H. J. Deeg, C. McFarland, K. R. Loeb, W. J. Valente, N. G. Ericson, E. A. Stevens, J. P. Radich, T. S. Mikkelsen, B. J. Hindson, and J. H. Bielas. 2017. Massively parallel digital transcriptional profiling of single cells. *Nat Commun* 8: 14049.
54. Qiu, X., Q. Mao, Y. Tang, L. Wang, R. Chawla, H. A. Pliner, and C. Trapnell. 2017. Reversed graph embedding resolves complex single-cell trajectories. *Nat Methods* 14: 979-982.
55. Moreno-García, M. E., K. Sommer, H. Shinohara, A. D. Bandaranayake, T. Kurosaki, and D. J. Rawlings. 2010. MAGUK-controlled ubiquitination of CARMA1 modulates lymphocyte NF-kappaB activity. *Mol Cell Biol* 30: 922-934.
56. Baumgarth, N. 2016. B-1 Cell Heterogeneity and the Regulation of Natural and Antigen-Induced IgM Production. *Front Immunol* 7: 324.

57. Victora, G. D., D. Dominguez-Sola, A. B. Holmes, S. Deroubaix, R. Dalla-Favera, and M. C. Nussenzweig. 2012. Identification of human germinal center light and dark zone cells and their relationship to human B-cell lymphomas. *Blood* 120: 2240-2248.
58. Hay, N. 2011. Interplay between FOXO, TOR, and Akt. *Biochim Biophys Acta* 1813: 1965-1970.
59. Ersching, J., A. Efeyan, L. Mesin, J. T. Jacobsen, G. Pasqual, B. C. Grabiner, D. Dominguez-Sola, D. M. Sabatini, and G. D. Victora. 2017. Germinal Center Selection and Affinity Maturation Require Dynamic Regulation of mTORC1 Kinase. *Immunity* 46: 1045-1058.e1046.
60. Benhamron, S., S. P. Pattanayak, M. Berger, and B. Tirosh. 2015. mTOR activation promotes plasma cell differentiation and bypasses XBP-1 for immunoglobulin secretion. *Mol Cell Biol* 35: 153-166.
61. Jellusova, J., M. H. Cato, J. R. Apgar, P. Ramezani-Rad, C. R. Leung, C. Chen, A. D. Richardson, E. M. Conner, R. J. Benschop, J. R. Woodgett, and R. C. Rickert. 2017. Gsk3 is a metabolic checkpoint regulator in B cells. *Nat Immunol* 18: 303-312.
62. Iwata, T. N., J. A. Ramírez-Komo, H. Park, and B. M. Iritani. 2017. Control of B lymphocyte development and functions by the mTOR signaling pathways. *Cytokine Growth Factor Rev* 35: 47-62.
63. Hideshima, T., P. Neri, P. Tassone, H. Yasui, K. Ishitsuka, N. Raje, D. Chauhan, K. Podar, C. Mitsiades, L. Dang, N. Munshi, P. Richardson, D. Schenkein, and K. C. Anderson. 2006. MLN120B, a novel IkappaB kinase beta inhibitor, blocks multiple myeloma cell growth in vitro and in vivo. *Clin Cancer Res* 12: 5887-5894.
64. Cantor, J., C. D. Browne, R. Ruppert, C. C. Féral, R. Fässler, R. C. Rickert, and M. H. Ginsberg. 2009. CD98hc facilitates B cell proliferation and adaptive humoral immunity. *Nat Immunol* 10: 412-419.
65. Cantor, J. M., and M. H. Ginsberg. 2012. CD98 at the crossroads of adaptive immunity and cancer. *J Cell Sci* 125: 1373-1382.
66. Limon, J. J., L. So, S. Jellbauer, H. Chiu, J. Corado, S. M. Sykes, M. Raffatellu, and D. A. Fruman. 2014. mTOR kinase inhibitors promote antibody class switching via mTORC2 inhibition. *Proc Natl Acad Sci U S A* 111: E5076-5085.
67. Tellier, J., W. Shi, M. Minnich, Y. Liao, S. Crawford, G. K. Smyth, A. Kallies, M. Busslinger, and S. L. Nutt. 2016. Blimp-1 controls plasma cell function through the regulation of immunoglobulin secretion and the unfolded protein response. *Nat Immunol* 17: 323-330.
68. Brohl, A. S., J. R. Stinson, H. C. Su, T. Badgett, C. D. Jennings, G. Sukumar, S. Sindiri, W. Wang, L. Kardava, S. Moir, C. L. Dalgard, J. A. Moscow, J. Khan, and A. L. Snow. 2015. Germline CARD11 Mutation in a Patient with Severe Congenital B Cell Lymphocytosis. *J Clin Immunol* 35: 32-46.
69. Xue, L., S. W. Morris, C. Orihuela, E. Tuomanen, X. Cui, R. Wen, and D. Wang. 2003. Defective development and function of Bcl10-deficient follicular, marginal zone and B1 B cells. *Nat Immunol* 4: 857-865.
70. Calado, D. P., B. Zhang, L. Srinivasan, Y. Sasaki, J. Seagal, C. Unitt, S. Rodig, J. Kutok, A. Tarakhovsky, M. Schmidt-Supprian, and K. Rajewsky. 2010. Constitutive canonical NF-κB activation cooperates with disruption of BLIMP1 in the pathogenesis of activated B cell-like diffuse large cell lymphoma. *Cancer Cell* 18: 580-589.
71. Jones, D. D., B. T. Gaudette, J. R. Wilmore, I. Chernova, A. Bortnick, B. M. Weiss, and D. Allman. 2016. mTOR has distinct functions in generating versus sustaining humoral immunity. *J Clin Invest* 126: 4250-4261.
72. Zhang, S., M. Pruitt, D. Tran, W. Du Bois, K. Zhang, R. Patel, S. Hoover, R. M. Simpson, J. Simmons, J. Gary, C. M. Snapper, R. Casellas, and B. A. Mock. 2013. B cell-specific deficiencies in mTOR limit humoral immune responses. *J Immunol* 191: 1692-1703.

73. Cho, S. H., A. L. Raybuck, K. Stengel, M. Wei, T. C. Beck, E. Volanakis, J. W. Thomas, S. Hiebert, V. H. Haase, and M. R. Boothby. 2016. Germinal centre hypoxia and regulation of antibody qualities by a hypoxia response system. *Nature* 537: 234-238.
74. Nakaya, M., Y. Xiao, X. Zhou, J. H. Chang, M. Chang, X. Cheng, M. Blonska, X. Lin, and S. C. Sun. 2014. Inflammatory T cell responses rely on amino acid transporter ASCT2 facilitation of glutamine uptake and mTORC1 kinase activation. *Immunity* 40: 692-705.
75. Shi, J. H., and S. C. Sun. 2015. TCR signaling to NF-κB and mTORC1: Expanding roles of the CARMA1 complex. *Mol Immunol* 68: 546-557.
76. Masle-Farquhar, E., A. Bröer, M. Yabas, A. Enders, and S. Bröer. 2017. ASCT2 (SLC1A5)-Deficient Mice Have Normal B-Cell Development, Proliferation, and Antibody Production. *Front Immunol* 8: 549.
77. Nicklin, P., P. Bergman, B. Zhang, E. Triantafellow, H. Wang, B. Nyfeler, H. Yang, M. Hild, C. Kung, C. Wilson, V. E. Myer, J. P. MacKeigan, J. A. Porter, Y. K. Wang, L. C. Cantley, P. M. Finan, and L. O. Murphy. 2009. Bidirectional transport of amino acids regulates mTOR and autophagy. *Cell* 136: 521-534.
78. Fenczik, C. A., R. Zent, M. Dellos, D. A. Calderwood, J. Satriano, C. Kelly, and M. H. Ginsberg. 2001. Distinct domains of CD98hc regulate integrins and amino acid transport. *J Biol Chem* 276: 8746-8752.
79. van den Brand, M., J. Rijntjes, K. M. Hebeda, L. Menting, C. V. Bregitha, W. B. Stevens, W. J. van der Velden, B. B. Tops, J. H. van Krieken, and P. J. Groenen. 2017. Recurrent mutations in genes involved in nuclear factor-κB signalling in nodal marginal zone lymphoma-diagnostic and therapeutic implications. *Histopathology* 70: 174-184.
80. Onaindia, A., L. J. Medeiros, and K. P. Patel. 2017. Clinical utility of recently identified diagnostic, prognostic, and predictive molecular biomarkers in mature B-cell neoplasms. *Mod Pathol* 30: 1338-1366.
81. Wu, C., N. F. de Miranda, L. Chen, A. M. Wasik, L. Mansouri, W. Jurczak, K. Galazka, M. Dlugosz-Danecka, M. Machaczka, H. Zhang, R. Peng, R. D. Morin, R. Rosenquist, B. Sander, and Q. Pan-Hammarström. 2016. Genetic heterogeneity in primary and relapsed mantle cell lymphomas: Impact of recurrent CARD11 mutations. *Oncotarget* 7: 38180-38190.
82. Gitlin, A. D., L. von Boehmer, A. Gazumyan, Z. Shulman, T. Y. Oliveira, and M. C. Nussenzweig. 2016. Independent Roles of Switching and Hypermutation in the Development and Persistence of B Lymphocyte Memory. *Immunity* 44: 769-781.
83. Tamahara, T., K. Ochiai, A. Muto, Y. Kato, N. Sax, M. Matsumoto, T. Koseki, and K. Igarashi. 2017. The mTOR-Bach2 Cascade Controls Cell Cycle and Class Switch Recombination during B Cell Differentiation. *Mol Cell Biol* 37.
84. Kotani, A., N. Kakazu, T. Tsuruyama, I. M. Okazaki, M. Muramatsu, K. Kinoshita, H. Nagaoka, D. Yabe, and T. Honjo. 2007. Activation-induced cytidine deaminase (AID) promotes B cell lymphomagenesis in Emu-cmyc transgenic mice. *Proc Natl Acad Sci U S A* 104: 1616-1620.
85. Pasqualucci, L., G. Bhagat, M. Jankovic, M. Compagno, P. Smith, M. Muramatsu, T. Honjo, H. C. Morse, M. C. Nussenzweig, and R. Dalla-Favera. 2008. AID is required for germinal center-derived lymphomagenesis. *Nat Genet* 40: 108-112.
86. Mandelbaum, J., G. Bhagat, H. Tang, T. Mo, M. Brahmachary, Q. Shen, A. Chadburn, K. Rajewsky, A. Tarakhovsky, L. Pasqualucci, and R. Dalla-Favera. 2010. BLIMP1 is a tumor suppressor gene frequently disrupted in activated B cell-like diffuse large B cell lymphoma. *Cancer Cell* 18: 568-579.
87. Bartlett, N. L., B. A. Costello, B. R. LaPlant, S. M. Ansell, J. G. Kuruvilla, C. B. Reeder, L. S. Thye, D. M. Anderson, K. Krysiak, C. Ramirez, J. Qi, B. A. Siegel, M. Griffith, O. L. Griffith, F. Gomez, and T.

A. Fehniger. 2018. Single-agent ibrutinib in relapsed or refractory follicular lymphoma: a phase 2 consortium trial. *Blood* 131: 182-190.

88. Xu, L., N. Tsakmaklis, G. Yang, J. G. Chen, X. Liu, M. Demos, A. Kofides, C. J. Patterson, K. Meid, J. Gustine, T. Dubeau, M. L. Palomba, R. Advani, J. J. Castillo, R. R. Furman, Z. R. Hunter, and S. P. Treon. 2017. Acquired mutations associated with ibrutinib resistance in Waldenström macroglobulinemia. *Blood* 129: 2519-2525.
89. Mullally, A., S. W. Lane, B. Ball, C. Megerdichian, R. Okabe, F. Al-Shahrour, M. Paktinat, J. E. Haydu, E. Housman, A. M. Lord, G. Wernig, M. G. Kharas, T. Mercher, J. L. Kutok, D. G. Gilliland, and B. L. Ebert. 2010. Physiological Jak2V617F expression causes a lethal myeloproliferative neoplasm with differential effects on hematopoietic stem and progenitor cells. *Cancer Cell* 17: 584-596.
90. Martin, F., and J. F. Kearney. 2001. B1 cells: similarities and differences with other B cell subsets. *Curr Opin Immunol* 13: 195-201.
91. Durand, C. A., K. Hartvigsen, L. Fogelstrand, S. Kim, S. Iritani, B. Vanhaesebroeck, J. L. Witztum, K. D. Puri, and M. R. Gold. 2009. Phosphoinositide 3-kinase p110 delta regulates natural antibody production, marginal zone and B-1 B cell function, and autoantibody responses. *J Immunol* 183: 5673-5684.
92. Choi, Y. S., J. A. Dieter, K. Rothaeusler, Z. Luo, and N. Baumgarth. 2012. B-1 cells in the bone marrow are a significant source of natural IgM. *Eur J Immunol* 42: 120-129.
93. Holodick, N. E., J. R. Tumang, and T. L. Rothstein. 2010. Immunoglobulin secretion by B1 cells: differential intensity and IRF4-dependence of spontaneous IgM secretion by peritoneal and splenic B1 cells. *Eur J Immunol* 40: 3007-3016.
94. Chou, M. Y., L. Fogelstrand, K. Hartvigsen, L. F. Hansen, D. Woelkers, P. X. Shaw, J. Choi, T. Perkmann, F. Bäckhed, Y. I. Miller, S. Hörkkö, M. Corr, J. L. Witztum, and C. J. Binder. 2009. Oxidation-specific epitopes are dominant targets of innate natural antibodies in mice and humans. *J Clin Invest* 119: 1335-1349.
95. Lalor, P. A., L. A. Herzenberg, S. Adams, and A. M. Stall. 1989. Feedback regulation of murine Ly-1 B cell development. *Eur J Immunol* 19: 507-513.
96. Reynolds, A. E., M. Kuraoka, and G. Kelsoe. 2015. Natural IgM is produced by CD5- plasma cells that occupy a distinct survival niche in bone marrow. *J Immunol* 194: 231-242.
97. Montecino-Rodriguez, E., H. Leathers, and K. Dorshkind. 2006. Identification of a B-1 B cell-specified progenitor. *Nat Immunol* 7: 293-301.
98. Crank, M. C., J. K. Grossman, S. Moir, S. Pittaluga, C. M. Buckner, L. Kardava, A. Agharahimi, H. Meuwissen, J. Stoddard, J. Niemela, H. Kuehn, and S. D. Rosenzweig. 2014. Mutations in PIK3CD can cause hyper IgM syndrome (HIGM) associated with increased cancer susceptibility. *J Clin Immunol* 34: 272-276.
99. Chiriaco, M., I. Brigida, P. Ariganello, S. Di Cesare, G. Di Matteo, F. Taus, D. Cittaro, D. Lazarevic, A. Scarselli, V. Santilli, E. Attardi, E. Stupka, S. Giannelli, M. Fraziano, A. Finocchi, P. Rossi, A. Aiuti, P. Palma, and C. Cancrini. 2017. The case of an APDS patient: Defects in maturation and function and decreased in vitro anti-mycobacterial activity in the myeloid compartment. *Clin Immunol* 178: 20-28.
100. Sasaki, Y., E. Derudder, E. Hobeika, R. Pelanda, M. Reth, K. Rajewsky, and M. Schmidt-Supprian. 2006. Canonical NF-kappaB activity, dispensable for B cell development, replaces BAFF-receptor signals and promotes B cell proliferation upon activation. *Immunity* 24: 729-739.
101. Abdelrasoul, H., M. Werner, C. S. Setz, K. Okkenhaug, and H. Jumaa. 2018. PI3K induces B-cell development and regulates B cell identity. *Sci Rep* 8: 1327.

102. Henley, T., D. Kovesdi, and M. Turner. 2008. B-cell responses to B-cell activation factor of the TNF family (BAFF) are impaired in the absence of PI3K delta. *Eur J Immunol* 38: 3543-3548.
103. Griffin, D. O., N. E. Holodick, and T. L. Rothstein. 2011. Human B1 cells in umbilical cord and adult peripheral blood express the novel phenotype CD20+ CD27+ CD43+ CD70-. *J Exp Med* 208: 67-80.
104. Kracker, S., J. Curtis, M. A. Ibrahim, A. Sediva, J. Salisbury, V. Campr, M. Debré, J. D. Edgar, K. Imai, C. Picard, J. L. Casanova, A. Fischer, S. Nejentsev, and A. Durandy. 2014. Occurrence of B-cell lymphomas in patients with activated phosphoinositide 3-kinase δ syndrome. *J Allergy Clin Immunol* 134: 233-236.
105. Compagno, M., Q. Wang, C. Pighi, T. C. Cheong, F. L. Meng, T. Poggio, L. S. Yeap, E. Karaca, R. B. Blasco, F. Langellotto, C. Ambrogio, C. Voena, A. Wiestner, S. N. Kasar, J. R. Brown, J. Sun, C. J. Wu, M. Gostissa, F. W. Alt, and R. Chiarle. 2017. Phosphatidylinositol 3-kinase δ blockade increases genomic instability in B cells. *Nature* 542: 489-493.
106. Avery, D. T., A. Kane, T. Nguyen, A. Lau, A. Nguyen, H. Lenthall, K. Payne, W. Shi, H. Brigden, E. French, J. Bier, J. R. Hermes, D. Zahra, W. A. Sewell, D. Butt, M. Elliott, K. Boztug, I. Meyts, S. Choo, P. Hsu, M. Wong, L. J. Berglund, P. Gray, M. O'Sullivan, T. Cole, S. M. Holland, C. S. Ma, C. Burkhart, L. M. Corcoran, T. G. Phan, R. Brink, G. Uzel, E. K. Deenick, and S. G. Tangye. 2018. Germline-activating mutations in. *J Exp Med* 215: 2073-2095.
107. Moens, L., and S. G. Tangye. 2014. Cytokine-Mediated Regulation of Plasma Cell Generation: IL-21 Takes Center Stage. *Front Immunol* 5: 65.
108. Xu, Z. Z., Z. G. Xia, A. H. Wang, W. F. Wang, Z. Y. Liu, L. Y. Chen, and J. M. Li. 2013. Activation of the PI3K/AKT/mTOR pathway in diffuse large B cell lymphoma: clinical significance and inhibitory effect of rituximab. *Ann Hematol* 92: 1351-1358.